# PREPARATION OF TI3C2TX MXENE BY VARIOUS FLUORIDE SALTS ETCHING FOR ADSORPTION OF ENROFLOXACIN

BY

CHANNARITH BE

A THESIS SUBMITTED IN PARTIAL FULFILLMENT OF THE
REQUIREMENTS FOR THE DEGREE OF MASTER OF
ENGINEERING (ENGINEERING TECHNOLOGY)
SIRINDHORN INTERNATIONAL INSTITUTE OF TECHNOLOGY
THAMMASAT UNIVERSITY
ACADEMIC YEAR 2022

THAMMASAT UNIVERSITY
SIRINDHORN INTERNATIONAL INSTITUTE OF TECHNOLOGY

THESIS

BY

CHANNARITH BE

ENTITLED

# PREPARATION OF TI3C2TX MXENE BY VARIOUS FLUORIDE SALTS ETCHING FOR ADSORPTION OF ENROFLOXACIN

was approved as partial fulfillment of the requirements for
the degree of Master of Engineering (Engineering Technology)

on January 31, 2023

Chairperson ______________________
(Associate Professor Pakorn Opaprakasit, Ph.D.)

Member and Advisor ______________________
(Associate Professor Paiboon Sreearunothai, Ph.D.)

Member and Co-adviser Chamorn Chawengkijwanich
(Chamorn Chawengkijwanich, Ph.D.)

Member T. Isobe
(Associate Professor Toshihiro Isobe, Ph.D.)

Director ______________________
(Professor Pruettha Nanakorn, D.Eng.)

| | |
|---|---|
| Thesis Title | PREPARATION OF TI3C2TX MXENE BY VARIOUS FLUORIDE SALTS ETCHING FOR ADSORPTION OF ENROFLOXACIN |
| Author | Channarith Be |
| Degree | Master of Engineering (Engineering Technology) |
| Faculty/University | Sirindhorn International Institute of Technology/ Thammasat University |
| Thesis Advisor | Associate Professor Paiboon Sreearunothai, Ph.D. |
| Thesis Co-Advisor | Chamorn Chawengkijwanich, Ph.D. |
| Academic Years | 2022 |

# ABSTRACT

The occurrence of the antibiotics in water and soil are now becoming a severe threat in many countries. Overuse of antibiotic drugs has promoted antibiotic-resistant bacteria in both human and animals. In response to the excessive antibiotic contamination in natural environment, removal of antibiotic residues is needed for accessing clean water and protecting water-related ecosystem. MXenes are a new family of two-dimensional transition metal carbides, nitride, and carbonitride which have demonstrated potentials in many applications due to their unique properties such as metallic conductivity, hydrophilicity, wide interlayer space, abundant surface functional groups, and ion intercalability. In this work, MXene ($Ti_3C_2T_x$) material was investigated for removal of enrofloxacin, an antibiotic drug frequently used in aquaculture, by using adsorption technique. MXene ($Ti_3C_2T_x$) was synthesized from MAX phase ($Ti_3AlC_2$) with acid/salts etchant from in-situ HF etching. The preparation of various fluoride salts in hydrochloric acid (HCl), including lithium fluoride (LiF), sodium fluoride (NaF), potassium fluoride (KF), Zinc fluoride ($ZnF_2$) were studied. We also investigated the influence of concentration of acid etchant and etching time to minimize the reaction. The results suggested that MXene could be produced upon 4 hours by using hydrochloric acid (9 mol/L) and fluoride salt (9 mol/L). The surface morphology analysis by scanning electron microscopy (SEM) indicated that all samples etched at 4 hours and 24 hours showed accordion-like structure in multilayer (MLs). The removal of Al element of synthesized

material confirmed by EDX analysis decreased after etching of 4 hours and 24 hours compared to that of the MAX phase precursor. The simultaneous cation intercalation caused the obtained MXene to have larger interlayer space as confirmed by XRD results.

Lithium cation intercalation of $Ti_3C_2$ showed vast inter-layer spacing compared to other fluoride salts etching system potentially due to its large solvation radii. As-prepared MX-Li-4h was further delaminated/fully exfoliated in DI water, LiCl, and ethanol by ultrasonication for 20 minutes. Well exfoliated/delaminated MXene was produced in DI water. From dynamic light scattering, the hydrodynamic particle size of the obtained $Ti_3C_2$/DI was approximately $380.2 \pm 4.7$nm with the negative zeta potential $-45$mV. Transmission electron microscopy (TEM) results confirmed the successful exfoliation of the obtained MXene sonicated in DI water (sMX/DI) with a few layers.

Adsorption of enrofloxacin (ENR) antibiotic onto MLs ion-intercalated MXene, which include MX-Li, MX-Na, MX-K and MX-Zn, the ENR adsorption seems to be slower than that of the monolayer MXene (sMX/DI) due to the MLs being occupied by the intercalated cations, which required longer time to adsorb the drug molecules. A multilayer MX-HF, etched by direct HF also show poorly performance due to smaller interlayer space which has low chance for ENR adsorbing at the active site inside layer structure.

ENR sorption onto monolayer MX (sMX/DI) has improved adsorption capacity compared to that of Li-MX multilayer which some adsorption sites occupied by $Li^+$. A delamination MX-Li-4h in TBAOH into single layer also revealed that monolayer MX binding with $TBA^+$ would not be likely to exchange with ENR. Thus, monolayer MX with abundant adsorption site is a better candidate than cation intercalated MLs MX or smaller interlayer space MLs MX for ENR adsorption performance.

For monolayer MXene (sMX/DI), the adsorption capacity reached the value of 8.35 mg $g^{-1}$ in 3 hours, which is higher than those of the MLs MXene MX-Li, MX-Na, MX-K, MX-Zn which took almost 10 hours to reach equilibrium with the lower adsorption capacity values of 6.80 mg $g^{-1}$, 3.65 mg $g^{-1}$, 4.76 mg $g^{-1}$, 2.76 mg $g^{-1}$, respectively. The adsorption isotherms were well fitted by the Langmuir model, which provides the maximum adsorption capacity of the monolayer MXene of 17.45 mg $g^{-1}$. The enrofloxacin adsorption is in the order of monolayer MXene > cation intercalated multi-layer MXene > multi-layer MXene.

**Keywords:** MXene, In-situ HF etching, Adsorption, Cation-exchange

# ACKNOWLEDGEMENTS

First of all, I would like to express sincere gratitude to my advisor, Assoc. Prof. Dr. Paiboon Sreearunothai as well as my co-advisor, Dr. Chamorn Chawengkijwanich who played a crucial role during my master’s degree and research. His guidance helped me in all the time of research and writing of this thesis. I could not have imagined having a better advisor and mentor for my master’s degree study.

I am also thankful to my thesis committee, Assoc. Prof. Dr. Pakorn Opaprakasit (Sirindhorn International Institute of Technology) and chairperson, Assoc. Prof. Dr. Toshihiro Isobe (Tokyo Institute of Technology), for their encouragement and insightful comments.

I am also thankful to the TAIST-Tokyo Tech scholarship and host university, Sirindhorn International Institute of Technology, Thammasat University for offering scholarship and the financial support. Furthermore, I would like to thank to all my fellow lab mates and senior at Functional Advanced Material and Engineering (FAME) for providing technical and laboratory support during my research.

Last but not least, I would like to thank my family: my parents Chanthou Kong and Sokoeurn Touch, my sister Chansreyroth Be for supporting me spiritually throughout my life.

Channarith Be

# TABLE OF CONTENTS

# LIST OF TABLES

# LIST OF FIGURES

# LIST OF SYMBOLS/ABBREVIATIONS

| **Symbols/Abbreviations** | **Terms** |
|---|---|
| XRD | X-ray Power Diffraction |
| SEM | Scanning Electron Microscopic |
| ENR | Enrofloxacin |
| EDX | Energy Dispersive X-ray |
| PSO | Pseudo Second Order |
| PFO | Pseudo First Order |
| CIP | Ciprofloxacin |
| ARB | Antibiotic Resistant Bacteria |
| TEM | Transmission electron microscopy |
| ICP-OES | Inductively coupled plasma atomic emission spectroscopy |
| DSL | Dynamic light scattering |
| ZP | Zeta potential |
| MLs | Mulilayer |
| $Li^+$ | Lithium |
| MX | MXene |
| TBAOH | Tetrabutylammonium hydroxide |
| sMX | Sonication MXene |

# CHAPTER 1
# INTRODUCTION

## 1.1 Background

In 2004, the concept of the 2D dimensional material was initially developed by graphene which peels off from the graphite material. Since then, 2D dimensional material has been dramatically interested in various research topics due to its unique physical and chemical properties in a wide range of applications A. Liu et al. (2020).A. Liu et al. (2020). In 2011, an emerging 2D dimensional material was discovered based on metallic carbide, carbonitrides and nitrite, namely MXene by Draxel University research team. MXene has developed in various kinds of applications due to multiple advantages such as high specific area, good electrical conductivity, high mechanical strength, activated metallic hydroxide sites and hydrophilicity in nature (Rasool et al., 2019).MXene has developed in various kinds of applications due to multiple advantages such as high specific area, good electrical conductivity, high mechanical strength, activated metallic hydroxide sites and hydrophilicity in nature (Rasool et al., 2019). The general formula of MXene is $M_{n+1}X_nT_x$ (n=1 to 3; M=transition metal, e.g., Ti, V, Nb, Mo; X= C and/or N; T= surface termination, e.g., −O, −OH, and −F which form on the surface of the outer M element during synthesis). The concept of 2D dimensional material MXene was produced from the bulk MAX phase polycrystalline, hexagonal carbides and nitrides which have the general formula: $M_{n+1}AX_n$, where n = 1 to 4, and M is an early transition metal, A is an A-group element, and X is either carbon and/or nitrogen. In order to get the structural layer of MXene, it was prepared by selective etching of group A element (Al, Si and Ge) from MAX phase precursor (M. Ghidiu, M. R. Lukatskaya, M.-Q. Zhao, Y. Gogotsi, & M. W. J. N. Barsoum, 2014b).(Ghidiu et al., 2014b). Regarding the MXene properties, the most prominent of MXene is benefits from their metallic conductivity, while some synthesized material can be semiconductors or superconductors, depending on the surface termination and the composition of the material. Due to their attractive structure, MXene has been explored on high efficiency of adsorption capability of pollutant in the wastewater. Its high specific surface area exhibits excellent adsorption of both cationic and anionic dye molecule (Yan et al., 2021). This is because of the chemically surface and mainly cause by electrostatic interaction (Rozmysłowska-Wojciechowska et al., 2019). For example, natural zeolite was investigated to adsorb of enrofloxacin antibiotic (Ötker & Akmehmet-Balcıoğlu, 2005). Rahman and Raheem (2022) fabricated zinc oxide impregnated graphene oxide/inulin (ZGI) for adsorption of enrofloxacin with greatly removal efficiency >90% and can be used up to 5 cycles. Akpotu et al. (2023)Its high specific surface area exhibits excellent adsorption of both cationic and anionic dye molecule (Yan et al., 2021). This is because of the chemically surface and mainly cause by electrostatic interaction (Rozmysłowska-Wojciechowska et al., 2019). For example, natural zeolite was investigated to adsorb of enrofloxacin antibiotic (Ötker & Akmehmet-Balcıoğlu, 2005). Rahman and Raheem (2022) fabricated zinc oxide impregnated graphene oxide/inulin (ZGI) for adsorption of enrofloxacin with greatly removal efficiency >90% and can be used up to 5 cycles. Akpotu et al. (2023) studied on adsorption enrofloxacin by composite GO-PEG thin film on the surface of Mont-$NH_2$, provided variety in chemical constitution and functionalities, facilitated the ability of uptake enrofloxacin molecule. Sukidpaneenid et al. (2023) also reported the performance of ENR adsorption in aqueous solution by using adsorbent-photocatalyst $Ti_3C_2$-$TiO_2$. The efficiency of degradation was mainly due to the MXene layer structure consists of titanium and carbon elements and inducing of titanium dioxide particle on the outer surface by using a rapid microwave hydrothermal treatment. It has been shown to be very efficient sorbent material and also photocatalytic material for eliminating ENR molecule.

Meanwhile, as growing of MXene material on remediation, research studies on simulation and prediction of different of fluoride salts etching, producing different size of cation intercalation are still a promising candidate since it could produce MXene in distinct chemical constitution, especially interlayer space . Especially, using MXene as an adsorbent to employ on removal of contamination in water.

## 1.2 Statement of problem

Antibiotics are the most potential drugs against bacteria which used to treat the bacterial infection. Furthermore, the improper dosage and unnecessary usage of antibiotics have polluted to aquatic environment and led to emerge antibiotic resistant gens (ARGs), antibiotic-resistant bacteria and the multidrug-resistant pathogenic (Kumar et al.).(Kumar et al.). Antibiotic resistance has already become a serious global health problem, with an estimated 10 million deaths per year by 2050 if not successfully addressed. Approximately 1.2 million fatalities in 2019 were confirmed to be attribute to antimicrobial resistant (Murray et al., 2022). Multiple antibiotic classes were discovered in receiving water and effluent at concentrations ranging from ng/L to mg/L. China has the highest number of antibiotic contaminations in East and Southeast Asia. Approximately 90 antibiotics from five major classes (SFs, FQs, TCs, MLs, and BLs) were studied in water samples with concentrations ranging from 0.1 to 1000 ng/L, with the median being 100ng/L. The predominance of antibiotic concentrations in China are found based on economic (e.g., population growth and antibiotic emission), geochemical, geographical, and hydrological factors (Chen, Jing, Teng, & Wang, 2018). Antibiotic contamination was identified in large quantities in sewage and wastewater treatment plants. Several antibiotic compounds, including ß-lactams, quinolones, tetracyclines, macrolides, sulfonamides, and others, can fix up to distinct subgroups. They are complex compounds that may have many functions inside the same molecule (Kümmerer, 2009). Besides from practical manner, antibiotic residues have caused significant harm to ecosystems due to their limited biodegradability over time. Antibiotic residue has been identified in surface water, groundwater, and drinking water during the last decade, according to some data. (Oulton, Kohn, & Cwiertny, 2010). Conventional water treatment techniques, including biological treatment, filtration, coagulation, flocculation and sedimentation, have been identified as ineffective antibiotic removal (Watkinson, Murby, & Costanzo, 2007). Advanced oxidation technologies that produce hydroxyl radical to decompose contaminants such as UV photolysis, photocatalysis, adsorption, photo-Fenton reaction, ionizing radiation were found to be successfully for antibiotics removal. However, the main challenge for all these methods was related to the application cost, catalyst management, residual toxicity, and various byproducts (Ikehata, Jodeiri Naghashkar, & Gamal El-Din, 2006). Therefore, removal of harmful residual in water is very challenging for protect the environment. Multiple antibiotic classes were discovered in receiving water and effluent at concentrations ranging from ng/L to mg/L. China has the highest number of antibiotic contaminations in East and Southeast Asia. Approximately 90 antibiotics from five major classes (SFs, FQs, TCs, MLs, and BLs) were studied in water samples with concentrations ranging from 0.1 to 1000 ng/L, with the median being 100ng/L. The predominance of antibiotic concentrations in China are found based on economic (e.g., population growth and antibiotic emission), geochemical, geographical, and hydrological factors (Chen et al., 2018). Antibiotic contamination was identified in large quantities in sewage and wastewater treatment plants. Several antibiotic compounds, including ß-lactams, quinolones, tetracyclines, macrolides, sulfonamides, and others, can fix up to distinct subgroups. They are complex compounds that may have many functions inside the same molecule (Kümmerer, 2009). Besides from practical manner, antibiotic residues have caused significant harm to ecosystems due to their limited biodegradability over time. Antibiotic residue has been identified in surface water, groundwater, and drinking water during the last decade, according to some data. (Oulton et al., 2010). Conventional water treatment techniques, including biological treatment, filtration, coagulation, flocculation and sedimentation, have been identified as ineffective antibiotic removal (Watkinson et al., 2007). Advanced oxidation technologies that produce hydroxyl radical to decompose contaminants such as UV photolysis, photocatalysis, adsorption, photo-Fenton reaction, ionizing radiation were found to be successfully for antibiotics removal. However, the main challenge for all these methods was related to the application cost, catalyst management, residual toxicity, and various byproducts (Ikehata et al., 2006). Therefore, removal of harmful residual in water is very challenging for protect the environment.

## 1.3 Objectives

In this work, we aim to investigate the factors that influence MXene ($Ti_3C_2T_x$) synthesis and further to exfoliate the multilayer MXene ($Ti_3C_2T_x$) into monolayer MXene ($Ti_3C_2T_x$). The primary synthesis of MXene was conducted in the top-down method using wet chemical etching (LiF-HCl) and further studied the influencing factors of acidic concentration, different fluoride salts, and etching time. Thereafter, the removal of pharmaceutical contaminant of an enrofloxacin by simple adsorption technique was carried out by using neat multilayer MXene ($Ti_3C_2T_x$) and monolayer MXene ($Ti_3C_2T_x$).

Part 1;

- To synthesized MXene ($Ti_3C_2T_x$) following the in-situ HF etching by various fluoride salts etching; 4 hours etching, and 24 hours etching were carried out
- Influence of acid etchant was studied
- Influence of fluoride salt etchant was studied
- Characterizations of the obtained material (SEM-EDX and XRD)
- Conversion of multilayer-MXene into monolayer-MXene using probe ultrasonication.

Part 2;

- To study the adsorption performance of synthesized material under dark condition
- To study the adsorption capacity between multilayer MXene ($Ti_3C_2T_x$) synthesized from various cation intercalation, and the monolayer MXene ($Ti_3C_2T_x$) obtained from fully exfoliation
- To study the mechanism of the adsorption performance by adsorption kinetic model and adsorption isotherm model.

## 1.4 Scope of study

- MXene was synthesized by using MAX phase as precursor and using hydrochloric acid (HCl) and fluoride salts (LiF, KF, ZnF, and NaF) as etchant agents.
- The influence of different concentrations of HCl etchant (1M, 4M, and 9M) were studied.
- The effect of etching time at 4 hours and 24 hours were employed.
- Fully exfoliation of MXene (MX-Li-4h) was sonicated in three dispersions (DI water, ethanol, and lithium chloride).
- Commercial enrofloxacin antibiotic were used as an artificial contaminant in aqueous solution experimentally.

# CHAPTER 2

# REVIEW OF LITERATURE

The main purpose of this chapter is to examine the relevant literature on MXene discovery, synthesis method, and the factor influence on the etching process. Furthermore, the discussion in this chapter will go into further detail on the problem of residual antibiotic pollutants in water and suitable absorbents for drug removal. There are number of approaches to remove large molecules of pharmaceutical contaminants in scientific studies, and MXene has been found as one of the sophisticated materials that pose a fasten adsorption of drug due to its unique properties, large surface area, ion intercalation, strong electrical conductivity, and environmentally friendly.

## 2.1 MAX Phase ($Ti_3AlC_2$)

MAX phases are polycrystalline nanolaminates layered of ternary carbide or nitride in metallic and ceramic material. The name of MAX phase chemically emphasizes the composition with the formular $M_{n+1}AX_n$ , where M stand for transition metal carbide nitride or carbonitride, A is an A group element (mostly group IIIA or IVA), and X is C and/or N (A. Zhou, 2012). MAX phase can be classified in a variety of crystalline structure groups, $M_2AX$ with n=1, $M_3AX_2$ with n=2, $M_4AX_3$ with n=3 based on the number of atoms M, A and X elements in each of molecule. These group also known as 211, 312, 413 materials. MAX phases are polycrystalline nanolaminates layered of ternary carbide or nitride in metallic and ceramic material. The name of MAX phase chemically emphasizes the composition with the formular $M_{n+1}AX_n$ , where M stand for transition metal carbide nitride or carbonitride, A is an A group element (mostly group IIIA or IVA), and X is C and/or N (A. Zhou, 2012). MAX phase can be classified in a variety of crystalline structure groups, $M_2AX$ with n=1, $M_3AX_2$ with n=2, $M_4AX_3$ with n=3 based on the number of atoms M, A and X elements in each of molecule. These group also known as 211, 312, 413 materials. Figure 2.1 shows each of chemical composition of MAX phase and synthesized material (Michel W. Barsoum & El-Raghy, 2001). The first synthesized MAX phase was $M_2AX$ in the 1960s. There were more than 40 of $M_2AX$ phases that have been successfully synthesized. After that, two differences $M_3AX_2$ ($Ti_3SiC_2$ and $Ti_3GeC_2$) were synthesized in 1967, and the same structure of $Ti_3AlC_2$ was also synthesized in the 1990s (A. Zhou, 2012). Thereafter, several of $M_4AX_3$ phases were added to the list in 2000s, including $Ti_4AlN_3$, $Ta_4AlC_3$, $Nb_4AlC_3$ and $V_4AlC_3$ shows each of chemical composition of MAX phase and synthesized material (Michel W. Barsoum & El-Raghy, 2001). The first synthesized MAX phase was $M_2AX$ in the 1960s. There were more than 40 of $M_2AX$ phases that have been successfully synthesized. After that, two differences $M_3AX_2$ ($Ti_3SiC_2$ and $Ti_3GeC_2$) were synthesized in 1967, and the same structure of $Ti_3AlC_2$ was also synthesized in the 1990s (A. Zhou, 2012). Thereafter, several of $M_4AX_3$ phases were added to the list in 2000s, including $Ti_4AlN_3$, $Ta_4AlC_3$, $Nb_4AlC_3$ and $V_4AlC_3$ (M. W. Barsoum, El-Raghy, & Procopio, 2000; Hu et al., 2007; Hu et al., 2008; Lin, Zhuo, Zhou, Li, & Wang, 2006). The chemical bonding in the MAX phases demonstrate as electronic properties which are useful in technology involving high energy efficiency, thermal tolerant, rigidity at high temperature (Magnuson & Mattesini, 2017).. The chemical bonding in the MAX phases demonstrate as electronic properties which are useful in technology involving high energy efficiency, thermal tolerant, rigidity at high temperature (Magnuson & Mattesini, 2017).

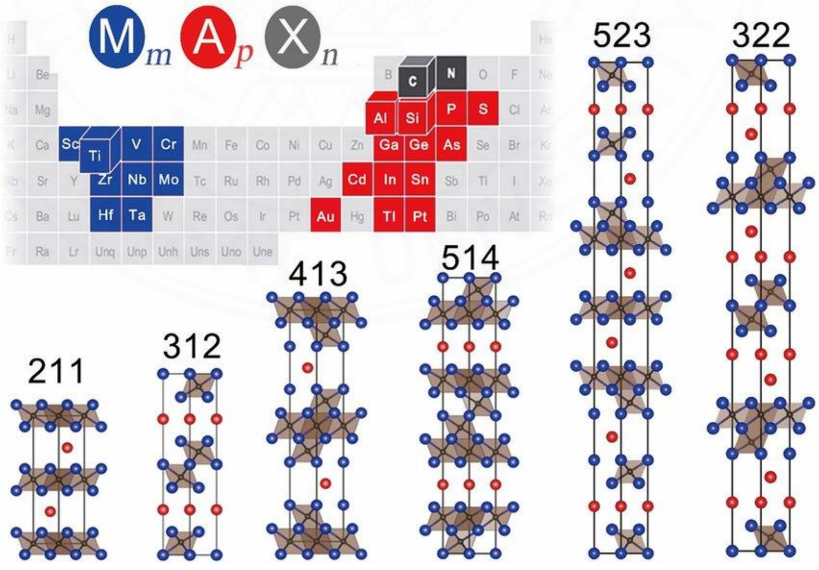

**Figure 2.1** Illustration of chemical elements of MAX phase ($Ti_3AlC_2$)

## 2.2 MXene ($Ti_3C_2T_x$)

The concept of the 2D dimensional material was initially developed by graphene which peels off from the graphite material in 2004. Since then, 2D dimensional material has gained tremendous interested in various research topics due to their special properties in chemical, mechanical and physical properties (A. Liu et al., 2020). In 2011, an emerging 2D dimensional material MXene was discovered by Drexel University research team. MXene family consists of transition metal carbide, carbonitrides and nitrite. Since then, 2D dimensional material has gained tremendous interested in various research topics due to their special properties in chemical, mechanical and physical properties (A. Liu et al., 2020). In 2011, an emerging 2D dimensional material MXene was discovered by Drexel University research team. MXene family consists of transition metal carbide, carbonitrides and nitrite. MXene has grown in popularity in a variety of applications because of its several benefits, including high specific area, strong electrical conductivity, high mechanical strength, activated metallic hydroxide sites, and ecologically benign features (Rasool et al., 2019).(Rasool et al., 2019). The general formula of MXene is $M_{n+1}X_nT_x$ (n=1-3; M=transition metal, e.g., Ti, V, Nb, Mo; X= C and/or N; T= surface termination, e.g., −O, −OH, and −F which form on the surface of the outer M element during synthesis). MXene material was derived from the MAX phase polycrystalline, hexagonal carbides and nitrides which have the general formula: $M_{n+1}AX_n$, where n = 1 to 4, and M is an early transition metal, A is an A-group element, and X is either carbon and/or nitrogen. In order to get the structural layer of MXene, it was synthesized by selective etching of group A element (Al, Si and Ge) from MAX phase precursor (Ghidiu et al., 2014b).In order to get the structural layer of MXene, it was synthesized by selective etching of group A element (Al, Si and Ge) from MAX phase precursor (Ghidiu et al., 2014b). Generally, MXene can be described in various kinds of structural materials which depends on the initial precursor of MAX phase. Three examples of MAX phase structures $M_2AX$, $M_3AX_3$ and $M_4X_3$ are shown in Figure 2.2 (a) and the exfoliate MXene illustrate in Figure 2.2 (b). Additionally, the MXene family comes with three different kinds of atomic structure, ranging from $M_2X$, $M_3X_2$, and $M_4X_3$, yielding tunability and opportunity to apply on many applications. Moreover, the surface of MXene which covers with single or mixed termination depending on the synthesis process and the MXene composition. Many studies showed that physical properties such as bandgap, metallically, magnetic and electronic mobility are associated with surface termination. MXene came out with unique properties and characteristics which renders them in many applications. The most prominent of MXene is benefits from their metallic conductivity, while some synthesized material can be semiconductors or superconductors, based on the surface termination and the composition of the material. The surface termination of the MXene sheets is defined after etching from MAX phase. Error! Reference source not found. has indicated over ten years of the progress and the d evelopment of the MXene from the beginning year of 2011 until 2021. In the past decade, the first discovery of MXene has been reported by etching the A element from the parent precursor $Ti_3AlC_2$ into a new material called $Ti_3C_2$ MXene.

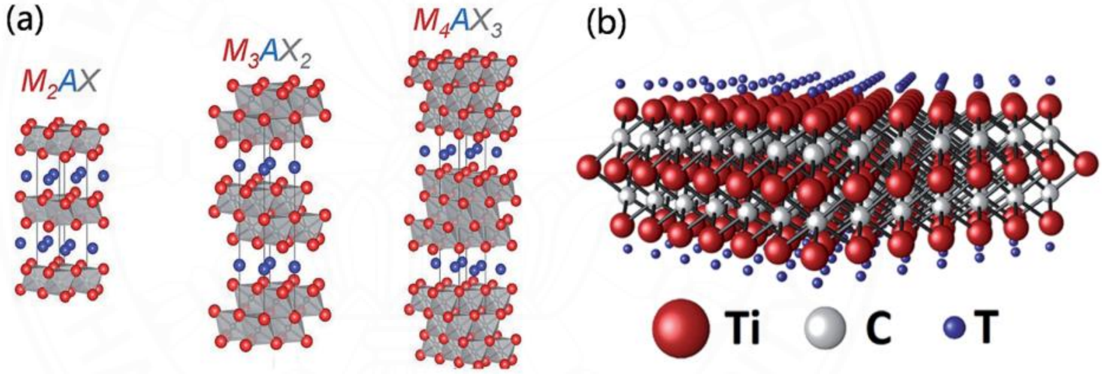

**Figure 2.2** (a) Crystalline structures of MAX phase (b) crystal structure of the single-sheet $Ti_3C_2T_x$, consisting of T as the termination group of ─O, ─F and/or ─OH.

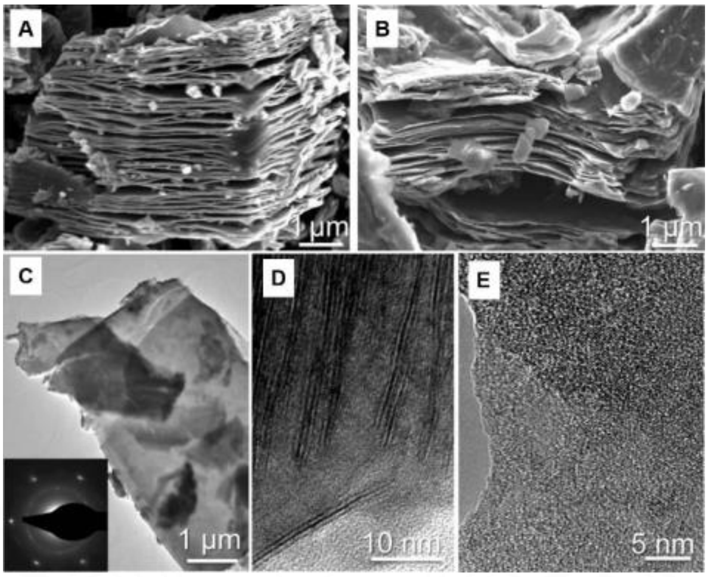

**Figure 2.3** SEM image of multilayer MXene and in-plane TEM image of MXene flake (Mashtalir et al., 2013). SEM image of multilayer MXene and in-plane TEM image of MXene flake (Mashtalir et al., 2013).

## 2.3 MXene synthesis overview

General synthesis approaches for 2D material were almost achieved mechanically by ball milling, shearing, ion intercalation, or surfactant-assisted solutions. However, all are required to exfoliate from bulk layer material with in-plane solid chemical bonding and weak out-of-plane bonding. Failure to synthesize MXene by mechanical exfoliation was reported since it could not break the metallic M-A bonding in-plane. Therefore, most of the MXene synthesis procedures were top-down or etching by chemical wetting to produced multilayer of MXene. Presently, there are several methods for synthesized MXene material. However, each synthesis procedure depends on the target application in which there are some modifications of the final product of MXene (Alhabeb et al., 2017). The most common method of synthesis MXene was HF etchants which is (50 wt%) concentrated solution dispersed into MAX phase. In this typical synthesis, M-A metallic bonding showed to weaken, and M-X remained strength, leading Al element almost etching out from the $M_{n+1}AX_n$ (Naguib et al., 2011b). However, each synthesis procedure depends on the target application in which there are some modifications of the final product of MXene (Alhabeb et al., 2017). The most common method of synthesis MXene was HF etchants which is (50 wt%)

concentrated solution dispersed into MAX phase. In this typical synthesis, M-A metallic bonding showed to weaken, and M-X remained strength, leading Al element almost etching out from the $M_{n+1}AX_n$ (Naguib et al., 2011b).

However, the synthesis route of MXene in a high concentration of hydrogen fluoride may cause a noticeable toxic during the synthesis time. Therefore, it is better for the research community to understand and ensure that the synthesis of MXene family should be safe and strictly performance. There are specific mechanisms that cause for most toxicity. Basically, hydrofluoric acid is one of the preferable etchants for MXene synthesis since it required few hours to synthesized. However, if the synthesis with pure hydrofluoric acid etching (HF Etching), a high concentration of hydronium ions could lead to standard acid burns. It also releases fluoride ions which are highly lipophilic, and it will penetrate deeply into human tissue if there is less precaution. In addition, it rapidly causes liquefactive necrosis in the contacted area (Christopher E Shuck et al., 2021). Hence, developing of *in situ* HF etching was recommended for synthesized in lab-scale and provided good etching of Al element similarly HF etching method.In addition, it rapidly causes liquefactive necrosis in the contacted area (Christopher E Shuck et al., 2021). Hence, developing of *in situ* HF etching was recommended for synthesized in lab-scale and provided good etching of Al element similarly HF etching method.

Another etching utilized fluoride-containing etchants with hydrochloric acid to produce HF forming called *in-situ* HF etching or acid salt etchants. *in-situ* HF was dependent on the concentration of fluoride salt or acidic and temperature which can successfully etching from 12 hours to days. The condition of individual etching depends on the purpose of the application. On the other hand, the synthesis step between the HF etching and *in-situ* HF etching are similar. In the synthesis procedure, fluoride salt such as (LiF, NaF, KF and $NH_4F$, etc.) were used for etching Al element (Al or Si) from MAX phase in the presence of hydrochloric acid (HCl). Thereafter the MXene sample will wash by deionized water or ethanol in several times. Cleaning step should be carried by centrifugation approximately 3500rpm to 5000 rpm until the supernatant pH value become neutral. The obtained MXene powder should dry in vacuum oven at 60 ˚C. Finally, MXene should store in desiccator to avoid moisture content since MXene easily to oxidize. Some studies have confirmed that $Ti_3C_2T_x$ easily to oxidized which turned the surface of MXene cover with the $TiO_2$. The final product after etching is in the form of multilayer MXene that combine by hydrogen or Van de Waals bonding, following by surface termination such as -F, -O, -Cl, -OH etc.

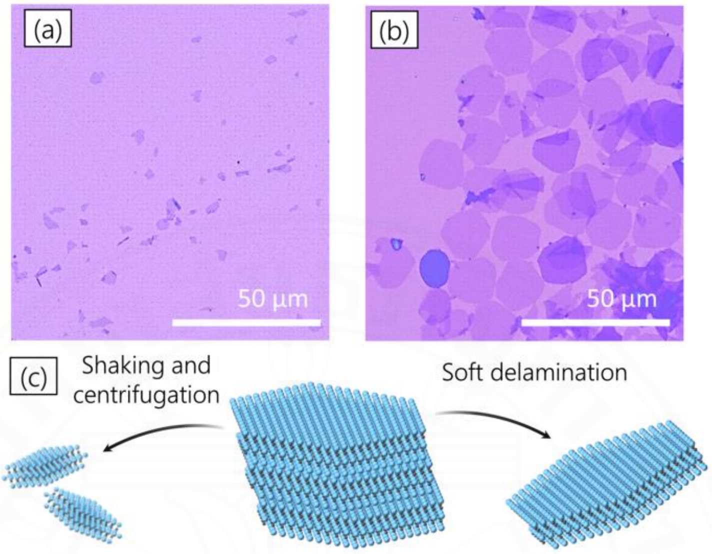

**Figure 2.4** Schematic illustrate of monolayer MXene flake obtained from hand shaking and soft delamination (Shekhirev, Busa, et al., 2022) schematic illustrate of monolayer MXene flake obtained from hand shaking and soft delamination (Shekhirev, Busa, et al., 2022)

### 2.3.1 Different F-salt etching

As report in the literature studies Z. Li et al. (2015); Mashtalir et al. (2013), MXene can further exfoliated by intercalation or delamination in the organic reagent including (DMSO, TBAOH, $NH_3.H_2O$ or urea). The purpose of intercalated with organic solvent is to increase the d-spacing of the MXene layer stacks. Therefore, each of MXene layer sheet could possibly separate by hand shaking or using power sonication. For the intercalation of organic solvent above is applied for MXene that synthesis via hydrofluoric acid. However, d-spacing in the lattice structure which give the interplanar distance is enlarged based on proportional to the size of the intercalate ions molecule if the etching method perform via fluoride salt etching with hydrochloric acid (Verger, Natu, Ghidiu, & Barsoum, 2019).However, d-spacing in the lattice structure which give the interplanar distance is enlarged based on proportional to the size of the intercalate ions molecule if the etching method perform via fluoride salt etching with hydrochloric acid (Verger et al., 2019).

As mentioned above, cations play a significant role to intercalate MXene structure. Ghidiu et al. 2014 report that fluoride salt etchant undergoes simultaneous ion intercalation, but HF etching did not. The main reason why HF-etched MXene are not ion exchangeable due to proportional of F termination are hydrophobic result in strong bond connection between MXene sheet (Natu et al., 2022). However, F-salt etched MXene after defluorination, a possible cation ($Na^+$ or $Li^+$) are easily ions exchangeable with smaller hydronium ions, making an osmosis swelling. For example, F. Liu et al. (2017)The main reason why HF-etched MXene are not ion exchangeable due to proportional of F termination are hydrophobic result in strong bond connection between MXene sheet (Natu et al., 2022). However, F-salt etched MXene after defluorination, a possible cation ($Na^+$ or $Li^+$) are easily ions exchangeable with smaller hydronium ions, making an osmosis swelling. For example, F. Liu et al. (2017) studied the effect of the nature of cation during etching $Ti_3AlC_2$ in various F-salt (LiF, NaF, KF and $NH_4F$) etchant mixture and varying different time and temperature etching. The results obtained from synthesis provide suitable synthesis condition for LiF at 50℃ 24 h, at 40℃ 48 h for NaF, 40℃ 48 h for KF and 24 h at 30 ℃ for $NH_4F$. However, remaining of LiF and $Na_3AlF_6$ appeared after successfully etching of Al element for LiF and NaF etchant sample. They also report that the fraction of LiF remaining because of large proportional of LiF salt much higher which some of $Li^+$ act as ions exchange with $H_3O^+$ after etching and some could not wash out because of low solubility in water. However, there was almost no detected residue K and Na on MXene which synthesized via NaF and KF. Another studied also mentioned about other salt etched beside LiF etchant, Benchakar et al. (2020) has demonstrated that $FeF_3$/HCl etchant significantly altered the surface termination, oxidation sensitivity and delamination ability. In their work, FeF3/HCl etching results in $Ti_3C_2T_x$@$TiO_{2-x}F_{2x}$ composite in one-pot synthesis in harsher etching condition. They also mentioned that the removal rate of Al element was much higher than LiF/HCl. Thus, by varying the temperature, concentration, temperature, and duration of synthesis, the fraction of $TiO_2$ can be controlled. Moreover, the c parameter value was calculated of 29.8 Å which are higher than LiF/HCl etching solution.

### 2.3.2 Molten salt etching

Molten salt assisted electrochemical etching system was introduce by Shen et al. (2021).Molten salt assisted electrochemical etching system was introduce by Shen et al. (2021). Because of the surface termination of 2D MXene material have significantly impacts to the application, modification of surface of 2D MXene were studied. Basically, the beginning of MXene etching system was introduce of -F surface termination due to acid etching. In this kind of synthesis material, molten salt assisted electrochemical etching (MS-E-etching) method was synthesized with fluorine-free $Ti_3C_2T_x$ without metallics.

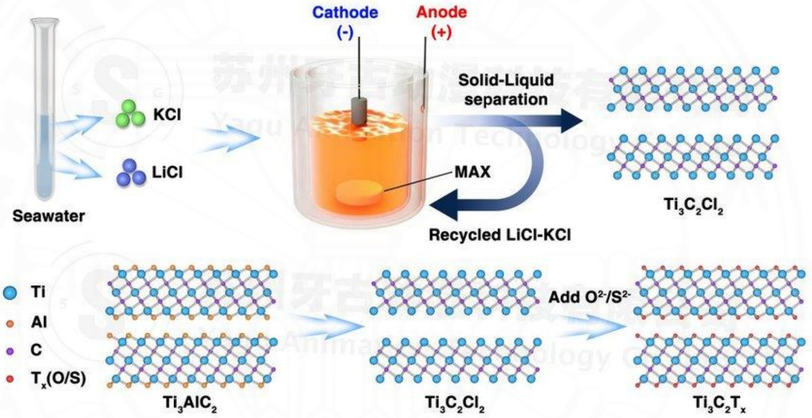

**Figure 2.5** Synthesis of MXene from MAX phase by MS-E-etching

**Table 2.1** Summary of MXene synthesis condition and its properties of each condition

| Synthesis Method | etchant condition | Temperature & Time | Properties | Application | Ref |
|---|---|---|---|---|---|
| HF direct etching | 50 wt.% | RT, 24 | Multilayer, Require intercalate with organic solvent to delaminated, Surface modification friendly | Energy storage Chemotherapeutic agent | (Anasori, Lukatskaya, & Gogotsi, 2017) |

| | | | | | |
|---|---|---|---|---|---|
| In-situ HF Fluoride salt and HCl (NaF, KF, LiF NH4F etc) | Vary depending on fluoride salt | Vary depend on fluoride salt | Multilayer<br>Cation intercalation and delamination<br>Less harmful | Water purification<br>Supercapacitor<br>Sensors<br>Antibacterial | (F. Liu et al., 2017) |
| In-situ HF<br>$FeF_3$/HCl | HCl 6M<br>2g $FeF_33H_2O$ | 50 h at 60℃ | Multilayer<br>$TiO_2$ at high temperature | Photocatalysis<br>Supercapacitor<br>Sensors | (Wang et al., 2017) |
| Hydrothermal etching | 37 wt % HCl<br>$NaBF_4$ | 16 h at 180℃ (Author suggest 16 h for the optimum time for avoid impurity of $AlF_3$) | High efficiency etching MXene<br>MXene flake | Adsorption of dye molecule | (C. Peng et al., 2018) |
| Electrochemical etching | HCl | Require long time for synthesis | Surface termination consist of $Cl^-$<br>-OH -O<br>Flouride-free | Obtain electrochemistry properties material | (Shahzad et al., 2017) |

### 2.3.3 Delamination of MXene

Single layer of MXene material has attatched tremorous interrest in environmental and electrochemical research field. Since multilayer particle of MXene has been widely investigated, the delamination process has received much attention in the liturature. The first stage of delamination of MXene was chemical intercalation in organic solvent (DMSO) follow by sonication (Mashtalir et al., 2013), which the large molecule of organic solvent intercalated and weakening the Van de Waals force of multilayer, causing delaminated into single flake. Thereafter, $Ti_3C_2T_x$ has also delaminated in another large organic molecule, e.g., ($TBA^+$) and ($TMA^+$ ). The first stage of delamination of MXene was chemical intercalation in organic solvent (DMSO) follow by sonication (Mashtalir et al., 2013), which the large molecule of organic solvent intercalated and weakening the Van de Waals force of multilayer, causing delaminated into single flake. Thereafter, $Ti_3C_2T_x$ has also delaminated in another large organic molecule, e.g., ($TBA^+$) and ($TMA^+$ ). It empasized that it was possible to exchange the large molecule of $TMA^+$ and $TBA^+$ with the existing cation $Li^+$ which $Ti_3C_2T_x$ fabricated by in-situ HF procedure (VahidMohammadi, Mojtabavi, Caffrey, Wanunu, & Beidaghi, 2019).(VahidMohammadi et al., 2019). Large molecule of intercalation has produced the MXene material become larger interspace which demonstrate as easily to delaminate. However, delaminated MXene results in high number of defect MXene flake which is unstable and readily oxidize. Some of several studied has mentioned that, the prefered method for delamination of MXene is simultanously chemical intercalation of $Li^+$ which act as an intercalant and etching agent. Recently work has published in another method for delamination of MXene ($Ti_3C_2T_x$ and $V_2CT_x$) by 3 roll shearing after MXene synthesis via in-situ HF etching. It also reported that the interspace from smaller intercalant $Li^+$ is applicable for shearing and produce large flake of monolayer MXene with a good electrochemical and conductivity (Inman et al., 2022b). It also reported that the interspace from smaller intercalant $Li^+$ is applicable for shearing and produce large flake of monolayer MXene with a good electrochemical and conductivity (Inman et al., 2022b).

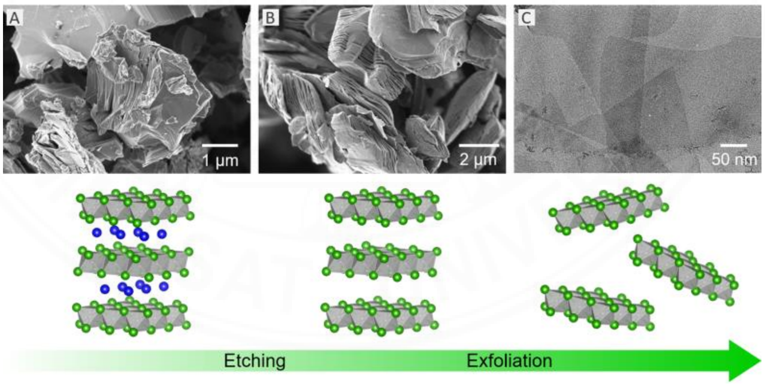

**Figure 2.6** Etching process of 2D MXene flake nanosheet (a) the MAX phase precursor, (b) multilayer MXene and (c) TEM micrograph of overlapping MXene single layer.

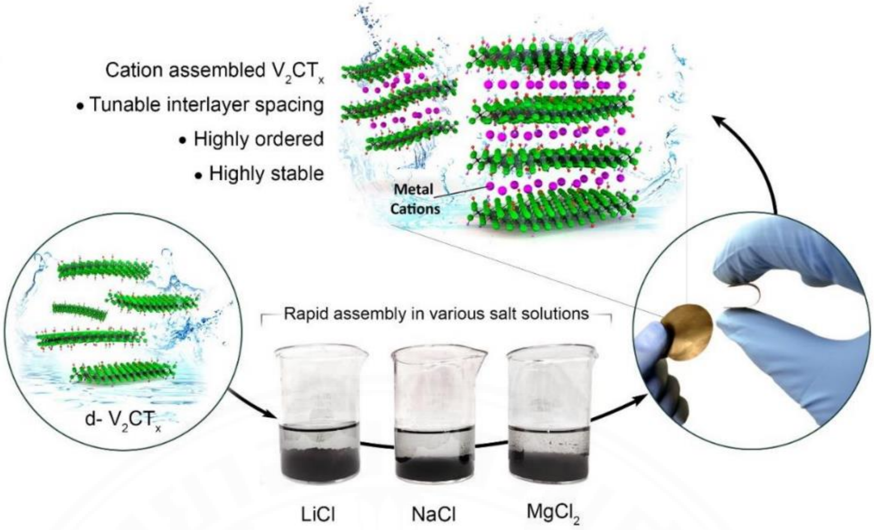

**Figure 2.7** Possible assembly of delamination MXene in salts solution

## 2.4 Application of MXene

MXene has potential criteria which emerged many applications, enabling of chemical transformation for achieving future sustainable energy. In 2016, MXene firstly explored chemistry catalytic via electrochemical hydrogen evolution reaction (HER) (Gao, O'Mullane, & Du, 2017). The promising of the large surface area, many number of active sites provides a crucial criterion for expanding in the future studies. The first starting point of MXene was applied in supercapacitor application which known as energy storage device with achieved the capacitance 440 F cm$^{-3}$ (130 F g$^{-1}$) and up to 900 F cm$^{-3}$ (245 F g$^{-1}$) in acidic electrolytes (M. Ghidiu, M. R. Lukatskaya, M.-Q. Zhao, Y. Gogotsi, & M. W. Barsoum, 2014a; Lukatskaya et al., 2013). MXene was also use in environmental and water treatment applications. The primary MXene water treatment membrane was prepared by vacuum-assisted filtration (VAF). The unique properties of MXene are their sheet assembly into layer stacks with a well-define interlayer spacing, which act as water selective channel. Various charge cations ($Mg^+$, $Ca^+$, and $Al^{3+}$) are smaller than the inter layer spacing of MXene layers which are beneficial to migrate cationic in the water (Ren et al., 2015). MXene can also use as photocatalytic application due to their altering surface chemistries. The multi-layer of $Ti_3C_2T_x$ which stand for photocatalyst reveal a degradation efficiency of methylene blue up to 81% under UV within 5 hours. However, it was not degrade in the dark condition even prolong for 20 hours (Mashtalir et al., 2014a). In addition, they also suggested that multi-layer of MXene provide capable adsorbent toward cationic molecule of methylene blue due to an increasing of inter-spacing which was observed during adsorption. Moreover, $Ti_3C_2T_x$ nanosheet also report as a good adsorbent for removal of some heavy metal (Pb, Cu, Cr etc). Shahzad et al. (2017), mentioned that delamination of $Ti_3C_2T_x$ flake enhance a good adsorption of cupper due to the nanosheet flake exhibit large surface area, hydrophilicity, and their unique surface functional group. In addition, the adsorption capacity of cupper was 78.45mg/g for 1 minute, corresponding to 80% of total of metal content. Recently, new approach of MXene has laden with bacteriophage to come across with antibacterial candidate for controlling bacteria contamination in water. Mansoorianfar, Shahin, Hojjati–Najafabadi, and Pei (2022), highlighted that negatively charge molecule of lipopolysaccharide of *shigella* outer membrane quickly attach with MXene, reducing bacteria 99% of artificial contamination sample. Noticeably, there was no regrowth of other bacteria which revealed as an outstanding antibacterial efficiency.MXene has potential criteria which emerged many applications, enabling of chemical transformation for achieving future sustainable energy. In 2016, MXene firstly explored chemistry catalytic via electrochemical hydrogen evolution reaction (HER) (Gao et al., 2017). The promising of the large surface area, many number of active sites provides a crucial criterion for expanding in the future studies. The first starting point of MXene was applied in supercapacitor application which known as energy storage device with achieved the capacitance 440 F $cm^{-3}$ (130 F $g^{-1}$) and up to 900 F $cm^{-3}$ (245 F $g^{-1}$) in acidic electrolytes (Ghidiu et al., 2014a; Lukatskaya et al., 2013). MXene was also use in environmental and water treatment applications. The primary MXene water treatment membrane was prepared by vacuum-assisted filtration (VAF). The unique properties of MXene are their sheet assembly into layer stacks with a well-define interlayer spacing, which act as water selective channel. Various charge cations ($Mg^+$, $Ca^+$, and $Al^{3+}$) are smaller than the inter layer spacing of MXene layers which are beneficial to migrate cationic in the water (Ren et al., 2015). MXene can also use as photocatalytic application due to their altering surface chemistries. The multi-layer of $Ti_3C_2T_x$ which stand for photocatalyst reveal a degradation efficiency of methylene blue up to 81% under UV within 5 hours. However, it was not degrade in the dark condition even prolong for 20 hours (Mashtalir et al., 2014a). In addition, they also suggested that multi-layer of MXene provide capable adsorbent toward cationic molecule of methylene blue due to an increasing of inter-spacing which was observed during adsorption. Moreover, $Ti_3C_2T_x$ nanosheet also report as a good adsorbent for removal of some heavy metal (Pb, Cu, Cr etc). Shahzad et al. (2017), mentioned that delamination of $Ti_3C_2T_x$ flake enhance a good adsorption of cupper due to the nanosheet flake exhibit large surface area, hydrophilicity, and their unique surface functional group. In addition, the adsorption capacity of cupper was 78.45mg/g for 1 minute, corresponding to 80% of total of metal content. Recently, new approach of MXene has laden with bacteriophage to come across with antibacterial candidate for controlling bacteria contamination in water. Mansoorianfar et al. (2022), highlighted that negatively charge molecule of lipopolysaccharide of *shigella* outer membrane quickly attach with MXene, reducing bacteria 99% of artificial contamination sample. Noticeably, there was no regrowth of other bacteria which revealed as an outstanding antibacterial efficiency.

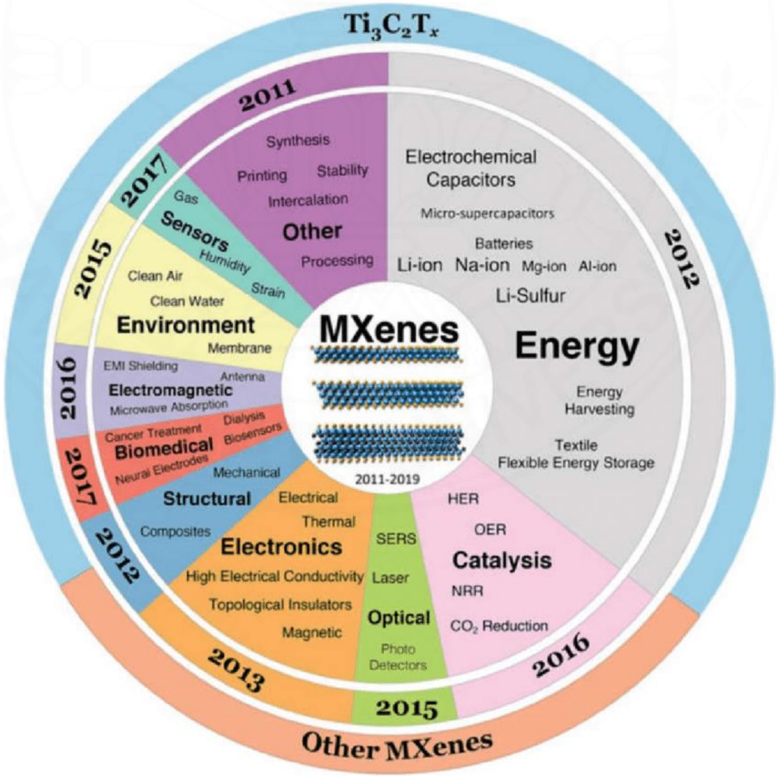

**Figure 2.8** The general application of MXene since the staring year of discovery (Anasori & Gogotsi, 2011)

## 2.5 Antibiotic overview

Antibiotic is a combination of two classical Greek words, anti ("against") and bios ("life"). Thus, antibiotics are the principal substance "against life". They are organic molecules derived from the low molecular weight, which is selectivity against bacteria life (Christopher & Timothy, 2016). It was well-known that antibiotic is a powerful drug which was used to treat disease caused by bacteria. The various activity of antibiotics can be the relevance of bacteriostatic, which slow down the growth of bacteria or inhibit the bacteria growth, and bactericidal means exclusively kill bacteria (Rhee & Gardiner, 2004).(Rhee & Gardiner, 2004). Antibiotics are a kind of medicine that fight against certain infections and can save lives when used in properly way. In the human body, before bacteria can cause symptoms, the immune system can generally try to fight with them. Sometimes, however, many harmful bacteria have occurred, and the immune system cannot handle them. Therefore, antibiotics are helpful in this situation to carry out their ability to struggle against bacteria infectious. Antibiotics are classified based on their chemical structure or mechanism of action. There are various chemical classes that may be broken down into subgroups, including ß-lactams, quinolones, tetracyclines, macrolides, sulfonamides, and others. They are complex compounds that may have many functions inside the same molecule (Kümmerer, 2009). Enrofloxacin is a member of the fluoroquinolone family, which is a subfamily of the quinolone family. It was widely used in animals at the beginning of the 1980s. ENR has a broad antimicrobial spectrum that is effective against most gram-negative and gram-positive bacteria but not anaerobic bacteria. (Trouchon & Lefebvre, 2016). ENR is classified as zwitterionic molecule with $pK_{a1}$ = (5.88-6.06) and a $pK_{a2}$ = (7.70-7.74). Due to protonation and deprotonation of ENR molecule, at lower pKa1 ENR molecule become positively charge due to the carboxyl acid group. At higher that pKa2, basic tertiary amine become negatively charge drug. So enrofloxacin doesn't bear charge between this two pH. They are complex compounds that may have many functions inside the same molecule (Kümmerer, 2009). Enrofloxacin is a member of the fluoroquinolone family, which is a subfamily of the quinolone family. It was widely used in animals at the beginning of the 1980s. ENR has a broad antimicrobial spectrum that is effective against most gram-negative and gram-positive bacteria but not anaerobic bacteria. (Trouchon & Lefebvre, 2016). ENR is classified as zwitterionic molecule with pKa1 = (5.88-6.06) and a pKa2 = (7.70-7.74). Due to protonation and deprotonation of ENR molecule, at lower pKa1 ENR molecule become positively charge due to the carboxyl acid group. At higher that pKa2, basic tertiary amine become negatively charge drug. So enrofloxacin doesn't bear charge between this two pH.

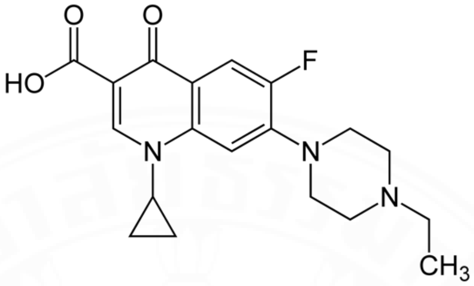

**Figure 2.9** Enrofloxacin chemical structure

### 2.5.1 Excessive use of antibiotics

Antibiotics are the foremost commonly endorsed medications within the world consumption. The utilize of these drugs has taken off over later decades in numerous nations, especially in low-middle income countries (LMICs). Worldwide antibiotics utilization expanded by 65% between 2000 and 2015, and the rate of antibiotic utilization expanded by 39%, 32 from 11.3 to 15.7 characterized everyday measurements (DDDs) per 1,000 individuals. However, the serious problem of antibiotic pollutant refers to antimicrobial resistant which microbial species can adapt to high level of antibiotics. Antimicrobial resistant (AMR) is a serious server to public health issue. WHO announced that monitoring of antibiotic consumption is needed for many low-income and middle-income country. Antibiotic resistance has as of now gotten to be an inescapable worldwide wellbeing risk, possibly coming about in an assessed 10 million fatality a year by 2050 in case not being successfully migrated.

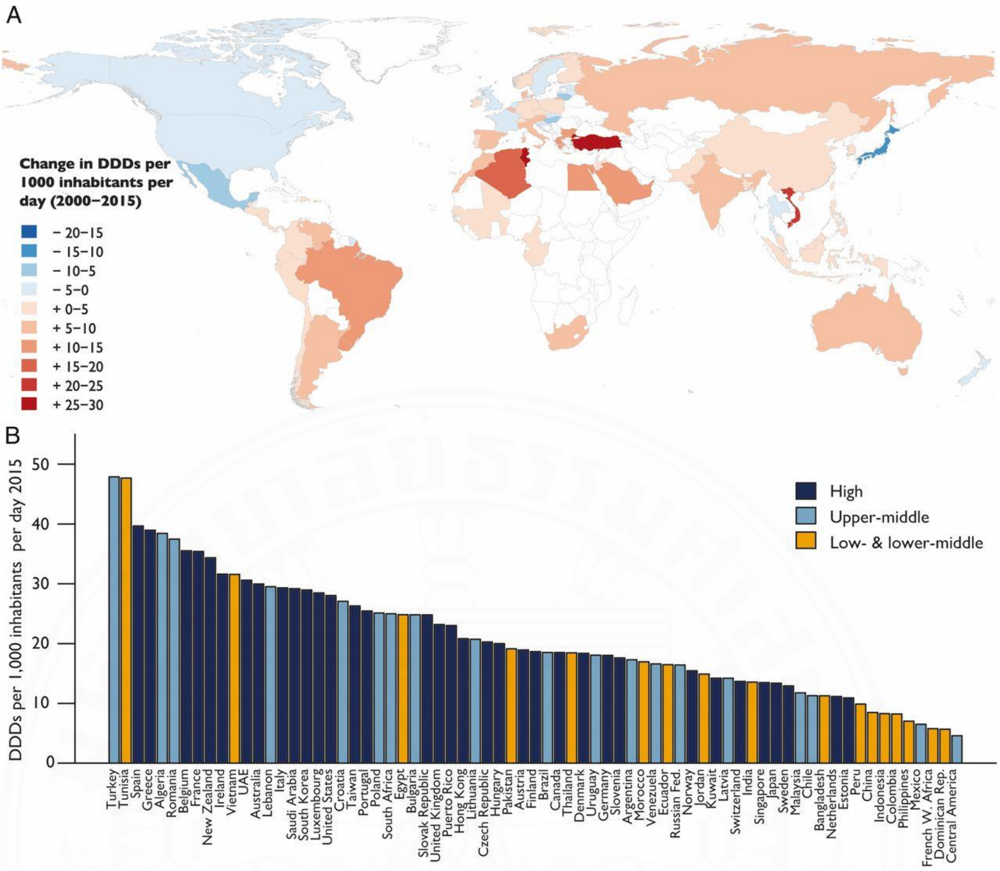

**Figure 2.10** Global antibiotic consumption by country: 2000–2015. (A) Change in the national antibiotic consumption rate between 2000 and 2015 in DDDs per 1,000 inhabitants per day, (B) Antibiotic consumption rate by country for 2015 in DDDs per 1,000 inhabitants per day (Klein et al., 2018). Global antibiotic consumption by country: 2000–2015. (A) Change in the national antibiotic consumption rate between 2000 and 2015 in DDDs per 1,000 inhabitants per day, (B) Antibiotic consumption rate by country for 2015 in DDDs per 1,000 inhabitants per day (Klein et al., 2018).

Since the discovery of penicillin in 1929, global antibiotic usage has risen, and numerous types of synthetic antibiotics have also been utilized in people, animals, and industries (Kümmerer, 2009; Q.-Q. Zhang, Ying, Pan, Liu, & Zhao, 2015). As a result, antibiotic contamination was found in the environment by discharging from household, hospital, wastewater treatment plants, and aquaculture livestock farms. (Kümmerer, 2009).(Kümmerer, 2009). Within the aquaculture industry, antibiotics is currently utilizing as a drug to prevent bacterial infections. Only small portion of the antibiotic has chemically absorbed, and most of them discharge into environment as the antibiotic residues. In livestock farming, antibiotic is imperative for promoting growth of livestock and preventing of the infection disease. Therefore, most of antibiotic contaminant resulting from the animal feces or urine (Briones, Sarmah, & Padhye, 2016). As the results, residual antibiotics occur in the river or lake through livestock farming, aquaculture, wastewater, hospital, and many other factors caused emerging Therefore, most of antibiotic contaminant resulting from the animal feces or urine (Briones et al., 2016). As the results, residual antibiotics occur in the river or lake through livestock farming, aquaculture, wastewater, hospital, and many other factors caused emerging.

Antibiotic was not employed on human but also use in animal especially for promoting growth of the aquaculture. According to European Surveillance of Veterinary Antimicrobial Consumption (ESVAC), which reported every year since 2011, Italy was the highest antibiotic consumption among European countries in agriculture. Antibiotics are being employed in a variety of industries, including home waste, hospitals, urban sewage, raising livestock, and aquaculture (He et al., 2016). Besides from practical manner, antibiotic residues have also caused severe damage to ecosystems, as they have low biodegradability over time. Over the past decade, some evidence has been observed that antibiotic residue has been found in surface water, groundwater and drinking water (Oulton et al., 2010). Conventional water treatment techniques, including biological treatment, filtration, coagulation, flocculation and sedimentation, have been identified as ineffective antibiotic removal (Watkinson et al., 2007). Advanced oxidation technologies that produce hydroxyl radical to decompose contaminants such as UV photolysis, photocatalysis, photo-fenton reaction, ionizing radiation were found to be successfully for removal of antibiotic. However, the main challenge for all these methods was related to the application cost, catalyst management, residual toxicity, and various byproducts (Ikehata et al., 2006).Antibiotic was not employed on human but also use in animal especially for promoting growth of the aquaculture. According to European Surveillance of Veterinary Antimicrobial Consumption (ESVAC), which reported every year since 2011, Italy was the highest antibiotic consumption among European countries in agriculture. Antibiotics are being employed in a variety of industries, including home waste, hospitals, urban sewage, raising livestock, and aquaculture (He et al., 2016). Besides from practical manner, antibiotic residues have also caused severe damage to ecosystems, as they have low biodegradability over time. Over the past decade, some evidence has been observed that antibiotic residue has been found in surface water, groundwater and drinking water (Oulton et al., 2010). Conventional water treatment techniques, including biological treatment, filtration, coagulation, flocculation and sedimentation, have been identified as ineffective antibiotic removal (Watkinson et al., 2007). Advanced oxidation technologies that produce hydroxyl radical to decompose contaminants such as UV photolysis, photocatalysis, photo-fenton reaction, ionizing radiation were found to be successfully for removal of antibiotic. However, the main challenge for all these methods was related to the application cost, catalyst management, residual toxicity, and various byproducts (Ikehata et al., 2006).

China is one of the most nations which devoured higher sum of antibiotic due to most high populated in the world. The total usage of antibiotic in China was 162,000 tons in 2013 (Q.-Q. Zhang et al., 2015). In addition, yearly consumption of human antibiotic in Vietnam, Brunei, Philippine, Japan, Mongolia, and South Korea were estimated to be 1086, 1.13, 260.5, 524.9, 133.2, 546.4 in 2015 as report by WHO. Figure 2.6. shows the human antibiotic consumption rate illustrate as DDD per 1000 inhabitants per day in 2015 (WHO, 2018). In China, more than 90 types of antibiotics belong to five class of antibiotic (SF, FQ, TCs, MLs, and Bls) were investigated in water, ranging from 0.1 to 1000ng/L (S. Li et al., 2018). As mentioned by Chen et al., (2018), the leftover of antibiotic in China due to poor treatment efficiency of sewage, surface runoff, and direct discharge from livestock industries (Chen et al., 2018).

China is one of the most nations which devoured higher sum of antibiotic due to most high populated in the world. The total usage of antibiotic in China was 162,000 tons in 2013 (Q.-Q. Zhang et al., 2015). In addition, yearly consumption of human antibiotic in Vietnam, Brunei, Philippine, Japan, Mongolia, and South Korea were estimated to be 1086, 1.13, 260.5, 524.9, 133.2, 546.4 in 2015 as report by WHO. Figure 2.6. shows the human antibiotic consumption rate illustrate as DDD per 1000 inhabitants per day in 2015 (WHO, 2018). In China, more than 90 types of antibiotics belong to five class of antibiotic (SF, FQ, TCs, MLs, and Bls) were investigated in water, ranging from 0.1

to 1000ng/L (S. Li et al., 2018). As mentioned by Chen et al., (2018), the leftover of antibiotic in China due to poor treatment efficiency of sewage, surface runoff, and direct discharge from livestock industries (Chen et al., 2018).

In Thailand, Oxytetracycline and Enrofloxacin were detected higher concentration approximately 3050 and 1590ng/L in water at Tha Chin River which determined as the influence from antibiotic usage from tilapia cage farming (Rico et al., 2014). In addition, six canals at Bangkok city, Thailand, were found high amount of Ciprofloxacin and Sulfathiazole ranging from 9-194ng/L and 29-107ng/L, respectively (Tewari, Jindal, Kho, Eo, & Choi, 2013). It also reported that, Ciprofloxacin concentration found in the domestic wastewater treatment plants mainly in return sludge, and aeration unit. Sulfamethoxazole predominantly is more difficult to degrade, and mostly shows high concentrations in effluent (Sinthuchai et al., 2021). Chan., et al has investigated the antibiotics in pig feed and drinking water which excreted with manure and wastewater. Tetracycline, macrolides, aminoglycosides, quinolones, sulfonamides, pleurmutilin and florfenicol classes have found as the main ingredients in feed and drinking water. It was also formed and settle as a sludge up to 79.5$\mu$g/L and 24.2mg/kg in pond during wastewater treatment (Chan, Chiemchaisri, Chiemchaisri, Boonsoongnern, & Tulayakul, 2022). Jansomboon et al., has reported that antibiotic residual also found in the *Pangasius catfish* product which imported to Thailand. As mentioned, antibiotic play a crucial role in promoting the livestock farming especially in fish farming. As the results, antibiotic pollutant has not found only in the water but also in the fish species by fish incomplete digestion. Jansomboon et al., has found that Enrofloxacin detected in *Pangasius catfish* in a range of 6.4 — 11.3 $\mu$g/kg which were higher than the recommendation of the US food and drug administration (US-FDA) level (Jansomboon, Boontanon, Boontanon, Liamleam, & Polprasert). In particular, the occurrence of the antibiotics possibly correlated with the population density for human antibiotic and relatively high amount for veterinary drug in agriculture or livestock area. There are still lack of information about the occurrence, distribution, and fate of antibiotic in surface water from several countries including South Korea, Cambodia, Laos, Myanmar and Timor-Lests (Anh et al., 2021).In Thailand, Oxytetracycline and Enrofloxacin were detected higher concentration approximately 3050 and 1590ng/L in water at Tha Chin River which determined as the influence from antibiotic usage from tilapia cage farming (Rico et al., 2014). In addition, six canals at Bangkok city, Thailand, were found high amount of Ciprofloxacin and Sulfathiazole ranging from 9-194ng/L and 29-107ng/L, respectively (Tewari et al., 2013). It also reported that, Ciprofloxacin concentration found in the domestic wastewater treatment plants mainly in return sludge, and aeration unit. Sulfamethoxazole predominantly is more difficult to degrade, and mostly shows high concentrations in effluent (Sinthuchai et al., 2021). Chan., et al has investigated the antibiotics in pig feed and drinking water which excreted with manure and wastewater. Tetracycline, macrolides, aminoglycosides, quinolones, sulfonamides, pleurmutilin and florfenicol classes have found as the main ingredients in feed and drinking water. It was also formed and settle as a sludge up to 79.5$\mu$g/L and 24.2mg/kg in pond during wastewater treatment (Chan et al., 2022). Jansomboon et al., has reported that antibiotic residual also found in the *Pangasius catfish* product which imported to Thailand. As mentioned, antibiotic play a crucial role in promoting the livestock farming especially in fish farming. As the results, antibiotic pollutant has not found only in the water but also in the fish species by fish incomplete digestion. Jansomboon et al., has found that Enrofloxacin detected in *Pangasius catfish* in a range of 6.4 — 11.3 $\mu$g/kg which were higher than the recommendation of the US food and drug administration (US-FDA) level (Jansomboon et al.). In particular, the occurrence of the antibiotics possibly correlated with the population density for human antibiotic and relatively high amount for veterinary drug in agriculture or livestock area. There are still lack of information about the occurrence, distribution, and fate of antibiotic in surface water from several countries including South Korea, Cambodia, Laos, Myanmar and Timor-Lests (Anh et al., 2021).

## 2.6 Adsorption of pollutant by using MXene material

Antibiotic effluents are notorious for being difficult to eliminate. Some evidence has been published in the last decade that antibiotic residue has been found in surface water, groundwater, and drinking water (Oulton et al., 2010). For eliminating antibiotics, several water treatment procedures such as biological treatment, filtration, coagulation, flocculation, sedimentation, adsorption, and solvent extraction have been investigated (Watkinson et al., 2007). Adsorption is seen to be the most promising of these since it is simple, cost-effective, and economical. There are several studies which used MXene to work on adsorption of antibiotic drug and other pollutant.Antibiotic effluents are notorious for being difficult to eliminate. Some evidence has been published in the last decade that antibiotic residue has been found in surface water, groundwater, and drinking water (Oulton et al., 2010). For eliminating antibiotics, several water treatment procedures such as biological treatment, filtration, coagulation, flocculation, sedimentation, adsorption, and solvent extraction have been investigated (Watkinson et al., 2007). Adsorption is seen to be the most promising of these since it is simple, cost-effective, and economical. There are several studies which used MXene to work on adsorption of antibiotic drug and other pollutant.

Another group of study was also conducted on the adsorption of selected pharmaceutical compounds (amitriptyline, verapamil, carbamazepine, ibuprofen, diclofenac). The study was chosen commercially $Ti_3C_2T_x$ for receiving universal results. The high potential of the adsorption capacity was due to the electrostatic interaction between the negatively charge of the MXene and the positively charge of the contamination of drug. To increase the adsorption efficiency, sonication of MXene at different frequency for increasing the high surface area and active site was also observed. The maximum of the adsorption was 241 mg $g^{-1}$ for sonicated $Ti_3C_2T_x$ MXene with the AMT adsorbate (Ghani et al., 2021).The maximum of the adsorption was 241 mg $g^{-1}$ for sonicated $Ti_3C_2T_x$ MXene with the AMT adsorbate (Ghani et al., 2021).

Sukidpaneenid et al. (2023) has proved that MXene-$TiO_2$ has had multi-role of adsorbent and photocatalyst for removal of antibiotic drug contamination from water. MXene was synthesized via LiF/HCl etching and further a rapid microwave hydrothermally composite in aqueous solution HCl to form MXene-$TiO_2$. In case of composite material, NaCl was included in the composite material since it was found that it could adsorb antibiotic well, where lithium content was removed by heat in microwave reactor with HCl and initiating form $Na^+$ and $TiO_2$ among the structure of MXene. The result found that the sodium intercalate in the MXene structure has a potential uptake the drug molecule through cation exchange. Furthermore, $Na^+$ could interfere the fastest growth of $TiO_2$ forming.

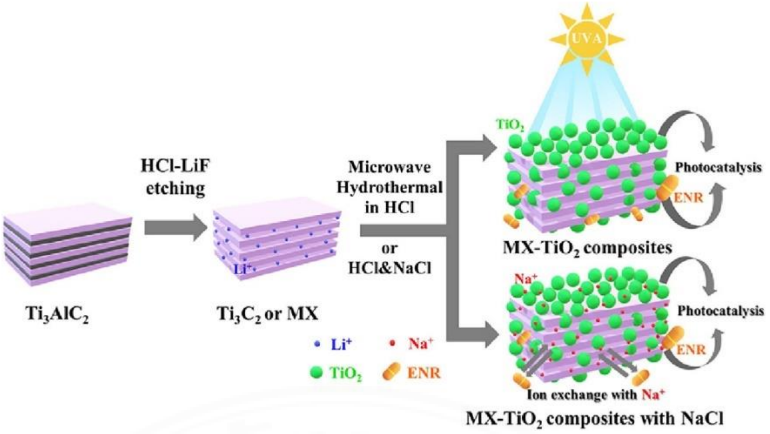

**Figure 2.11** Multi-function of MXene adsorbent composite with $TiO_2$ enhance the removal of ENR antibiotic (Sukidpaneenid et al., 2023). multi-function of MXene adsorbent composite with $TiO_2$ enhance the removal of ENR antibiotic (Sukidpaneenid et al., 2023).

Recently study has revealed on the enhancement of adsorption of Tetracycline by using ALK-MXene, mainly discussed on surface complexation. The synthesis MXene material was followed in the literature report (Q. Peng et al., 2014).(Q. Peng et al., 2014). Alkalization reaction was further synthesized after first step HF etching for intercalated $Na^+$ by using NaOH. In this study, MXene-rich hydroxyl surface intercalated with $Na^+$ was used to remove the antibiotic contaminant Tetracycline from wastewater. The study has indicated that it has slightly affect by the changing temperature of adsorption. However, it mainly effected by pH changing due to the protonation and deprotonation of the tetracycline molecule in various pH range. In addition, in the system of only TC adsorption, hydroxyl group on the surface of the ALK-MXene plays majority interaction with tetracycline during adsorption process as it can be seen by the XPS results of -OH peak at 531.23 eV move to lower direction of 530.95 eV. Author also revealed that before and after adsorption of tetracycline, material didn’t change the structure which confirmed by XRD and XPS results (Dao, Hao, Bi, Sun, & Huang, 2022a).Author also revealed that before and after adsorption of tetracycline, material didn’t change the structure which confirmed by XRD and XPS results (Dao et al., 2022a).

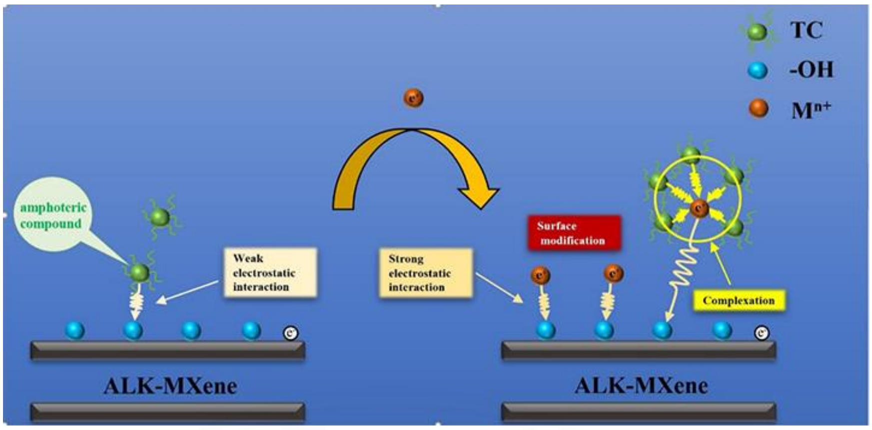

**Figure 2.12** Surface complexation of ALK-MXene for adsorption of tetracycline antibiotic (Dao, Hao, Bi, Sun, & Huang, 2022b)

A. Liu et al. (2020) has developed a laminated membrane for separate of pharmaceutical which polluted to water environment. The assembly of the titanium carbide shows good performance than most polymeric nanofiltration membranes. The separation mechanism is mainly size-selective, pH. This outstanding separation performance is enabled by the highly regular 2D structure, which introduces a new concept for designing sub nanochannels/nanochannels. This Ti3C2Tx membrane broadens the use of lamellar membranes in drug purification, sewage treatment, and medical wastewater treatment.

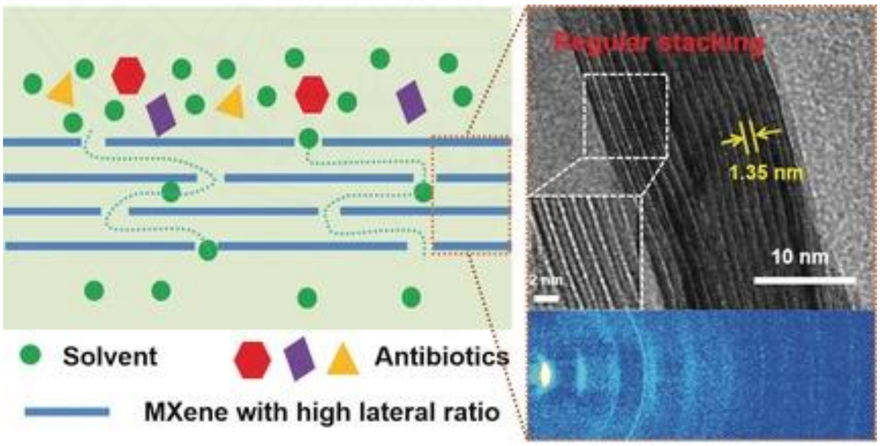

**Figure 2.13** Antibiotics separation with MXene membranes based

## 2.7 Adsorption mechanism

To eradicate contaminants in water, a considerable number of studies have been conducted on the adsorption behavior of nanomaterials, which have superior chemical and physical properties such as wide surface area, small size, and high stability when compared to typical bulk materials. Specifically, it is low cost compared to other technologies such as filtration, biological treatment, coagulation, flocculation, sedimentation solvent extraction (Watkinson et al., 2007).Specifically, it is low cost compared to other technologies such as filtration, biological treatment, coagulation, flocculation, sedimentation solvent extraction (Watkinson et al., 2007). Adsorption is known as mass transfer, which involves the accumulation of substances that interact at two phases, such as liquid−liquid, liquid−solid, gas−solid, and gas−liquid. It is considered as a complex phenomenon that is primarily determined by the surface chemistry or nature of the sorbent, sorbate, and the system circumstances in between the two phases. Thereafter, it finally adhered at the adsorbent surface. The adsorbate is the substance being adsorbed, and the adsorbing material is known as the adsorbent. The effect of adsorption can vary depending on the initial loading of adsorbent, pH value, time interaction, temperature and the nature of the adsorbent and adsorbate. The amount of adsorption of molecule at equilibrium phase can be determined using the given formular:

$$q_t = \frac{(C_0 - C_t) \times V}{m} \tag{2.1}$$

Where:

$q_t$ : adsorption amount at time t (mg/g)

V : volume of solution (L)

m : mass of adsorbents (g)

$C_0$ : initial concentration of contaminant (mg/L)

$C_t$ : concentration of contaminant at time t (mg/L)

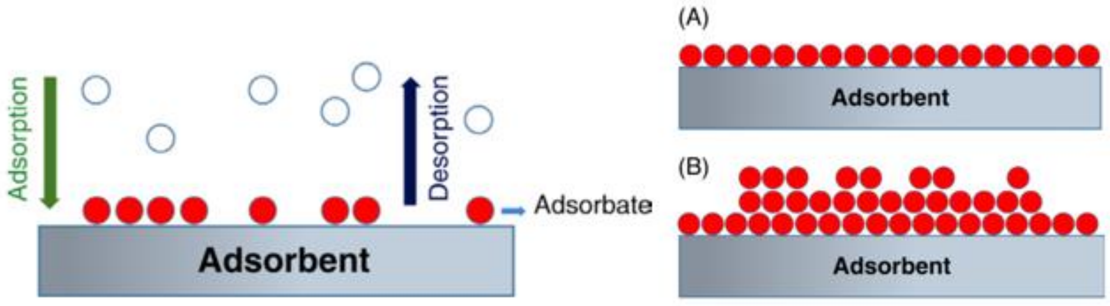

**Figure 2.14** The illustration of the adsorption on the surface of the adsorbent.

Most of the industrial adsorbents fall into three different types

1. Oxygen-containing material: Basically, hydrophilicity and polar compound
2. Carbon based material: Basically, non-polar
3. Polymer based material: Typically, polar and non-polar depending on the functional group in the polymer matrix

**Table 2.2** Comparison between physical adsorption and chemical adsorption

| Chemical adsorption | Physical adsorption |
|---|---|
| • Covalent bond formed between the surface and the adsorbed material<br>• Slow<br>• High temperature is needed<br>• Activated energy is required<br>• Monolayer are formed<br>• Irreversible | • Electrostatic and Van de Waal force are involved<br>• Fast<br>• Occurs at low temperature and decrease with increase temperature<br>• Activated energy is not required<br>• Multilayers are form<br>• Reversible |

### 2.7.1 Adsorption kinetic

The aim of the adsorption kinetic implementation is to comprehend the mechanism of adsorption of the capacities of molecules to be adsorbed. In the adsorption system, adsorption models such as the pseudo-first order model, the pseudo-second order model, and the intraparticle diffusion model are widely use in the adsorption system. Because of the kinetic model could support the understanding of the adsorption mechanism.

1) Pseudo-first order kinetics model (PFO)

PFO denoted the kinetic process of the liquid-solid phase adsorption in which reaction rate is limited by the individual mechanism and all binding or adsorption sites are time dependent. The pseudo-first order model was developed by Lagergren. The main assumption of kinetic model is the following:

- Absorption occurs only at the specific binding site, which localized on the surface adsorbent.
- Adsorption energy does not depend on the formation of a layer on adsorbent surface.
- No interaction occurs between the adsorbed molecules on the surface of the adsorbent.

2) Pseudo-second order model (PSO)

Two assumptions underlying the pseudo-second order model. The first assumption is that two reactions will occur simultaneously during the adsorption process, and the second assumption is that one of the reactions will occur at a faster rate and will reach equilibrium quickly, while the other reaction will occur at a slower rate and will continue until the adsorption process is complete.

### 2.7.2 Adsorption isotherm

Adsorption isotherms explain the distribution of adsorbed molecules from the liquid phase to the surface of the solid phase at equilibrium. Adsorption isotherms are the equilibrium relationships that characterize the interaction of adsorbate ions with the adsorbent's surface. Adsorption isotherms are graphs or curves created at a constant pH and temperature that are used to study the process of adsorption (Foo & Hameed, 2010).Adsorption isotherms are graphs or curves created at a constant pH and temperature that are used to study the process of adsorption (Foo & Hameed, 2010). Adsorption equilibrium happens when an adsorbate in any phase comes into sufficient contact with the adsorbent. The Langmuir, Freundlich, and Elovich isotherms are all commonly employed in adsorption processes. Adsorption processes can occur in either a homogeneous or heterogeneous layer, according to the Langmuir and Freundlich theory of adsorption. It is determined by the number of active sites on the adsorbents' surface (Foo & Hameed, 2010).It is determined by the number of active sites on the adsorbents' surface (Foo & Hameed, 2010).

1. Langmuir adsorption isotherm

The Langmuir isotherm assumes that the adsorbent's surface has a fixed number of adsorption sites of identical size and shape. It also implies that each unoccupied site may hold one molecule and that a consistent quantity of heat is generated during the process. For these reasons, the Langmuir isotherm is also known as the homogeneous adsorption isotherm. This isotherm best depicts the chemisorption type of adsorption. The adsorbed and free molecules are in dynamic equilibrium with one another. This indicates that the adsorption and desorption processes are in balance throughout the mechanism. The most fundamental assumption of this isotherm model is that adsorption results in a single layer of adsorbed molecules and that there is no adsorbate transmigration in the surface plane. The intermolecular attractive force between molecules reduces as the distance between them increasing, according to the Langmuir isotherm concept. The following nonlinear equation is used to calculate the Langmuir adsorption parameters.

$$Q_e = \frac{Q_{\max} K C_e}{1 + K Q_e} \tag{2.2}$$

Where:

$Q_{max}$ : Langmuir constant indicating measures of monolayer adsorption capacity (mg/g)

K : Langmuir constant indicating adsorption rate (L/mg)

$C_e$ : equilibrium concentration (mg/L)

$Q_e$ : the amount of uptake per gram of the adsorbent at equilibrium (mg/g)

2. Freundlich adsorption isotherm

In contrast to the Langmuir isotherm model, which is limited to monolayer adsorption, the Freundlich isotherm model is applicable to multilayer adsorption and explains non-ideal and reversible adsorption. According to Foo and Hameed (2010), the adsorption mechanism produces a heterogeneous adsorbate layer rather than a homogenous monolayer. According to Foo and Hameed (2010), the adsorption mechanism produces a heterogeneous adsorbate layer rather than a homogenous monolayer. "The stronger binding sites are occupied first, and adsorption energy drops exponentially until the adsorption process completes," according to Freundlich isotherm theory. The following non-linear equation is used to calculate the parameters of the Freundlich adsorption isotherms.

$$Q_e = K_L (C_e)^{1/n} \tag{2.3}$$

Where:

$Q_e$ : amount of adsorbed per gram of the adsorbent at equilibrium (mg/g)

$K_L$ and n : Freundlich constants that indicate the adsorption capacity and intensity

$C_e$ : equilibrium concentration (mg/L)

# CHAPTER 3

# MATERIALS AND METHODS

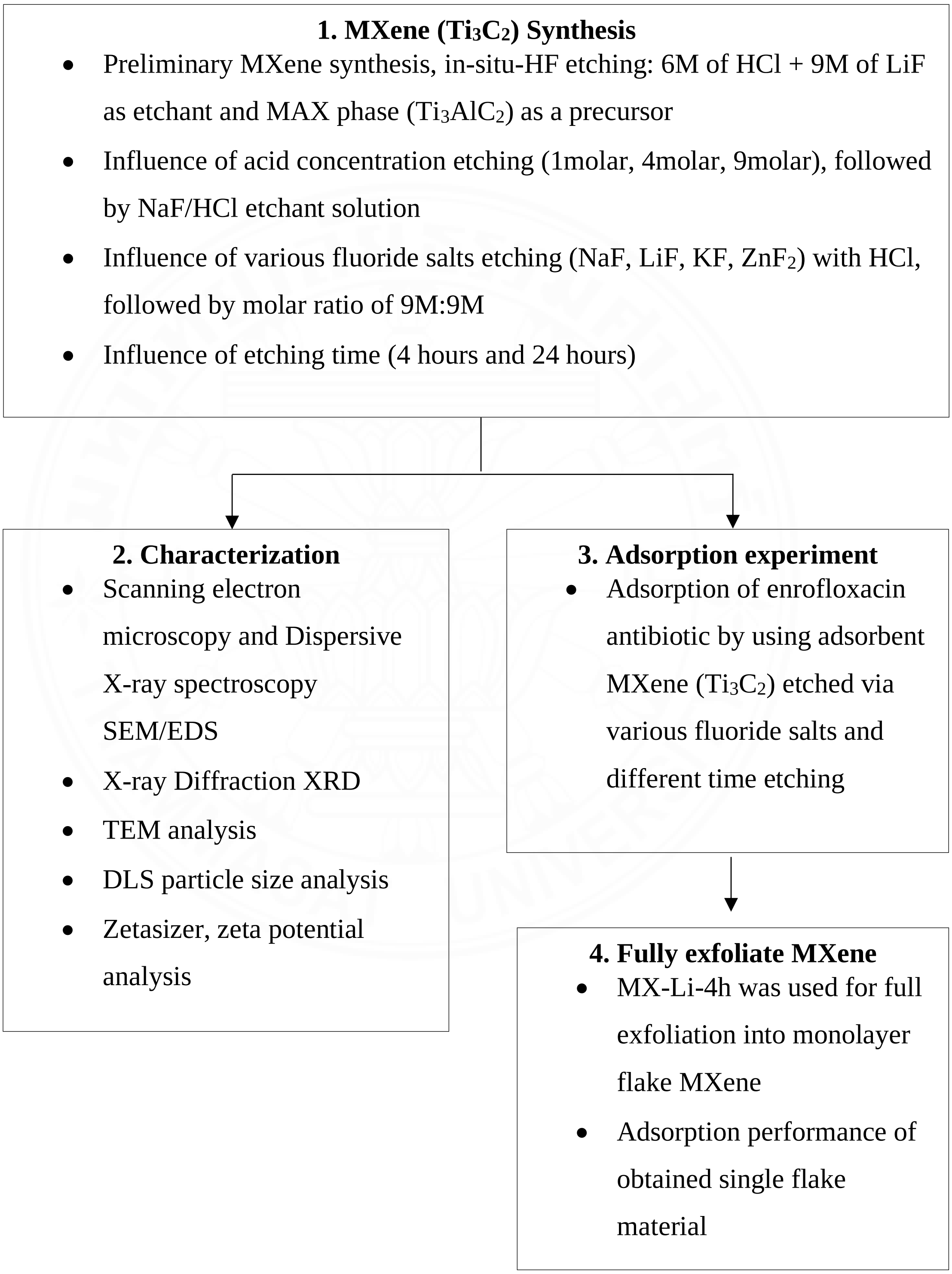

**1. MXene ($Ti_3C_2$) Synthesis**

- Preliminary MXene synthesis, in-situ-HF etching: 6M of HCl + 9M of LiF as etchant and MAX phase ($Ti_3AlC_2$) as a precursor
- Influence of acid concentration etching (1molar, 4molar, 9molar), followed by NaF/HCl etchant solution
- Influence of various fluoride salts etching (NaF, LiF, KF, $ZnF_2$) with HCl, followed by molar ratio of 9M:9M
- Influence of etching time (4 hours and 24 hours)

**2. Characterization**

- Scanning electron microscopy and Dispersive X-ray spectroscopy SEM/EDS
- X-ray Diffraction XRD
- TEM analysis
- DLS particle size analysis
- Zetasizer, zeta potential analysis

**3. Adsorption experiment**

- Adsorption of enrofloxacin antibiotic by using adsorbent MXene ($Ti_3C_2$) etched via various fluoride salts and different time etching

**4. Fully exfoliate MXene**

- MX-Li-4h was used for full exfoliation into monolayer flake MXene
- Adsorption performance of obtained single flake material

### 3.1 Materials

MAX phase ($Ti_3AlC_2$) was purchased from Luoyang Tongrun Info Technology Co., Ltd, China. Hydrochloric acid (HCl), lithium fluoride (LiF), and sodium chloride (NaCl) were purchased from Carlo Erba, Acros organics, and Loba Chemie, respectively. Sodium Fluoride (NaF), Potassium Fluoride (KF), Zinc Fluoride ($ZnF_2$), Sodium Hydroxide (NaOH), were purchased from Carlo Erba, KEMAUS, Alfa Aesar, Thermo Fisher Scientific, Carlo Erba, respectively. Enrofloxacin ($C_{19}H_{22}FN_3O_3$) was purchased from General drugs house Co., Ltd, Thailand.

### 3.2 MXene ($Ti_3C_2T_x$) Synthesis

### 3.2.1 Preliminary MXene ($Ti_3C_2T_x$) synthesis

In the preliminary synthesis, in-situ HF etching was used to avoid using highly hazardous compounds in the synthesis, and the synthesis technique was slightly modified from the previous report (Ghidiu et al., 2014a).(Ghidiu et al., 2014a). Lithium fluoride (LiF) and hydrochloric acid (HCl) were utilized as the etchant solution in this synthesis. 10mL of HCl (6M) was added with 2.33g of LiF (9M). The mixture was stirred for 20 minutes to dissolve the salts sufficiently. 1g of MAX phase ($Ti_3AlC_2$) was gently added to the mixture to prevent the exothermic reaction. The mixture was stirred at 50℃ for 24 hours. After that, the suspension was washed with DI water until pH $\geq 5$ by centrifugation (5000 rpm for 10 minutes for each cycle). The supernatant was discarded, and the bottom like-clay sediment was collected and dried for 12 hours in a vacuum oven at 60°C. In order to make comparison with the previous work by (Sukidpaneenid et al., 2023), MXene was also synthesized as described in that work, i.e. at lower fluoride salt concentration (2.5M of LiF). In brief, 6mol/L of HCl and 2.5mol/L of LiF were prepared. Temperature was maintained at 50℃ and reaction time was kept for 24 hours. In order to make comparison with the previous work by of (Sukidpaneenid et al., 2023), MXene material was also synthesized as described in that work, i.e. atin lower fluoride salt concentration etching (2.5M of LiF). In brief, 6mol/L of HCl and 2.5mol/L of LiF were prepared. Temperature was maintained at 50℃ and reaction time was kept for 24 hours.

### 3.2.2 Influence of HCl acid etching of MXene ($Ti_3C_2T_x$) synthesis

In this typical synthesis, MXene ($Ti_3C_2T_x$) was synthesized by *in-situ* hydrochloric acid (HCl) and sodium fluoride salt (NaF). Various concentrations of HCl were used (1M, 4M and 9M) with the fixed concentration of the NaF (9M). 10mL of each HCl was used with the target concentration of fluoride salt (NaF) 9mol/L. The mixture was stirred for 20 minutes to sufficiently dissolve the salt. 1g of MAX phase ($Ti_3AlC_2$) was slowly added in the mixture to avoid the exothermic reaction. The suspension was was stirred at 50 ˚C for 24 h. During etching, each of the synthesis batch was also sampling at 4 hours for the study on the effect of the etching time.

Thereafter, MXene suspension was soaked in DI water and additional stirring for 3 hours to intercalate water molecules into the MXene sheet. In addition, in the form of acidic condition, hydronium $H_3O^+$ ion will undergo further ion exchange with the $Na^+$ cation. As a result, we could get simultaneously $Na^+$ intercalation during etching as well as $Na^+$ which benefit from defluorination of the NaF by-product. After incubation, the suspension was washed with DI water (5000 rpm for 10 minutes for each cycle). Washing step was performed until the pH reach approximately (pH 5-6). The pH monitoring in each washing cycle illustrate in APPENDIX A (Figure 1). After that, the sediment-like clay was separate and vacuum-dried for 12 hours. In this investigation synthesis, etching time and acid concentration etching were examined.

### 3.2.3 Influence of other fluoride salts (LiF, NaF, $KF_2$, $ZnF_2$) etching of MXene ($Ti_3C_2T_x$)

In this synthesis part, the study on the effect on different fluoride salt was investigated by taking suitable acid etching conditions from the previous section (**3.2.2**), namely 9M HCl, 9M salts, 4h etching, 3h water incubation and wash until pH >5. The effect of fluoride was chosen LiF, NaF, KF, $ZnF_2$, as an etchant with hydrochloric acid (9mol/L). The synthesis step was followed from section **3.2.2** which consisted of chemical wet etching, water incubation, washing, and drying. In brief, 1g of MAX phase was immersed in 10 mL of hydrochloric acid (9mol/L) with the target concentration of fluoride salt 9mol/L. After that, the suspension was incubated in pure water for 3 hours before further washing until pH reaches 5-6 (centrifugation at

5000rpm for 10 minutes each cycle). Finally, MXene sediment was then dry in oven for overnight and ground with mortar to obtain fine particles.

### 3.2.4 Further exfoliation of MXene

For the fully exfoliation of MXene, Li-$Ti_3C_2$ etched at 4 hours was chosen to be further delaminated into a few layers or a monolayer MXene since the solvated $Li^+$ intercalated MXene possessed larger interlayer distance than other cations. In detail, 50 mg of multilayer-Li-$Ti_3C_2$ 4h was soaked in three different dispersions such as DI water, ethanol, and lithium chloride (9mol/L), separately. Each suspension was sonicated for 20 min (1min on and 30 sec off) using probe ultrasonication. After sonication, the well disperse suspension was centrifugated at 6,000 rpm to separate the sediment and the supernatant. The supernatant of each suspension was checked the absorbance spectra by UV-Vis spectrophotometer and the sediment part were also collected and drying in vacuum oven 60℃ . Thereafter, powder sample was collected and kept for further experiment.

Another exfoliation technique also prepares by using Tetrabutylammonium hydroxide (TBAOH) which is a large organics molecule, frequently used in the intercalation of MXene ($Ti_3C_2$), and further handshaking for delamination into few-layer or single layer. In brief, 200mg of MLs MXene (Li-$Ti_3C_2$ 4h) was soak in 40% v/v of TBAOH 50mL, for overnight. The obtained solution was then centrifuged to separate the unreacted intercalant. Then, it was washed with DI water for 3-5 cycles. The sediment like-clay was then dry in vacuum oven 60℃ and kept for further experiment.

## 3.3 Characterization

Scanning electron microscopy (SEM) was used to characterize the surface morphology of the MAX phase and produced MXene. Elemental composition of the materials was identified by the energy dispersive X-ray spectrometry (EDX). The condition of the SEM consists of 5kV of voltage, 10 unit of spot intensity. The condition of EDS was performed at 15kV of voltage and 20 units of spot intensity. The element qualitative of C, Al, Ti, F, O, Zn, Na and K were analyzed. Transmission Electron Microscopy (TEM, JEOL JEM-2100 plus, Japan) was used to characterize the monolayer of the MXene using accelerated voltage of 200 kV. In brief, 40mg of MXene sample was placed in DI water (40mL) and probe sonication for 20 minutes in pulse mode (1 min on, 30 sec off), using 60% amplitude before the TEM analysis. The sample solution was then dropped onto copper grid and left for drying at room temperature for 24h. In case of multilayer MXene ($Ti_3C_2T_x$), 40 mg of MXene powder was placed in DI water (40mL) and overnight before TEM analysis. XRD patterns were collected by (Bruker AXS Model D8 Advance, Germany), using Cu Kα (1.5406 Å) and operated at 40 kV and 40 mA. The range of 2θ was scanned from 5° to 70° with increment 0.02 degree/ and 0.2 second/step. To obtain the interplane distance, d-spacing of was calculated by Bragg's equation.

In case of multilayer MXene ($Ti_3C_2T_x$), 40 mg of MXene powder was placed in DI water (40mL) and stirring overnight before TEM analysis. XRD patterns were collected by power diffraction (Bruker AXS Model D8 Advance, Germany), using Cu Kα (1.5406 Å) and operated at 40 kV and 40 mA. The range of 2θ was scanned from 5° to 70° with increment 0.02 degree/stem and 0.2 second/step. To obtain the interplane distance, d-spacing of materials was calculated by Bragg's equation.

$$n\lambda = 2d\sin\theta \tag{3.1}$$

Where λ is the wavelength of the incident X-ray (1.5418Å ), $\theta$ is peak position, $n$ is order of diffraction and $d$ is d-spacing Å.

Surface charge chemistry and the hydrodynamic particle size and size's distribution were measured using Zetasizer Nano ZSs, Melvern. The concentration of NaCl (0.01M) is used as the supporting suspension electrolyte media to neutralization of the charge of MXene material. 30mg of MXene was dispersed in 30 mL of 0.01M NaCl. In order to avoid the aggregation of MXene particles, 1 minute of probe sonication with, using 60% amplitude was applied before analysis. A refractive index, RI=2.15, and the absorption 0.900 was used in this measurement with the fast response of sample equilibrium at 10 sec. For In case of the variation of zeta potential as a function of pH, 0.1M of hydrochloric acid (HCl) and 0.1M of sodium hydroxide (NaOH) were used to adjust the pH change in the range of 2–10. The suspension was then analyzed for the zeta potential using Zetasizer Nano ZSs. The zeta potential of $Ti_3C_2T_x$ nanoflake were measured at a concentration 1 mg $mL^{-1}$. The experiment was performed in monomodal mode for the fast measurement and to avoid possible aggregation of the MXene nanoflake aggregation.

### 3.4 Adsorption capability and adsorption kinetic

All experiments were conducted in the dark to prevent the of enrofloxacin or any of the material photocatalytic activity. 150 mg of MXene was dispersed into 150 mL of fresh enrofloxacin at an initial concentration 10 mg/L. Multi-layer MXene including (MX-Li, MX-Na, MX-K, MX-Zn) which were etched 4h and 24h were utilized. The suspension was stirred in a dark condition for 10 hours. The sample was withdrawn at specific time intervals between (10mins to 600mins). The withdrawal suspension was then filtered through 0.22$\mu$m of nyron syringe before analyzing the absorbance by UV-Vis spectrophotometer at 272nm (PerkinElmer, Lambda 650).

In case of few-layer or monolayer MX, the MXene sample obtained from further exfoliation in follow sonication and intercalation were used. sMX/DI, sMX/Et, sMX/LiCl and MX/TBAOH were used in the ENR adsorption follow the above experiment step. In brief, adsorbent was weight 100 mg and disperse in 100mL of fresh enrofloxacin. The suspension was incubation in the dark and sample was collected at specific time (10min-350min) for checking absorbance via UV-Vis spectrophotometer. After ENR adsorption experiment, the suspension after filtering was kept for further analysis of Li cation leaching upon adsorption experiment.

For ENR adsorption by using multilayer and monolayer MXene under dark conditions, adsorption kinetics is fitted to the pseudo-first order and the pseudo-second order model to obtain the rate parameters (Eq.2 and Eq.3) whereas the adsorption capacity of MXene is calculated by (Eq.3).

In addition, another set of experiment for the adsorption capacity at different pH was also conducted with the set initial concentration of ENR 10mg/L. Monolayer MXene (sMX/DI) was selected only to use in this experiment. ENR solution was adjusted the pH value ranging from pH 2 until pH 10. The MXene loading MXene adsorbate was 1g/L and the suspension was shaken in the dark condition for 24 hours to reach the equilibrium adsorption. Zetapotential of monolayer MXene (sMX/DI) was also measured in the same range pH of the adsorption experiment.

$$q_t = q_e(1-e^{-k_1 t}) \tag{3.2}$$

$$q_t = \frac{q_e k_2 t}{(1+q_e k_2 t)} \tag{3.3}$$

Where $q_e$ (mg/g) and qt (mg/g) are the amount of antibiotic adsorbed on the materials at equilibrium and at time, respectively, $k_1$ ($\text{min}^{-1}$) and $k_2$ (g/mg.min) at the pseudo-first order and pseudo-second order rate constants, t (min) is time.

$$q_e = \frac{(C_0 - C_e)\times V}{m} \tag{3.4}$$

Where $q_e$ is the adsorption capacity (mg/g), $C_0$ is the initial concentration, $C_e$ is the concentration at equilibrium (mg/L), m is mass of adsorbent (g), V is the volume of solution containing solute (L).

### 3.4.1 Li cation leaching upon sMX adsorption

In case of Li cation leaching, the solution which obtained from sMX adsorption experiment was further analysis by using inductively couple plasma (ICP) spectroscopy (Optima 8000 ICP-OES, PerkinElmer, USA). In brief, ENR solution after sMX adsorption, was diluted with DI water into low concentration. The dilution factor was recorded and the obtained concentration from ICP-OES was substituted into actual concentration.

The lithium content before and after adsorption in the sample were also analyzed. For analyzing Li cation content in solid sample. MX solid sample were sonicated in DI water using probe sonication for 10 minutes before ICP measurement.

$$Li_{(mg/g)} = \frac{(C_{Li} \times DF \times V)}{m} \tag{3.5}$$

where C is the concentration of lithium obtained from ICP measurement (ppm), DF is dilution factor, V is volume (L), and m is sample weight in (g)

### 3.5 Adsorption isotherm

Adsorption isotherm was conduct by using known concentration of ENR solution. A stock concentration was prepared and dilute to desired concentration as mentioned in the Table 3.1 The mass loading of adsorbate utilized in the ENR solution were maintained at 1 mg mL$^{-1}$. The adsorption capacity time was set to 24 hours to get equilibrium adsorption performance. An initial ENR solution was carried out at pH 5 and the incubation was performed at ambient temperature. Langmuir isotherm and Freundlich isotherm was conducted to examine the maximum adsorption capacity. The equation of the isotherm describe as below:

Langmuir Isotherm Equation

$$Q_e = \frac{Q_{\max} K C_e}{1 + K Q_e} \tag{3.6}$$

Freundlich Isotherm Equation

$$Q_e = K_d (C_e)^{1/n} \tag{3.7}$$

where Ce and Qe describe the concentration and adsorption capacity at equilibrium time, respectively, $Q_{max}$ is the maximum adsorption capacity. $K_d$ is the distribution of coefficient from Freundlich isotherm, and K is Langmuir constant representing of energy of adsorption.

**Table 3.1** Condition of adsorption isotherm parameters

| Initial Concentration $[C_0]_{ENR}$ | Mass adsorbate (mg) | Volume (mL) | pH |
|---|---|---|---|
| 10 ppm | 20.00 | 20 mL | 5.06 |
| 20 ppm | 19.60 | 20 mL | 5.09 |
| 30 ppm | 19.90 | 20 mL | 5.04 |
| 40 ppm | 20.0 | 20 mL | 5.08 |
| 50 ppm | 20.30 | 20 mL | 5.06 |
| 60 ppm | 20.80 | 20 mL | 5.04 |
| 80 ppm | 19.90 | 20 mL | 5.01 |
| 100 ppm | 20.90 | 20 mL | 5.07 |
| 150 ppm | 20.20 | 20 mL | 5.01 |

# CHAPTER 4
# RESULTS AND DISCUSSION

## 4.1 Preliminary results of MXene synthesis

### 4.1.1 Sample characterization of $Ti_3C_2T_x$ (MX)

The exfoliation of the Al element from MAX phase is an important part of the successfully synthesized MXene material. Instead of using direct hazardous HF etching, fluoride salt/acid etching which was commonly known as *in-situ* HF etching was introduced by (Naguib et al., 2012). However, the removal of aluminum from MAX phase differs in temperature, time, concentration of fluoride salt and acid. In addition, *in-situ* HF etching was one of the methods which reported simultaneously cation intercalation $Ti_3C_2T_x$. Instead of using direct hazardous HF etching, fluoride salt/acid etching which was commonly known as *in-situ* HF etching was introduced by (Naguib et al., 2012). However, the removal of aluminum from MAX phase differs in temperature, time, concentration of fluoride salt and acid. In addition, *in-situ* HF etching was one of the methods which reported simultaneously cation intercalation $Ti_3C_2T_x$. However, it depends on the concentration of etching agent (Alhabeb et al., 2017).(Alhabeb et al., 2017).

In this preliminary study, we used this approach to further understand the cation intercalated by using various fluoride salt etching with MAX phase precursor. The first preliminary synthesized of MXene was focused on different concentration of salt LiF-HCl etching. The synthesized was separated into two synthesis routes, lower salt concentration and higher salt concentration of LiF. The lower salt of LiF (2.5mol/L) etching was sonicated 1 minutes after completely washing followed previous study of Sukidpaneenid et al. (2023), while higher salt (9mol/L) etching did not require. For the acid solution, hydrochloric acid (6mol/L) was utilized.

From **Figure 4.1** Illustrate the schematic of in-situ HF etching method for synthesis of MLs MXene material. In the case of high LiF-HCl etchant condition, it was expected that the $Li^+$ intercalated $Ti_3C_2T_x$ clay interlayer and possibly delamination without sonication.

**Figure 4.1** Schematic illustration of the in-situ HF etching of the MXene (Ti3C2Tx) material.

Scanning electron microscope (SEM) images which is shown in **Figure 4.2** indicate the surface morphology of MAX phase and MXene synthesis material of 2.5LiF-$Ti_3C_2$ and 9LiF-$Ti_3C_2$. The exfoliation of the MXene ($Ti_3C_2$) in multilayer sheet was achieved. The accordion-like structure MXene multilayer was defined in both synthesis route. MXene sheet with lower lithium fluoride (2.5 LiF-$Ti_3C_2$), which followed previous synthesis method (Sukidpaneenid et al., 2023) as shown in **Figure 4.2c**, showed fewer layers packed due to the ultrasonication process, which attempts to delaminate the structure of MXene.

However, it could be observed that the obtained MXene were still packed and not completely separated into individual sheets yet. This could be due to the strong bonding between the MXene layers.

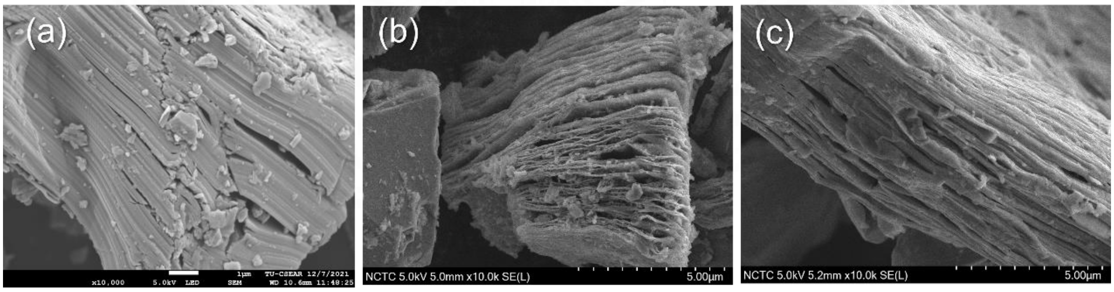

**Figure 4.2** SEM image surface morphology (a) the precursor MAX phase ($Ti_3AlC_2$), (b) 9M-LiF-$Ti_3C_2T_x$ (c) 2.5M-LiF-$Ti_3C_2T_x$ using 6M HCl: Condition; etched at 24 hours under 50℃.

According to Alhabeb et al. (2017), during etching $Li^+$ ions simultaneously intercalate into the $Ti_3C_2$ layers. Thus, $Li^+$ ions play an important role to increase the c-lattice parameter, causing the $Ti_3C_2$ MXene structure to delaminate easier. However, as shown in **Figure 4.2** illustrated above that the MXene particles were still packed in multi-sheets and still have accordion-like structure. According to Wu, Shang, Deng, Tao, and Yang (2020) reported that MXene nanosheet particularly were prone to aggregation and restack due to the Van de Waals force.

High concentration of fluoride salt etching (9MLiF-$Ti_3C_2T_x$) could not quite completely delaminate the MXene structure into monolayer MXene even the reactant LiF concentration was increased, although the Al was removed from the parents $Ti_3AlC_2$ MAX phase as was evident from the EDS measurement. The atomic % of Al element from each synthesis route has decreased from 12.6% in the original MAX phase to 2.26 and 2.19 % for sample etched by 2.5M LiF and 9M LiF, respectively.

**Table 4.1** Elemental composition analysis by EDS, summary of the sample MAX phase, MX (9LiF,6HCl), supernatant of MX(9LiF,6HCl) and MX (2.5MLiF, 6HCl)

| Materials | Elemental composition (Atomic percent) | | | | | |
|---|---|---|---|---|---|---|
| | Ti | Al | C | O | F | Cl |
| | At% | At% | At% | At% | At% | At% |
| MAX phase | 48.55 | 12.55 | 38.47 | - | - | - |
| MX (9LiF, 6HCl) | 23.03 | 3.0 | 18.06 | 11.07 | 43.82 | 1.02 |
| MX (2.5LiF,6HCl) | 36.82 | 2.26 | 23.24 | 20.72 | 15.01 | 1.96 |
| MX supernatant (9LiF, 6HCl) | 25.02 | 0.66 | 9.97 | 17.32 | 45.60 | 25.02 |

The selective removal of Al element can be confirmed by the disappearance of the Ti3AlC2 peaks in the XRD pattern. The X-ray diffractograms of representative samples are shown in Figure 4. 3 After etching with LiF/HCl, the characteristic diffraction peaks of the Ti3AlC2 at 19.15° was disappeared.

Meanwhile, the (002) peak at 9.75° of MX-LiF has become broaden and shifted to lower angle from 9.75° to 6.48°, indicating the Ti-Al bond was broken and Ti3C2 was formed (Naguib et al., 2011a). Furthermore, d-spacing value indicates the expanding of inter-space in-between MXene structure, causing by simultaneous cation intercalation of Li+.

As a results with this synthesis, the peaks of Ti3AlC2 still exist at 38.33°. However, the peaks at 38.33° and 45° possibly could be assigned to that of the LiF, which came from the incomplete washing and that some of LiF remained in the sample. Besides, sharp peaks at 36.69° and 44.97° were assigned to TiC impurity frequently found containing in the MAX phase due to its preparation (Aiguo Zhou, Wang, & Hunag, 2003).

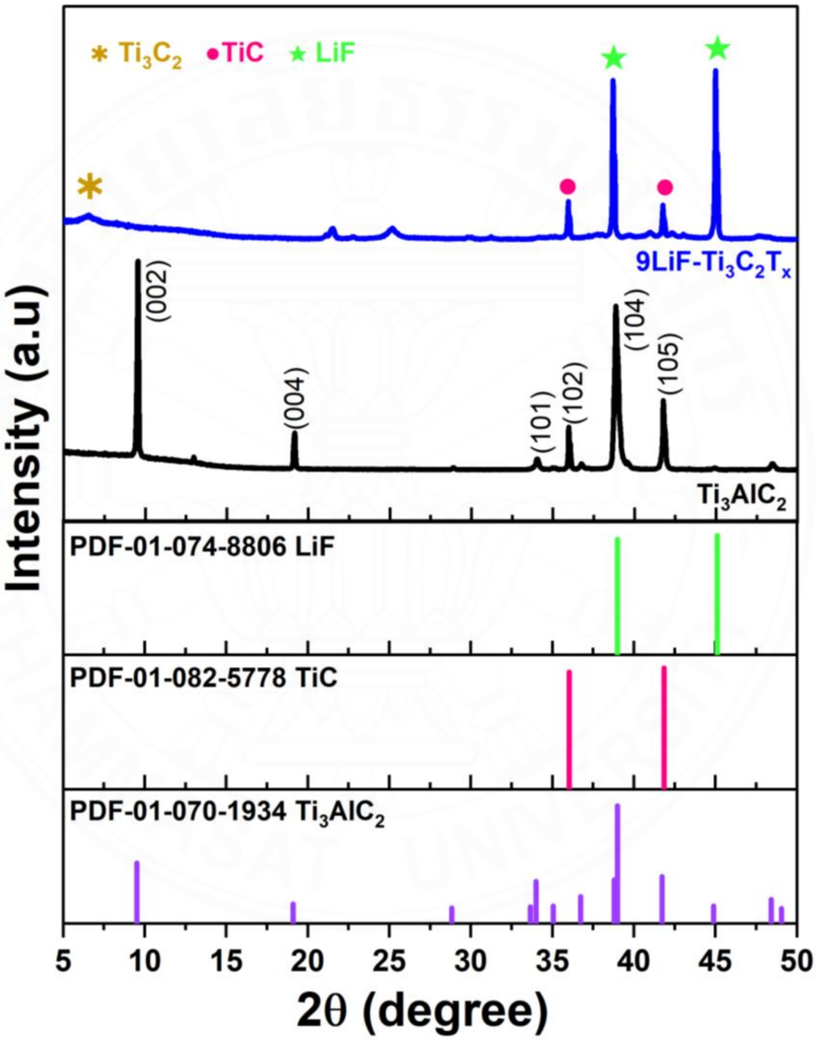

**Figure 4. 3** XRD patterns of MAX phase precursor and MXene synthesis via 6M HCl, 9M LiF etchant, 24h

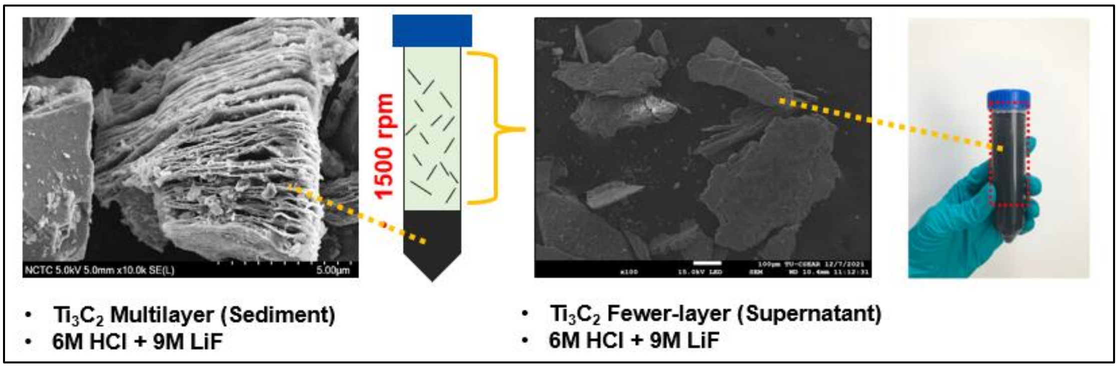

**Figure 4.4** SEM images of $Ti_3C_2$ synthesis via 6M HCl, 9M LiF by centrifugation separation at lower speed (1500rpm).

It is interesting to characterize MXene in the supernatant, which was not settled by centrifuge during the washing step. In this part, the 9MLiF-$Ti_3C_2T_x$ was centrifuged at intermediate speed of 1,500 rpm in the first washing cycle, for collecting the smaller fraction of particles dispersed in the supernatant.

The SEM image in Figure 4.4 showed fewer layer of MXene (Ti3C2Tx) obtained in the supernatant. High concentration of fluoride salt at 9M system could lead thin sheets of MXene (Ti3C2Tx), caused by the simultaneous intercalation of Li+ cation while Al was etched away by the in-situ generated HF. As a results, a few-layer and multi-layer MXene was achieved in the supernatant, while multilayer MXene is fractionated in the centrifuge sediment (Lipatov et al., 2016b). It was suggested that small intercalant ions were inserted between layers in the multilayer MXene, expanding the inter-layer space, and aiding the delamination of the packed MXene into a monolayer, or a few layer MXene.

From this preliminary synthesis we can assume that MX can be more exfoliate well in high concentration LiF, which causes the layer-structure to be more expanding. This could be useful for further delamination as some of the fewer layer MXene fraction can be obtained via fractionation centrifugation at intermediate speed. Acid etching concentration also a factor that can increase the speed of etching since high amount of acid/salts etchant combination produce HF to remove Al element out from MAX phase.

## 4.2 The study on $Ti_3C_2T_x$ (MX) synthesis via various fluoride salts etching

To further understand the influence of the cation caused MXene layer to be open, various kind of fluoride salts including sodium fluoride (NaF), zinc fluoride ($ZnF_2$), lithium fluoride (LiF), and potassium fluoride (KF) were utilized.

In this part, different concentrations of hydrochloric acid (HCl) were varied for faster etching of Al element from MAX phase. Sodium fluoride (NaF) was chosen to study on the effect of the (HCl) etching and the concentration of NaF was set to be 9M.

### 4.2.1 Effects of HCl concentration and etching time using NaF

To further clarify how the MAX phase was etched as a function of HCl concentrations and time in combination with NaF (9M). The X-Ray diffraction patterns of samples etched at different HCl concentrations and times are shown in **Figure 4. 5**.

In 1M and 4M HCl, the results of XRD shows that the peak of Ti3AlC2 still remained, while at 9M the peaks of Ti3AlC2 has disappeared. This is clear evidence that lower concentration of hydrochloric acid could not etch the Al element due to less amount of H+ and F- generated in the in-situ etching system. When the HCl concentration was increased to 9M, XRD pattern revealed that the characteristic peak (004) and (104) of Ti3AlC2 were completely removed after in-situ HF etching at 4 hours and 24 hours for the sample that was etched through 9M HCl and 9M NaF.

For the successfully etched sample, the typical broadening and downshift of (002) peak to the lower angle indicates the material's larger interlayer space, which exfoliated the Al element out and was replaced by intercalant Na+ cation and water molecule among MXene structure.

According to Bragg equation ($2d\sin\theta = n\lambda$), from 2θ of 7.08° and 7.07°, d-spacing of the material calculated to be 12.49Å and 12.50 Å, respectively. This result is similar to the previous studies which used direct HF etching followed with NaOH to from $Na^+$ intercalation in-between MXene structure (Ghani et al., 2021). In addition, d-spacing results was also consistent matched to another study of etching from NaF-HCl which mentioned of using 40℃, producing successfully disappeared of MAX phase ($Ti_3AlC_2$) (F. Liu et al., 2017).

Noticeably, the (002) peak of MXene strongly appeared at 4 hours etching and became weaker after extending etching until 24 hours, emphasizing the amount of simultaneously cation intercalation, causing the accordion-like structure to be more opening and expanding.

Based on the results, two conclusions can be drawn for the fabrication of MXene that concentration of HCl and time were important factors influencing etching of MXene material. The higher HCl concentrations the faster MXene produced.

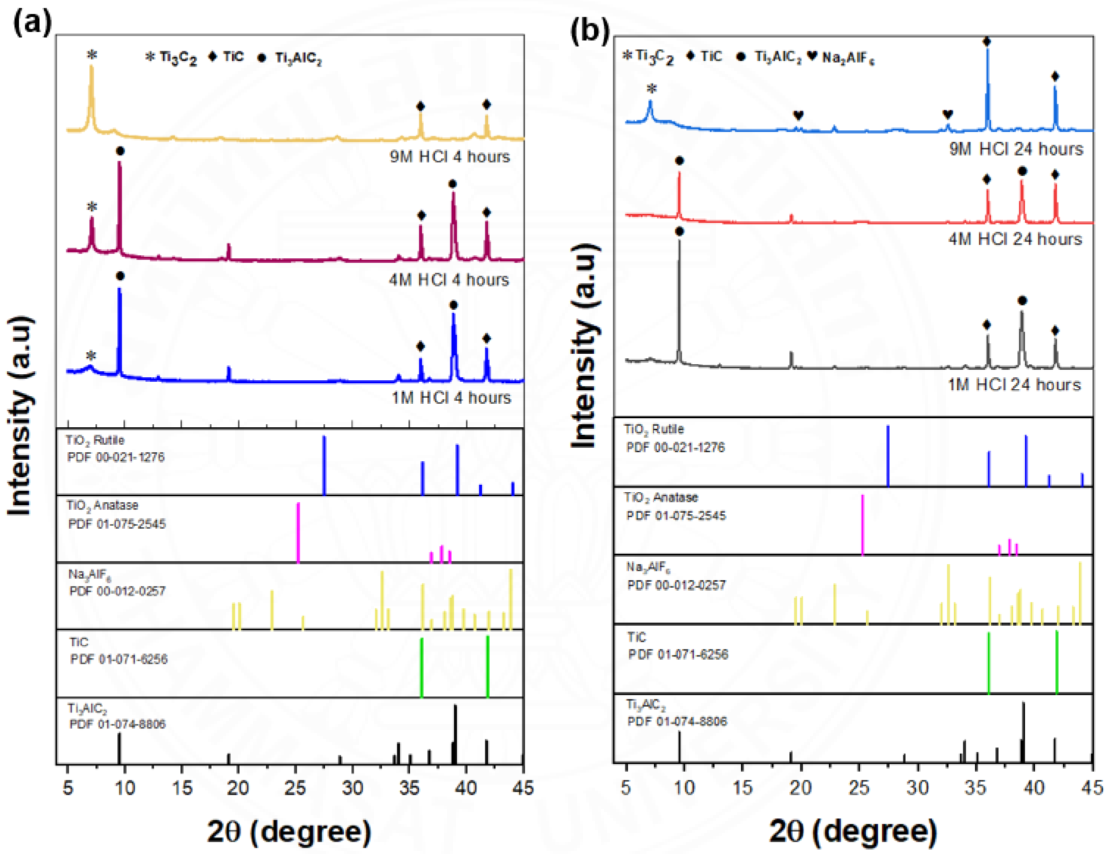

**Figure 4. 5** XRD patterns of $Ti_3C_2$ after etching at various concentrations of HCl for 4h (left panel), and 24h (right panel) in combination with 9M NaF. It can be seen that in both 4h and 24h at 1M and 4M HCl, MAX phase still remains. However, when HCl was increased to 9M, the MAX phase was almost completely removed. The MXene peak at 7.07 deg also appears higher for 4h compared to that of 24h.

### 4.2.2 Effects of different fluoride salts on exfoliation of MXene

As per mentioned in above section, high concentration of 9M HCl, can transform MAX phase into layer-structure MXene faster. In this part, various kind of fluoride salts is utilized to study on the effect of fluoride salts etching. Specifically, XRD diffraction peak will examine the phase change of each sample. The position of the (002) peak which is inversely proportion to the d-spacing was compared. LiF, NaF, KF, and $ZnF_2$, NaF and KF were used at 9M concentration along with 9M of HCl. Reaction of each synthesis was set at 4 hours and 24 hours.

From the XRD measurement, MXene ($Ti_3C_2T_x$) can be effectively exfoliated by *in-situ* HF etching solution at 4 hours for all conditions. The XRD was used to indicate the interlayer spacing between MX nanosheets which were intercalated by different cation species along with the co-intercalated water molecule (Lukatskaya Maria et al., 2013). The peak at 9.5 can be used to indicate the completeness of Al removal. For successful etching, the peak at 9.5° will be shifted to lower angle. Etching in LiF, there were still the diffraction peak at 9.5 of the MAX phases in the product. The d-spacing of each material etched at 4h was calculated to be 13.17 Å, 12.49 Å, 12.42 Å, 12.19 Å for sample etched by LiF, NaF, KF, $ZnF_2$, respectively. It is also interesting to compare also the 10%HF, in the previous study (Natu et al., 2022), the (002) peak for HF-MX was observed at $2\theta = 9°$ corresponding to the d-spacing of 9.7Å. (Lukatskaya Maria et al., 2013; Mashtalir et al., 2013).

For $Zn^{2+}$ has a charge of +2 and binds strongly with the MXene sheets resulting in slight contraction of the MXene sheet compared to other monovalent cations. It could also be observed that for $Zn^{2+}$, the longer etching times resulting in more contraction, possibly due to the better diffusion of Zn in between the layers, which caused the sheets to be more compacted.

**Table 4.2** D-spacing parameter obtained from XRD measurement along with solvated cation radius and cation radius.

| Etching solution | $2\theta$ (°) 4h | $2\theta$ (°) 24h | d-spacing 4h | d-spacing 24h | Solvated cation radius (Ramasubramanian, Reddy, Zaghib, Armand, & Ramakrishna, 2021) | Cation radius (Ramasubramanian et al., 2021) | Amount of Cation in MX from EDS 4h / 24h (at%) |
|---|---|---|---|---|---|---|---|
| LiF+HCl | 6.71 | 6.31 | 13.17 | 14.01 | 3.82 | 0.6 | ND by EDS |
| NaF+HCl | 7.08 | 7.07 | 12.49 | 12.50 | 3.58 | 0.95 | 2.83 / 7.30 |
| KF+HCl | 7.12 | 6.75 | 12.42 | 13.09 | 3.31 | 1.33 | 2.31 / 3.50 |
| $ZnF_2$+HCl | 7.25 | 7.39 | 12.19 | 11.96 | 4.3 | 0.74 | 0.44 / 0.69 |
| HF (Natu et al., 2022) | - | 9.00 | - | 9.7 | | | |

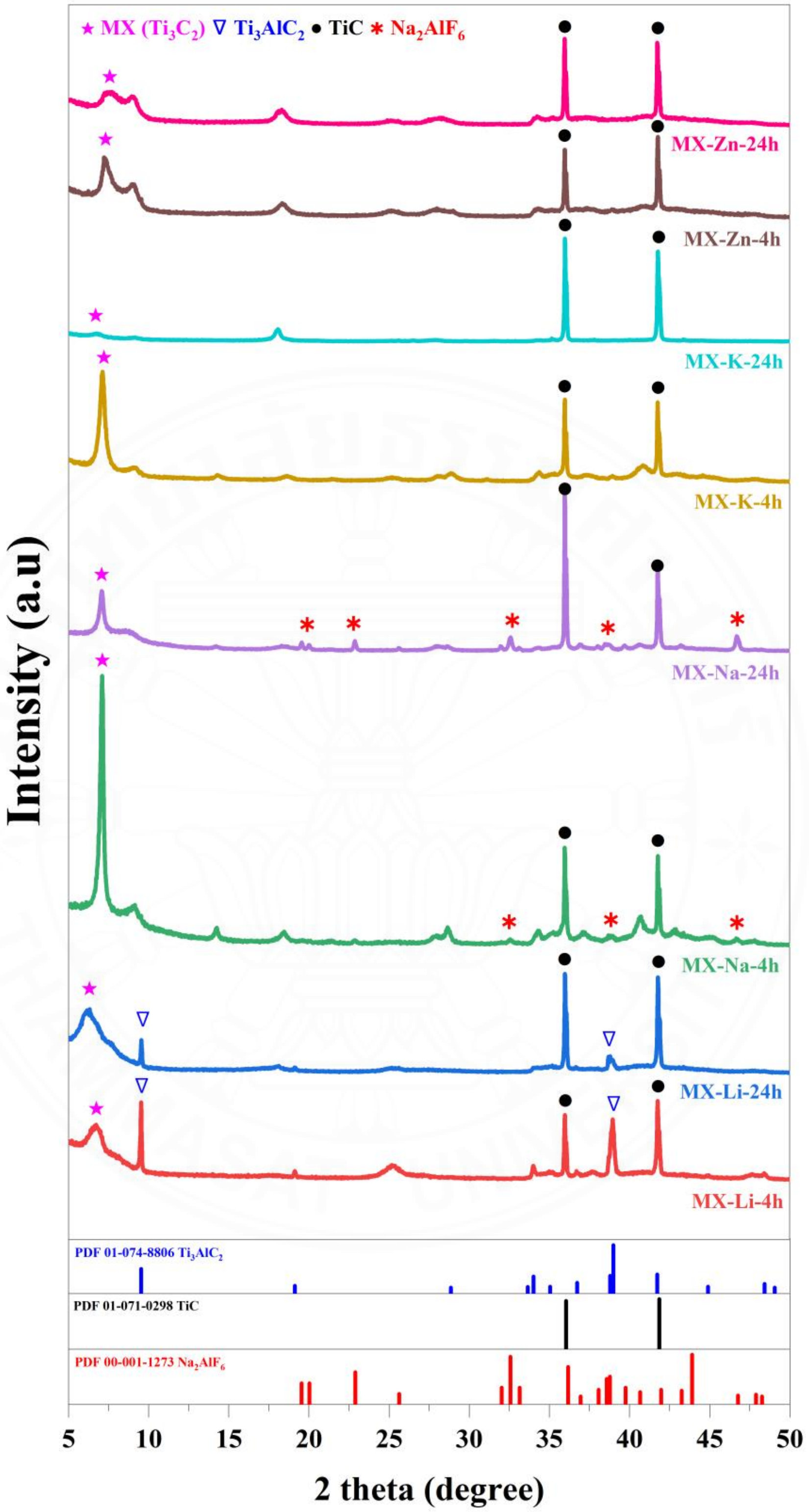

**Figure 4.6** Power diffraction (XRD) patterns of MXene ($Ti_3C_2$) or MX, obtained by various fluoride salts etching at 9M of LiF, NaF, KF, $ZnF_2$ with 9M of HCl at 4h and 24h etching. Standard powder diffraction peak of $Ti_3AlC_2$, TiC and $Na_2AlF_6$ are shown as comparison at the bottom.

Furthermore, after 24 hours etching has completed, it noticed that the intensity of each synthesis system has decreased indicating that the planes have become less well defined. The d-spacing value became slightly increased probably because there was more fraction of cations intercalated into the structure.

This is also in a good agreement with EDS results that elemental composition of each individual etching system, cation has slightly increased after 24 hours etching. In case of LiF/HCl, it was observed that MAX phase was not quite completely removed even after 24h. For NaF/HCl etchant, EDS results also indicate a very good etching of Al at 4h. However, expanding of etching time to 24h, resulting in producing of the impurity of $Na_2AlF_6$ which is consistent to that amount of –F and Al as shown in **Table 4.3**.

It is also interesting to observe the surface morphology by SEM and elemental composition analysis by EDS of obtained MXene material which etched via various 9M fluoride salts with 9M HCl at two different etching times 4h and 24 h.

For LiF, NaF, KF etchant system, MXene product shows typical multilayers stack for both 4h and 24h etching as shown in **Figure 4.7** (a–f). Interestingly, at 4h etching, the MXene sheet structure seemed to be more open at 24h etching. The cation contents were also increased at 24h. This is also observed from XRD results that the appearance of existing peak of $Na_2AlF_6$ remain in the sample. F. Liu et al. (2017) also report that some sodium aluminum fluoride compounds may still remain since it does not easily wash out by water.

$Zn^{2+}$ has two positively charge, it may crosslink in the MXene layer and pull the layer to become close to each other. **Figure 4.7**(g–h) show the SEM image of $ZnF_2$/HCl etching at 4h and 24h. The results indicate that the dense multilayers at 4h and not significantly different after 24h. This is maybe due to Zn cation has bigger in radii size and little amount of Zn cation was intercalated. The bi-modal peaks in the case of Zn2+ may be due to different amount of water molecules co-intercalated with the Zn2+, resulting in comparable two different types of d-spacing values. The Al was removed almost completely in the $ZnF_2$ system, compared to other systems, this was potentially due to the higher F content using 9M $ZnF_2$ , which probably can generate more in-situ HF upon combination with HCl, more efficiently than other monovalent fluoride salts.

Therefore, batch synthesis of MXene product via LiF/HCl, NaF/HCl, KF/HCl and $ZnF_2$/HCl were produced at 4 hours, supporting by the high concentration of acid (9M HCl) and high concentration of fluoride salts (9M). Furthermore, extending the reaction time to 24 hours, MXene structurally change by the intercalation of cation inserting to the MXene layer structure. However, keeping long time of reaction is also produce by-product of insoluble salts in NaF/HCl etching and KF/HCl etching system.

In summary, batch synthesis of MXene via LiF/HCl, NaF/HCl, KF/HCl and ZnF2/HCl were successfully etched at 4 hours, supporting by the high concentration of acid (9M HCl). Furthermore, extending the reaction time to 24 hours, MXene structural change by the intercalation of cation inserting to the MXene layer structure.

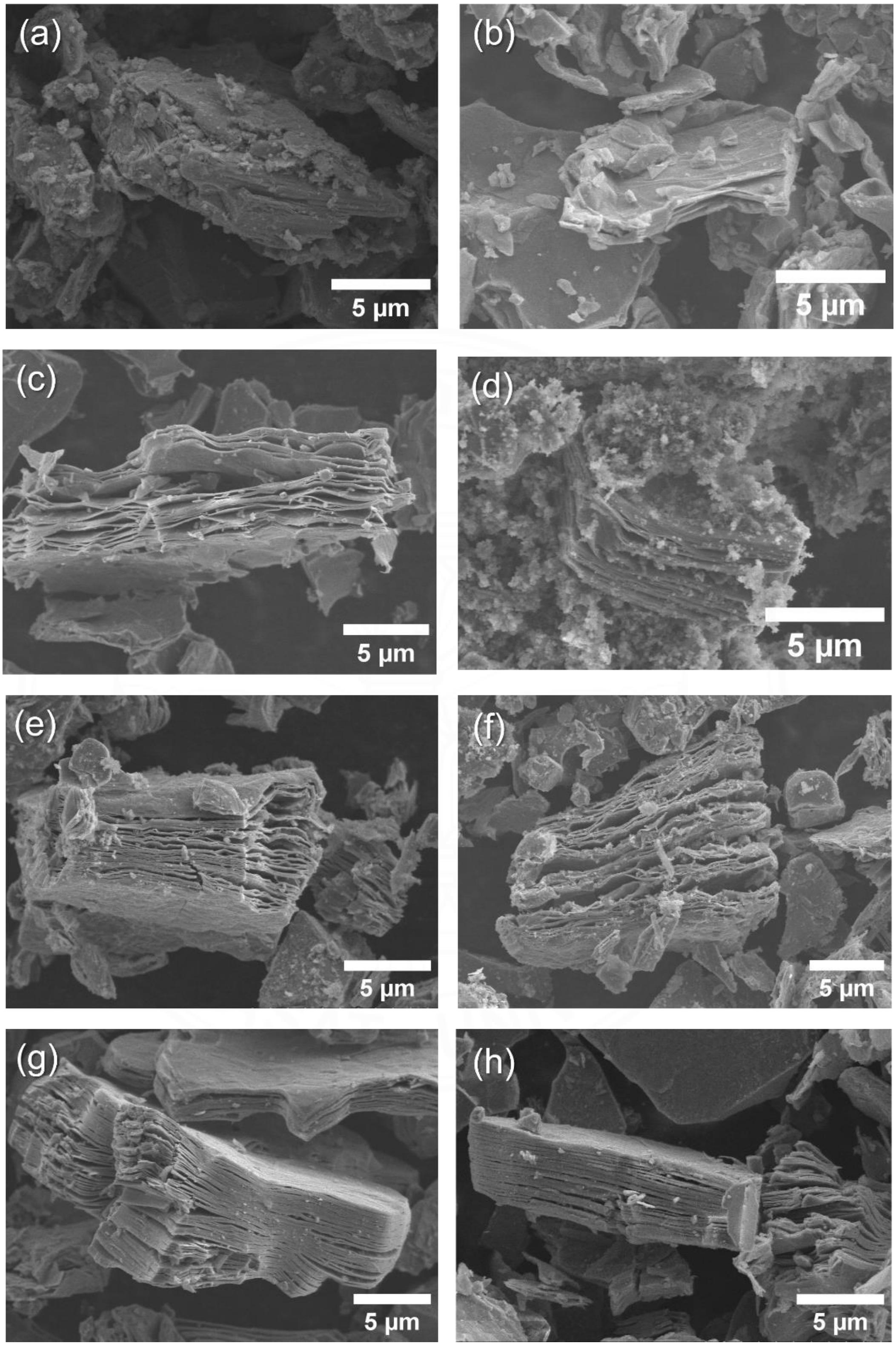

**Figure 4.7** SEM image of MXene etched via various fluoride salts, (a–b) LiF/HCl etching, (c–d) NaF/HCl etching, (e–f) KF/HCl etching, (g–h) $ZnF_2$/HCl etching; left side was etched at 4 hours and right side was etched at 24 hours.

**Table 4.3** Elemental composition of $Ti_3C_2$ MXene or MX sample etched via various fluoride salt 9M with HCl 9M and etching time of 4h and 24h.

| Element content | Atomic % content | | | | | | | |
|---|---|---|---|---|---|---|---|---|
| | MX-Li | | MX-Na | | MX-K | | MX-Zn | |
| | 4h | 24h | 4h | 24h | 4h | 24h | 4h | 24h |
| Ti | 20.47 | 13.86 | 23.07 | 19.85 | 32.76 | 18.01 | 31.20 | 24.53 |
| Al | 0.35 | 0.09 | 1.00 | 2.15 | 0.52 | 1.48 | 0.16 | 0.16 |
| C | 28.50 | 38.49 | 36.99 | 23.67 | 39.11 | 39.82 | 27.56 | 28.49 |
| O | 41.11 | 39.10 | 20.63 | 12.63 | 12.22 | 14.53 | 31.78 | 34.35 |
| F | 8.60 | 7.45 | 15.23 | 34.20 | 13.09 | 21.89 | 8.87 | 11.79 |
| Cl | 0.97 | 1.01 | 0.25 | 0.21 | - | - | - | - |
| Li | ND* | ND* | - | - | - | - | - | - |
| Na | - | - | 2.83 | 7.30 | - | - | - | - |
| K | - | - | - | - | 2.31 | 3.50 | - | - |
| Zn | - | - | - | - | - | - | 0.44 | 0.69 |
| Al/Ti | 0.017 | 0.006 | 0.043 | 0.108 | 0.001 | 0.082 | 0.005 | 0.006 |

*ND: EDS could not detect Li content

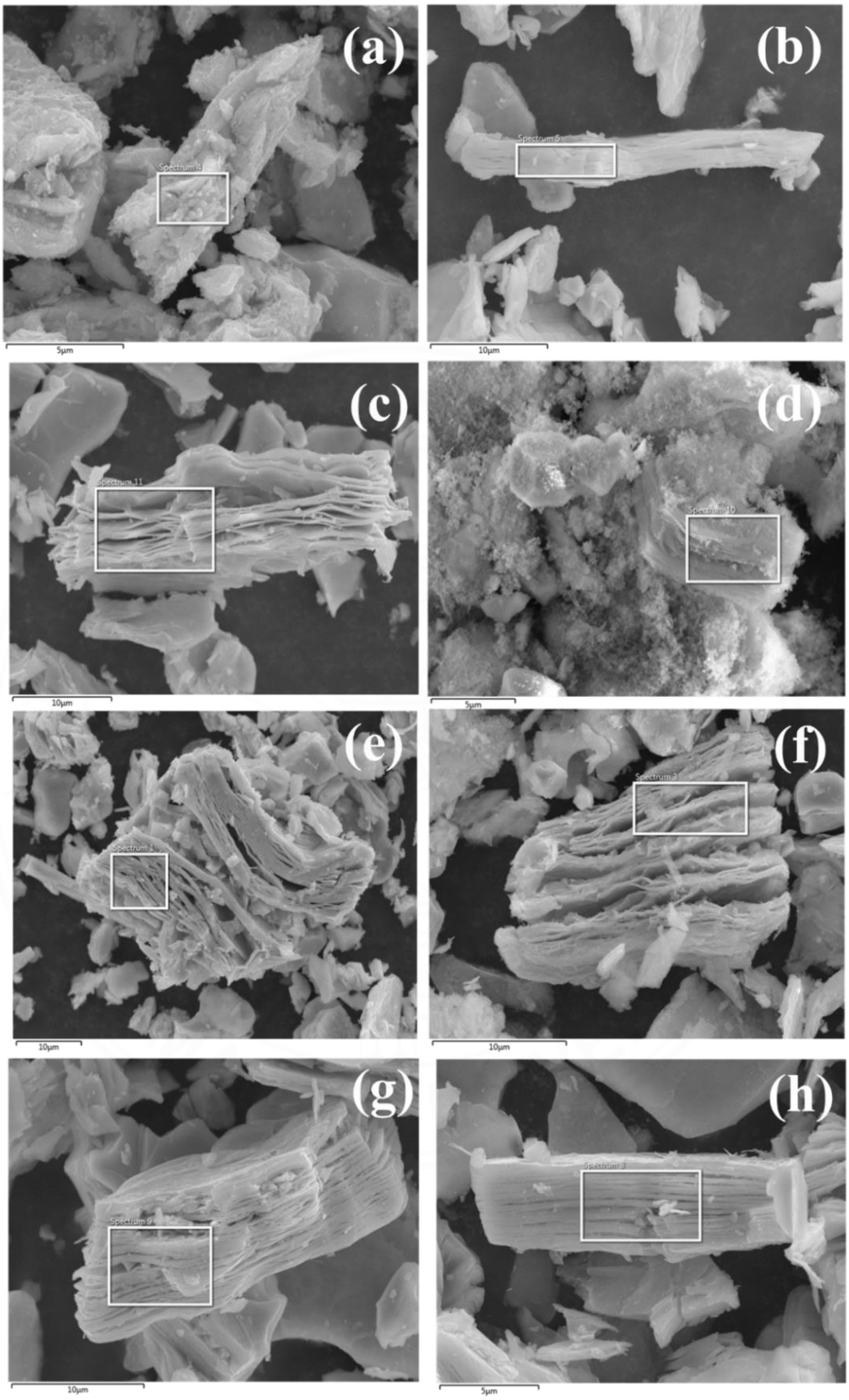

**Figure 4.8** Elemental analysis of Ti3C2 MXene powders etched via different fluoride salts as measured by EDX, (a-b) LiF/HCl etching, (c-d) NaF/HCl etching, (e-f) KF/HCl etching, (g-h) ZnF2/HCl etching; left side was etched at 4 hours and right side was etched at 24 hours

## 4.3 Adsorption capacity of ENR onto MLs MXene

The adsorption uptake of ENR onto intercalation-MXene was carried out. MXene sample which was etched at 4 hours and 24 hours by various fluoride salts were used in this study. Many studies reported that intercalation process on 2D material like MXene has a good performance in pollutant removal (Mashtalir et al., 2014a; Wan et al., 2016).

**Figure 4.9** shows the ratio of $C/C_0$ of ENR concentration after using adsorbents (Li-$Ti_3C_2$, Na-$Ti_3C_2$, K-$Ti_3C_2$, Zn-$Ti_3C_2$) etched at 4 hours and 24 hours. MLs MXene which has large interlayer space showed higher ENR adsorption. Cation intercalation into MXene facilitates later intercalation. The order of ENR adsorption ability was Li- > Na- > K- > Zn-Mx, which also correlates with the order of d-spacing that d-spacing of Li- > Na- > K- > Zn-Mx.

For MLs MXene etched for 24h, which had slightly larger interlayer spacing compared to that etched at 4h. However, their ENR adsorption was smaller than 4h. This is maybe due to the better stabilization of cations in MX-24h than those system etched for shorter time of 4h. Due to high concentration of cations in the etching media, they slowly diffuse into MX layers and would not come out easily, especially if the exchange with ENR is not so energetically much more favorable, then the exchange kinetic would be slow. Thus, the ENR adsorption capacity of all etching system at 24 h become less as can be seen in the concentration ratio C/C0 in **Figure 4.9.**

It is also interesting to observe the ENR adsorption kinetic of MLs MXene material which etched at 4h and 24h. The adsorption kinetics were fitted to pseudo first-order model $q_t = q_e(1-e^{-k1t})$, and the pseudo second-order, $q_t = q_e^2k_2t / (1 + q_ek_2t)$, where $q_e$ and $q_t$ are the adsorption capacity and adsorption equilibrium at time $t$, $k_1$ and $k_2$ are the rate constants for the pseudo first-order model and pseudo second-order model, respectively. The fitting results of the adsorption kinetics are summarized in **Table 4.4** and found that pseudo-second order model with higher $R^2$ value seem to fit better than pseudo-first order model.

Therefore, it can be assumed that cation intercalation is a key factor for expanding the MLs MX interlayer space to be more opening structure, thus ENR molecule could possibly enter and binding at active sites, or subsequent intercalation with larger organic molecules become possible. However, for longer etching time some of these salts might reach favorable sites within MX structure and fully occupy the MX sites. The further exchange becomes slightly less favorable in such case.

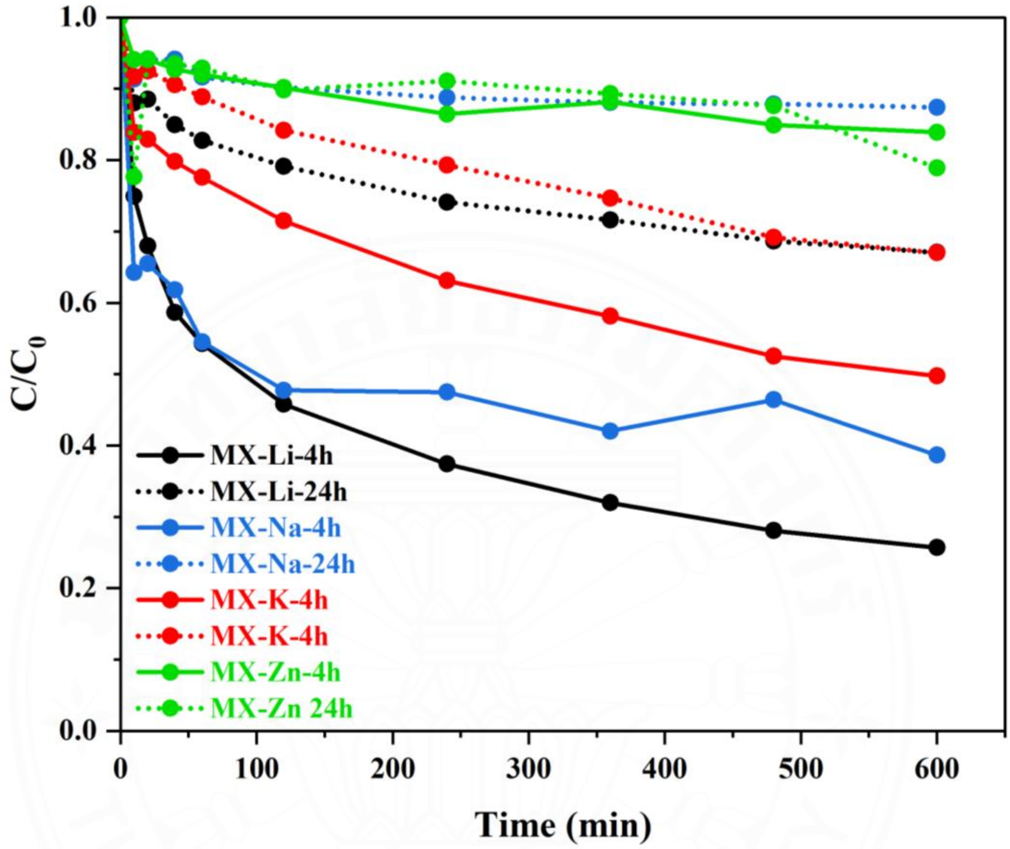

**Figure 4.9** Removal of enrofloxacin (ENR) by MLs MXene ($Ti_3C_2T_x$) synthesis via various fluoride salts etching. Condition: MLs ($Ti_3C_2T_x$) etching at 4hrs and 24hrs, adsorbent 1g $L^{-1}$, initial ENR 10mg $L^{-1}$, under dark condition, $C/C_0$ is the ratio between the ENR concentrations at time *t* and at initial time.

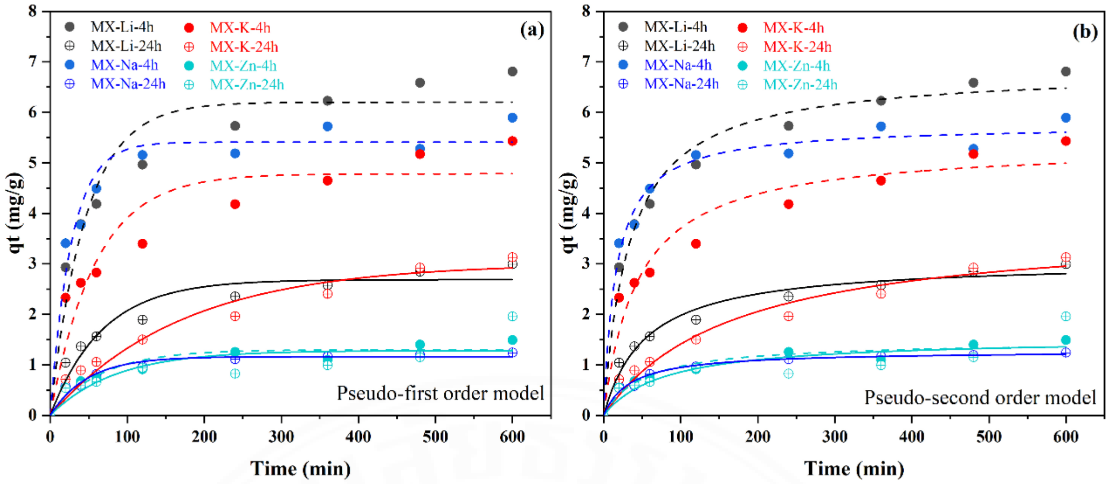

**Figure 4.10** Adsorption kinetic model of ENR antibiotic onto MLs MXene adsorbent material (a) pseudo-first order model, (b) pseudo-second order model. Dash and solid lines: fitting of the models to MX etched for 4h and 24h, respectively.

**Table 4.4** Kinetic parameters of ENR adsorption under dark condition using MX adsorbent synthesized at various fluoride salts and etching time of 4h and 24h.

| Samples | ENR adsorption under dark condition | | | | | | |
|---|---|---|---|---|---|---|---|
| | | Pseudo-first order model | | | Pseudo-second order model | | |
| | $q_{experiment}$ *(mg/g)* | $q_e$ (mg/g) | $k_1$ ($\times 10^{-3}$ min$^{-1}$) | $R^2$ | $q_e$ (mg/g) | $k_2$ ($\times 10^{-3}$ g/(mg·min)) | $R^2$ |
| MX-Li-4h | 6.80 | 6.20 | 21 | 0.938 | 6.84 | 4.3 | 0.983 |
| MX-Li-24h | 2.99 | 2.68 | 14 | 0.928 | 2.94 | 5.9 | 0.973 |
| MX-Na-4h | 5.89 | 5.41 | 36 | 0.961 | 5.75 | 10.5 | 0.982 |
| MX-Na-24h | 1.24 | 1.16 | 20.6 | 0.949 | 1.27 | 22.4 | 0.978 |
| MX-K-4h | 5.43 | 4.78 | 16.8 | 0.877 | 5.36 | 4.1 | 0.941 |
| MX-K-24h | 3.12 | 3.01 | 5.8 | 0.943 | 3.78 | 1.5 | 0.964 |
| MX-Zn-4h | 1.49 | 1.29 | 15.3 | 0.891 | 1.47 | 13 | 0.934 |
| MX-Zn-24h | 1.95 | 1.28 | 11.8 | 0.605 | 1.53 | 8.2 | 0.682 |

*MX: $Ti_3C_2$

## 4.4 Adsorption capacity of ENR onto single layer MXene

Since it was observed that the MXene obtained still have packed structure though with larger inter-layer space. It is interesting to try whether further exfoliation could help increase ENR adsorption capacity. The multilayer MX-Li-4h was used as precursor for further exfoliation.

### 4.4.1 Further exfoliation of the multilayer MX

As observed in previous section that even with 9M and 24h, the obtained MXene was still a multilayer structure. MXene will be further delaminated using a probe sonication. The effects of different media, which are DI water, LiCl, and ethanol, were tested. The possibility of delamination into a single layer has been reported in a few studies by hand shaking or delamination from typical LiF/HCl etching (Lipatov et al., 2016a; Shekhirev, Ogawa, et al., 2022; Christopher E. Shuck et al., 2021). T. Zhang et al. (2017) reported that ethanol can help exfoliation/delamination of MX material. Maleski, Mochalin, and Gogotsi (2017) also reported that dispersion medium including DI water, ethanol were a good dispersion after sonication. In addition, LiCl is also commonly used to delaminate MXene (Inman et al., 2022a).

MX-LiF-4h sample etched at 4 hours will be used as a precursor since its d-space, due to solvated lithium intercalation, was larger than other fluoride salt etching systems, and thus offers higher chance for delamination of the packed MXene into a few-layered or a monolayer MXene.

**Figure 4.11** schematically illustrates the procedure herein to prepare monolayer MXene flake by probe sonication the precursors in different solvents for 10 minutes. Sample sonicated in DI water had very good dispersion and cannot be settled down easily.

The dark solution was analyzed for their UV-Vis absorbance. The UV-Vis absorbance of MXene sonicated in DI water showed the highest absorbance followed by that in ethanol and LiCl. This result of UV-Vis absorbance spectra indicated that MXene sonicated in DI water were better exfoliated, compared to that in ethanol and LiCl. To obtain sediment, the dispersion has to be centrifuged at 12,000rpm for 1 hour to ensure sufficient sediment settling down and collection.

**Figure 4.12** which shows the dynamic light scattering size (DLS) of pristine multilayer MXene and sonicated MXene. TEM images were also taken which revealed the layer structure of the MX. The value of particle size distribution was obtained around 1,526 nm for the parent MXene (MX-Li-4h) and around 380 nm for the sMX/DI. In case of sMX/LiCl system, MX sample was settled down after centrifugation 10 minutes. This is due to the presence of 9M LiCl salts potentially neutralize the charge and flocculating MX. The zeta potential measurement seemed to also confirm this picture where sMX/LiCl possessed less negatively charged as shown in **Table 4.5**.

Maleski et al. (2017) have illustrated that medium with surface tension higher than 40mN/m produced a stable colloidal solution of MXene. Consistent with this picture, MXene sonicated in ethanol, which has the surface tension of 22 mN/m at 293K, could not produce stable suspension of MXene, while MXene sonicated in DI water (surface tension of 72 mN/m) results in stable suspension. MX sonicated in ethanol did not result in high dispersion, probably due to the stacking forces amongst MXene sheets are still larger than their interactions with ethanol.

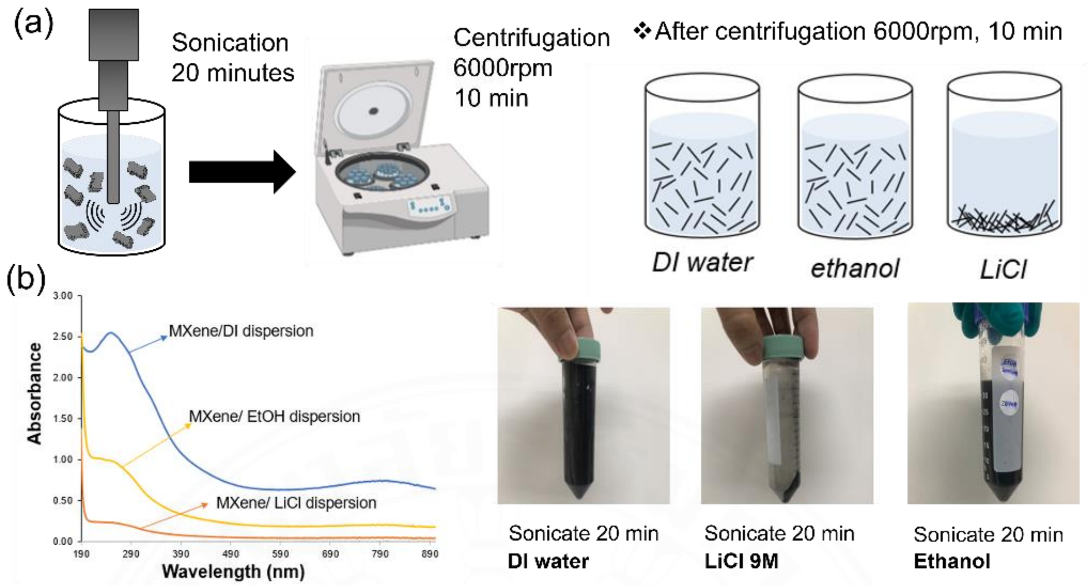

**Figure 4.11** (a) Diagram showing sonication of MX-Li4h in various media and the corresponding photos of the solution taken at10 minutes after centrifugation. Before sonication, MX-LiF-4h powder could be settled down at the bottom of the vial in all media type easily. (b)The UV-Vis absorbance of the supernatants taken at 10 min. after centrifugation, MX-Li-4h sonicated in DI water was highly dispersed and cannot be settled down, resulting in high UV-Vis absorbance. In contrast, MX-Li-4h sonicated in 9M LiCl was still easy to be settled.

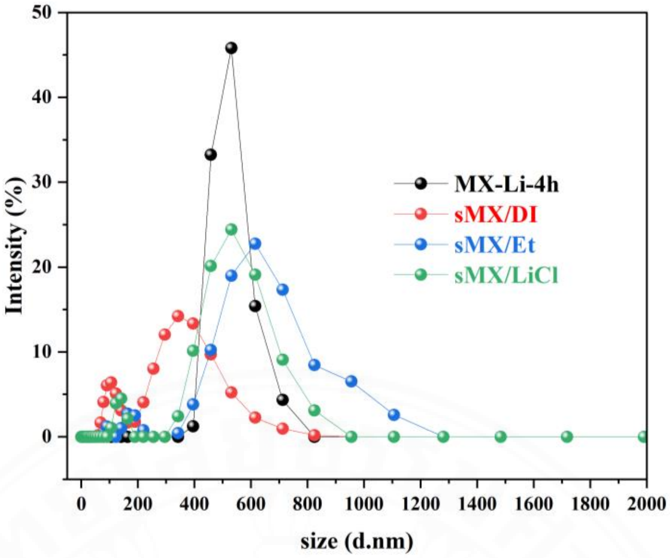

**Figure 4.12** Particle size distribution measurement by dynamic light scattering (DLS) technique of MX sample sonicate in DI water (sMX/DI), ethanol (sMX/Et), LiCl (sMX/LiCl), along with the MX-Li-4h precursor.

**Table 4.5** DLS particle size of MX sonicate in DI water, ethanol, LiCl MX-Li-4h precursor, along with zeta potential measurement.

| Sample | DLS Particle size (Z-avg, nm) | Size from 1st major peak (nm) | Size, average from 2 major peaks (nm) | Zeta potential (mV) |
|---|---|---|---|---|
| Parent MX-Li-4h | 1595±129.6 | 526 | 526 | -40.0 |
| sMX/LiCl | 1221±16 | 475 | 387 | -13.2 |
| sMX/EtOH | 1057±106.4 | 645 | 645 | -21.6 |
| sMX/DI | 380.2±4.7 | 360 | 289 | -45.7 |
| MX/TBAOH (Parent MX-Li-4h + TBAOH incubation 24h | 1362±177.2 | 621 | 621 | -45.9 |

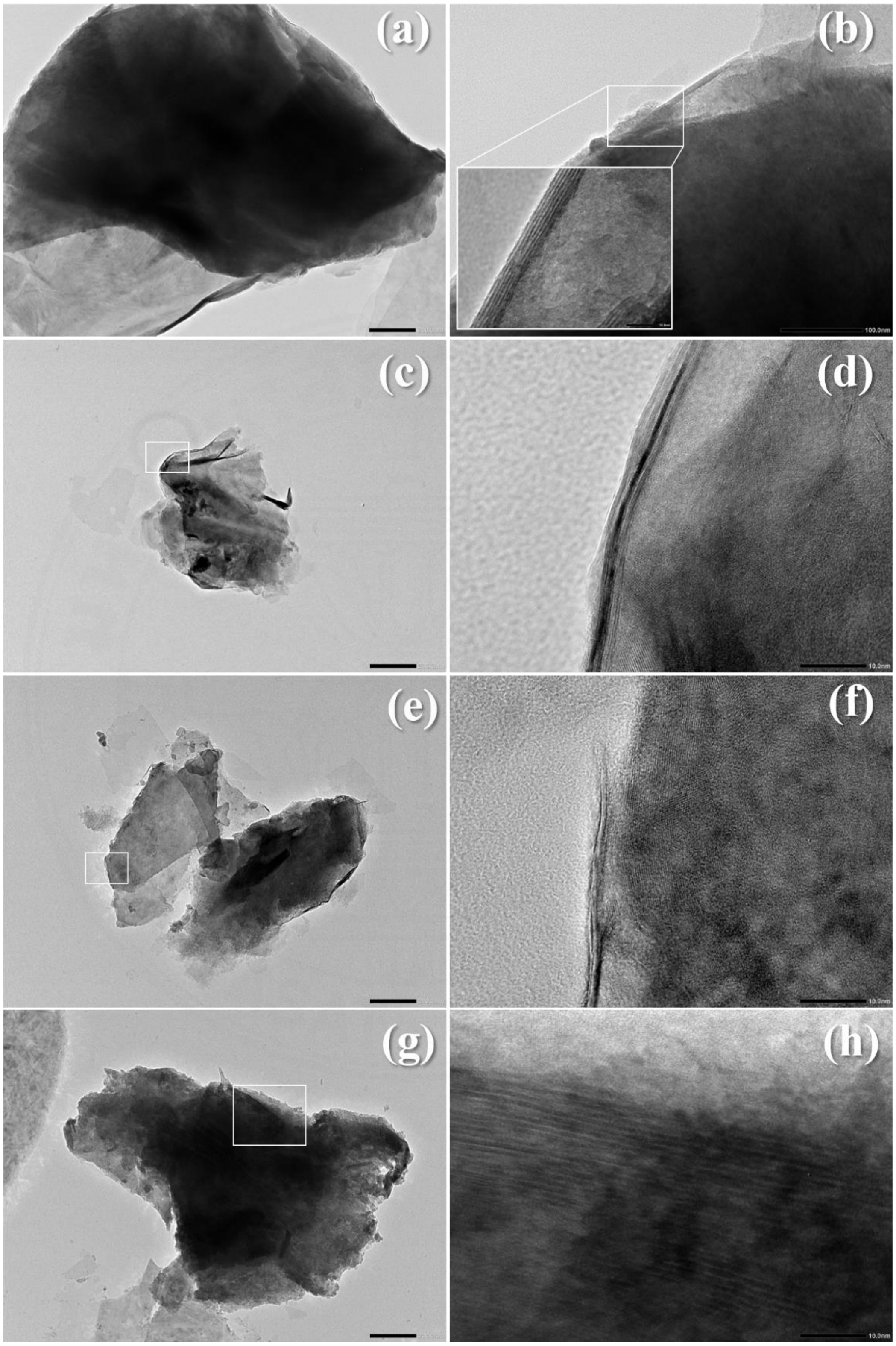

**Figure 4.13** TEM images of, (a) MX-Li-4h precursor before exfoliation, (b) MX after further exfoliation by 20 min sonication in DI water (sMX/DI), (c) in ethanol (sMX/EtOH), (d) in 9M LiCl (sMX/LiCl).

The parent multilayer MX (MX-Li-4h) with bigger organic molecule, tetrabutylammonium hydroxide (TBAOH) was utilized for weakening the $Ti_3C_2$ layer, which was reported that it could delaminate the $Ti_3C_2$ layer to a few-layer MX, or single layer, simply by hand shaking (Naguib et al., 2011a).

In this work, we also conducted similar procedure, by taking MX precursor (MX-Li-4h) intercalated with TBAOH overnight. The results show that the obtained MX was exfoliated into a single nanoflake as confirmed by TEM analysis image in Error! Reference source not found.. The particle size distribution by DLS illustrate 1,361±108.6 nm which is close to that of the neat MX. Therefore, delamination of MX by intercalation with TBAOH was successful to separate the multi stack MX layer into few-layer or single layer. This investigation is also in a good agreement to previous report which delaminate $V_2CT_x$ and $Ti_3CNT_x$ in TBAOH (Naguib, Unocic, Armstrong, & Nanda, 2015).

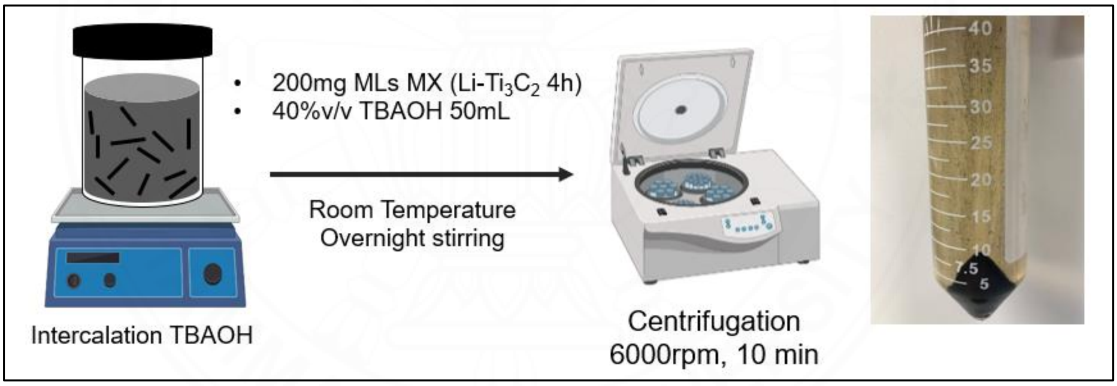

**Figure 4.14** Schematic illustration of the MXene $Ti_3C_2$ delamination via intercalation MX in TBAOH, photograph at right side indicate the suspension was collected after 10 minutes centrifugation.

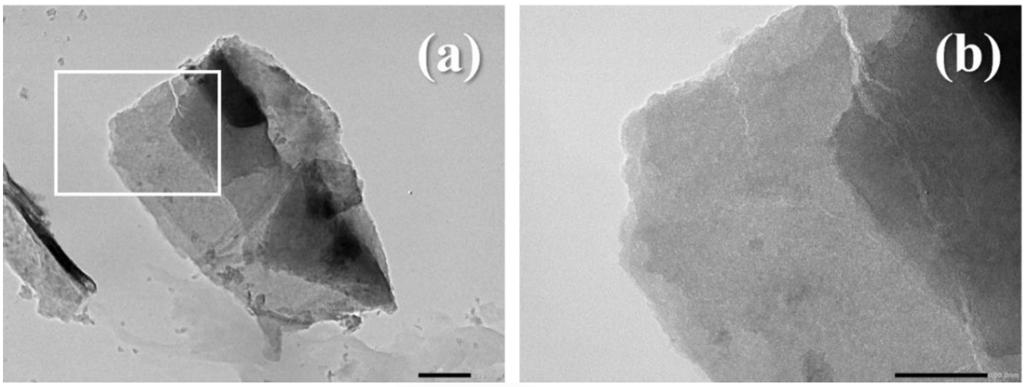

**Figure 4.15** TEM image of MXene $Ti_3C_2$ nanosheet intercalation in TBAOH, (a) MX/TBAOH sample (magnification ×30k), (b) MX/TBAOH (magnification ×100k)

The obtained sonicated MXene, or single layer MX above were then used to test for ENR removal. **Figure 4.16** indicates the ENR removal using MXene that was sonicated in DI water (sMX/DI), in ethanol (sMX-Et) and 9M LiCl (sMX-LiCl). It can be seen that sMX/DI removes ENR faster than those sonicated MXene fabricated via ethanol or LiCl.

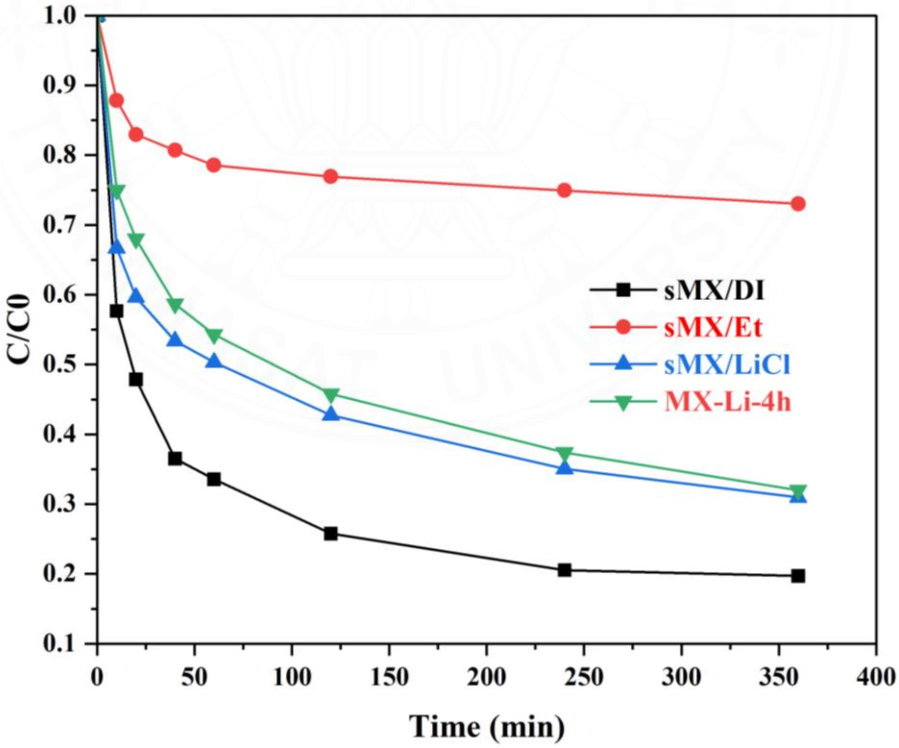

**Figure 4.16** Removal of ENR by MX that has been exfoliated further by sonication in different media. Conditions: sMX/DI centrifugation 12000rpm, sMX/LiCl and sMX/EtOH centrifugation 6000rpm, ENR 10 mg $L^{-1}$ and adsorbent loading 1g $L^{-1}$

In term of adsorption capacity ($q_t$), sMX/DI could adsorb ENR molecule approximately 8.35 mg $g^{-1}$, while sMX-LiCl and sMX-EtOH had qt 6.40 mg $g^{-1}$ and 2.15 mg $g^{-1}$, respectively. In this particular adsorption technique, we investigated that sMX/DI could uptake ENR quite rapidly within 2 hours due to delamination of single flake MXene providing high surface area negatively charge as confirm by zeta potential (-45.7 mV).

In comparison to multilayer MXene discussed in (section 4.2), MX-Li-4h also adsorb ENR. However, since MXene with the $Li^+$ intercalation has the sandwich structure of multilayer, the chance for ion-exchange with the drug molecules is slower than those MXene which have single layer. To assess to kinetic of contaminant adsorption onto sMX and MX. **Figure 4.17** and **Table 4.6** are the kinetics adsorption of ENR and the summarize of the rate parameters obtained from fitting kinetic models.

It can be seen that the speed of adsorption of Ti3C2/DI is very fast in comparison to MLs MXene (Li-MX 4h) and even faster than those sample which sonicate in ethanol and LiCl. This could be explained with the fact that sMX/DI, ENR adsorption is mainly occupied and the outer surface of the MXene, while MX-Li-4h, adsorption is mainly through cation-exchange of Li cation inside the interlayer space of the MX structure, and thus may has slower rate of ENR adsorption. This is also consistent to that the rate constant $k_1$ shows quite high for sMX/DI which may emphasize that facile adsorption may cause by the electrostatic interaction with the drug molecule. For sMX/Et, the kinetic constant was quite rapid due to its low adsorption capacity, and only small number of adsorption sites available and saturated rapidly.

The lithium cation leaching out during ENR adsorption. **Figure 4.18** shows the amount of Li cation leaching upon ENR sorption was measured. **Table 4.7** also shows the Li content in the sample before and after ENR adsorption experiment.

Interestingly, lithium cation was almost undetectable for ENR adsorbing with $Ti_3C_2$/DI. This can be explained that cation exchange of lithium and antibiotic drug may not involve in the adsorption performance. The predominance of the adsorption capacity of ENR onto MXene monolayer (sMX/DI) is consequently due to the attachment on the outer surface, as well as the engagement from surface termination, which promotes electrostatic interaction with enrofloxacin. This investigation is also similar to few studies in which MXene was used as adsorptive materials (Mashtalir et al., 2014b)

Furthermore, it is also interesting to observe the amount of Li content in the MXene before and after adsorption experiment in order to confirmed that Li cation definitely not involve in the adsorption capability of sMX/DI. **Table 4.6** shows the lithium content in the solid samples before and after adsorbing ENR. In the samples of sMX/Et and sMX/LiCl illustrate that the amount of Li cation inside the solid sample is gradually decreased which was consistent to the amount of Li cation has leached out upon adsorption experiment. However, the amount of Li cation inside sMX/DI does not significantly change before and after adsorption. This can be revealed that Li cation probably does not incorporate in the adsorption mechanism.

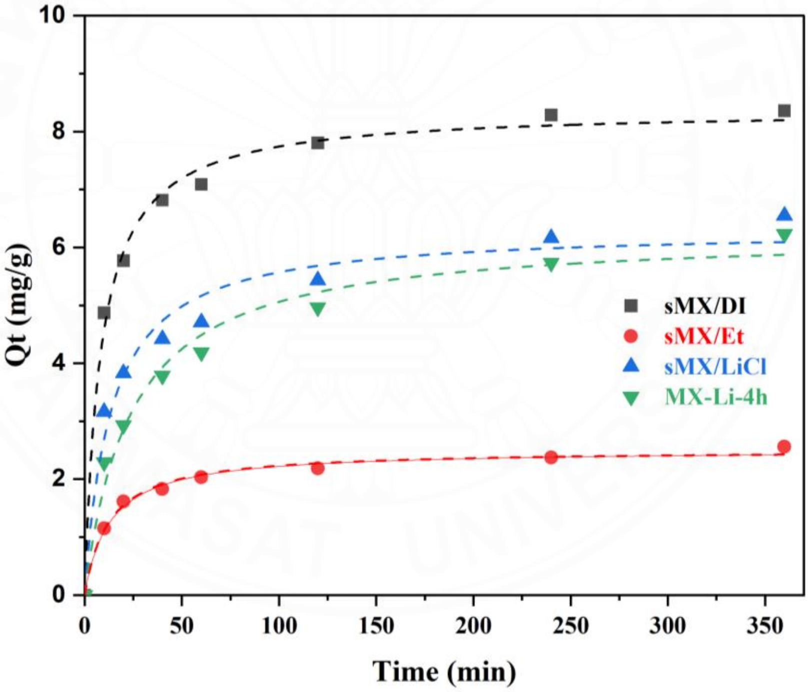

**Figure 4.17** Adsorption kinetic model of ENR antibiotic onto MX sample sonication in DI water (sMX/DI), ethanol (sMX/Et), 9M LiCl (sMX/LiCl)

**Table 4.6** Adsorption parameters evaluated from kinetic models of different adsorbents of monolayer MXene (Ti3C2Tx) which prepared by different dispersions.

| Kinetic models | Parameters | MLs MXene | s-MX | | |
|---|---|---|---|---|---|
| | | MX-LiF-4h | s-MX/DI | s-MX/EtOH | s-MX/LiCl |
| Pseudo-second order model | $K_2$ (g/mg.min) ($\times 10^{-3}$ ) | 5 | 14 | 32 | 12 |
| | $q_e$ (mg g-1) | 6.72 | 8.38 | 2.51 | 6.32 |
| | $R^2$ | 0.974 | 0.994 | 0.992 | 0.973 |

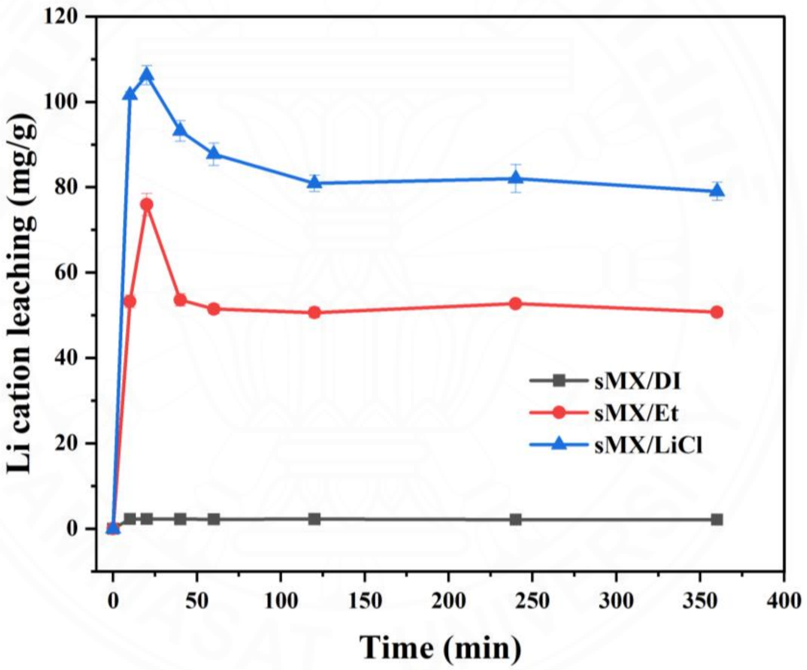

**Figure 4.18** Lithium cation leaching during the ENR adsorption using sonicated MX

**Table 4.7** Li content in the samples before and after adsorption along with the adsorption capacity of ENR

| Samples | Li content (mg/g) | | ENR Adsorption capacity (mg/g) |
|---|---|---|---|
| | Before adsorption | After ENR adsorption | |
| MX-Li-4h | 226.69 | 93.9 | 6.8 |
| sMX/LiCl | 136.10 | 31.17 | 6.4 |
| sMX/EtOH | 112.49 | 29.86 | 2.2 |
| sMX/DI | 5.78 | 5.68 | 8.4 |
| MX/TBAOH | 46.63 | 19.80 | 1.00 |
| MX-HF | - | - | 1.49 |

In addition, it is also observed the performance of delaminated MXene which has intercalated with other large organic based (TBAOH). This typical intercalation technique was also reported as monolayer like-flake MXene by using handshaking or soft sonication.(Naguib et al., 2015) In this part, MLs MXene (MX-Li-4h) was utilized to intercalate TBAOH. 40% v/v of TBAOH was used to intercalated MLs MXene overnight. TBAOH was successful exchanged with Li as shown by the reduction in the Li content after TBAOH intercalation in **Table 4.7**. However, MX/TBAOH shows poor ENR removal. This could be explained that the tetrabutylammonium adsorbs strongly to the MX binding sites, and do not want to be exchanged for the ENR molecule. This leads to the very poor ENR uptake in the MX/TBAOH system.

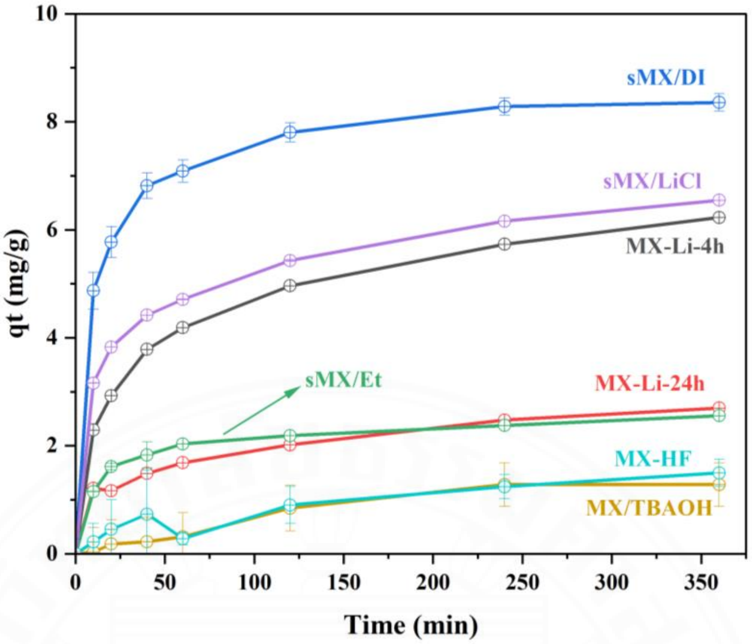

**Figure 4.19** Comparison of adsorption performance of monolayer MXene (sMX/DI, sMX/LiCl, MX/TBAOH) and multilayer MXene, MX-Li-4h, MX-HF

**Figure 4.19** shows the comparison of adsorption performance of all MXene samples from the multilayer MX-Li-4h, sMX, and conventional MX-HF obtained from previous work.(Katugampalage et al., 2019) MX-HF was synthesize via direct HF acid. In brief, MAX phase etched in 50% HF solution, 24 hours and washed several cycles until pH of 6. This MX-HF obtained was previously characterized to have multilayer structure and has no cation intercalation with small d-spacing of 9.7 A.

The ENR sorption now provides further insights. It can be seen that MX-HF with small interlayer spacing, shows very little ENR adsorption, while multilayer MX-Li-4h shows better ENR sorption performance, but less than sonicated MX in DI water (sMX/DI). TEM results showed that sonication in DI led to a few layers or single layer MX and can adsorb ENR better. Further comparison of ENR adsorption performance by MX sonicated in LiCl, shows that Li was not necessary for ENR adsorption as MX sonicated in 9M LiCl, whose sites were still fully occupied by Li, adsorb ENR not as well as sMX/DI, where most of the sites were probably not occupied by Li.

The Li intercalation was necessary in MX delamination, but not in its ion-exchange adsorption with other molecules later. The layer structure was also not important in this case to trap the ENR molecule. Single layer MX with abundant adsorption sites, not occupied by $Li^+$ or $TBA^+$ can already adsorb ENR, better and faster than the layered structure. Single-layer or a few-layer MX that has been delaminated using TBAOH also did not provide much ENR adsorption due to the fact that the MX sheets were occupied with $TBA^+$, which has stronger binding affinity to the MX sheets than the bulky ENR molecule. The structures of the TBAOH and ENR are also shown as in **Figure 4.20**

| Structure of TBAOH ($C_{16}H_{37}NO$) | Structure of Enrofloxacin ($C_{19}H_{22}FN_3O_3$) |
|---|---|
| 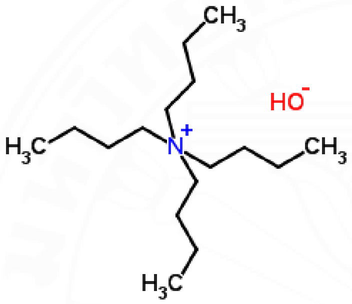 | 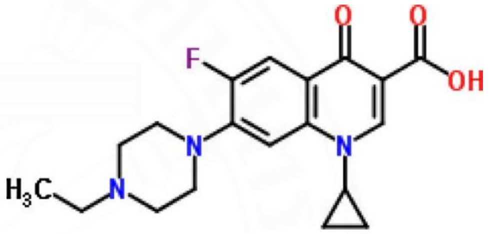 |

**Figure 4.20** Comparison of chemical structure of Tetrabutylammonium hydroxide and enrofloxacin.

In terms of affinity order to MX sheets, it seemed that $TBA^+ > Li^+ >$ ENR. ENR could compete to $Li^+$ for MX adsorption sites but seemed not very much as a lot of Li would still remain in the MX-Li-4h, or sMX/LiCl. For sMX/DI, no change in Li content was found after ENR adsorption. It could also be observed that for MX-Li-24h, the ENR adsorption became lower compared to MX-Li-4h, which was probably in line with the fact that MX binding affinity to solvated $Li^+$ may be similar or larger affinity than MX binding to ENR molecule. Therefore, ENR adsorption is in order of monolayer MXene > cation intercalated multi-layer MXene > multi-layer pristine HF-etched MXene.

## 4.5 Adsorption Isotherm of ENR by sMX/DI

To obtain adsorption capacity, adsorption isotherm (room temperature, 27 °C) of the SMX/DI for ENR adsorption was also conducted. In addition, initial ENR concentration of 10-150 mg/L and pH 5.0 were used as obtained from the optimum condition from pH dependent in (section 4.6).

By fitting the adsorption experiment data to two different adsorption isotherms, it can be used to explain the distribution of adsorbate molecules on the solid-liquid interface during the adsorption process. The Langmuir and Freundlich adsorption isotherm are used for fitting as shown in **Figure 4.21**. According to data obtaining in **Table 4.8**, it could be observed that the Langmuir model provides a better fitting than Freundlich model which is in accordance with monolayer binding of ENR on MX adsorption sites. The maximum adsorption capacity obtained from the model is then 17.45 mg g-1, with a rather weak adsorption affinity constant of 0.19 L/mg.

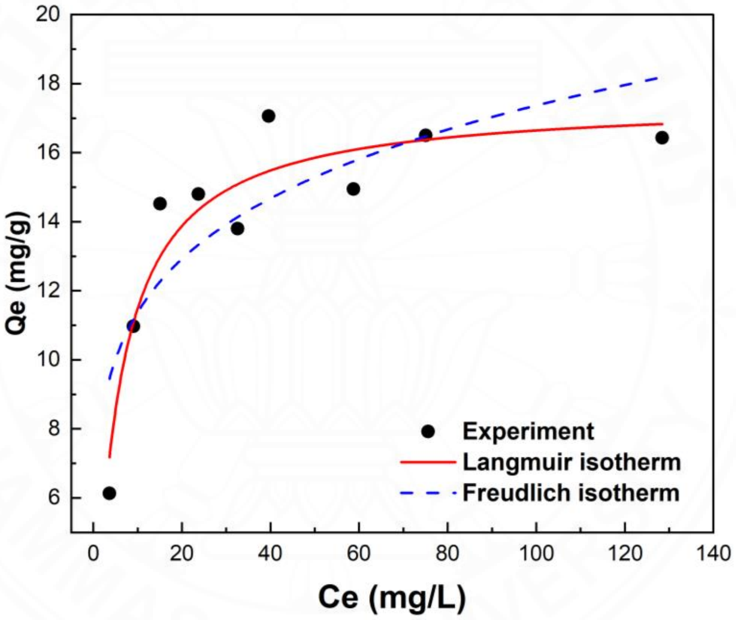

**Figure 4.21** Adsorption isotherm of ENR onto monolayer MXene: Condition: adsorbent loading 1g L-1, initial pH=5.0, ambient temperature

**Table 4.8** Adsorption isotherm parameters obtained from fitting isotherm models to experimental data at ambient temperature of 27 °C.

| | | |
|---|---|---|
| Langmuir | $Q_{max}$ (mg $g^{-1}$) | 17.45 mg/g |
| | $K_L$ (L $mg^{-1}$) | 0.1903 |
| | $R^2$ | 0.9010 |
| Freundlich | 1/n | 0.1837 |
| | $K_F$ | 7.4509 |
| | $R^2$ | 0.7036 |

### 4.6 Effect of background pH on ENR adsorption

Enrofloxacin, its molecule confers the characteristics of being zwitterionic drugs which turns drug molecule against variety of Gram-positive and Gram-negative bacteria. A zwitterionic drug could vary into 4 species in solution: as cation, neutral, anion, and zwitterion depending on the pH of the medium. Enrofloxacin drug acts as an ionic organic compound with the dissociation constant of $pK_{a1}$ = 5.15 and $pK_{a2}$ = 8.26. Adsorption is the process of mixing influence by properties of adsorbent and adsorbate.

Therefore, these indicate that solution pH is an important factor for adsorption performance because of enrofloxacin species can be changed, depending on the pH condition. Adsorption capacity against respected solution pH solution is depicted in **Figure 4.22**. MXene ($Ti_3C_2T_x$) is originally negative charge because of its combination of surface termination, it would prefer to adsorb mostly the positively charge of contaminant antibiotic. Zeta potential and adsorption capacity of monolayer MXene ($Ti_3C_2T_x$) at different pH are also shown in **Figure 4.22**. With increasing pH from 2.0 to 10.0, the surface charges of monolayer MXene ($Ti_3C_2T_x$) flake gradually increased as more negatively charge from -19.7 mV to -47.1 mV. At optimum condition, the maximum adsorption capacity was obtained at pH 5.0 since of the adsorbent monolayer MXene remains negatively charge (-41.9mV), facilitating the electrostatic interaction between adsorbent and adsorbate. Thereafter, it gradually decreased the adsorption behaviour when the enrofloxacin become anionic. This is due to the repulsion of charge between the adsorbent and adsorbate since enrofloxacin molecule deprotonate and become anionic at pH 8.25. At lower pH value (≤2.0), enrofloxacin still remain cationic form. However, the presence of the proton from pH adjustment will possibly reassembly the MXene ($Ti_3C_2T_x$) layer into multilayer and would not be likely to adsorb or exchange with the enrofloxacin molecule.

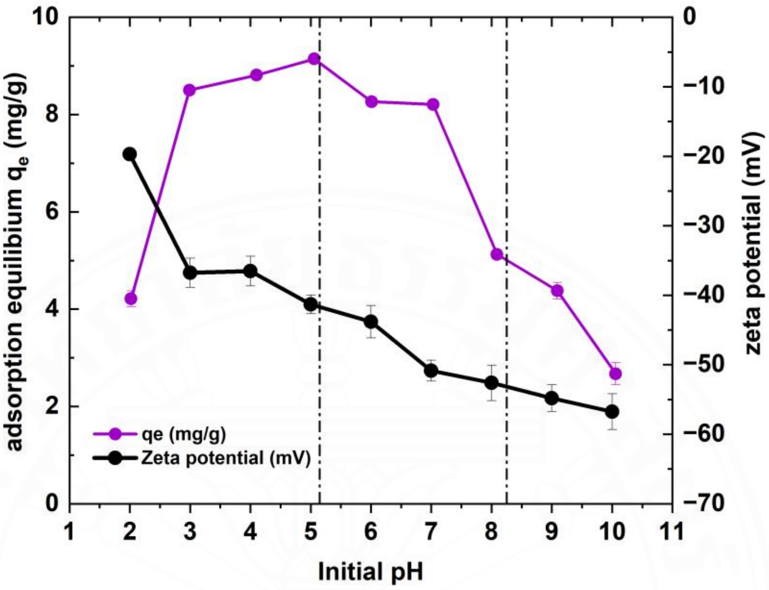

.

**Figure 4.22** ENR adsorption capacity and zeta potential of the sMX/DI as a function of pH

## 4.7 Temperature dependance of ENR adsorption

From **Figure 4.23** shows the adsorption of multilayer MX (MX-Li-4h) and fewer-layers MXene (sMX/DI) at different temperature of 0, 25, 50, 75℃. In brief, the adsorption experiment was sequentially conducted in series of 24 hours in each temperature condition. At lower temperature 0℃, sMX/DI remains good performance in comparison to multilayer MXene system. The uptake of ENR molecules progressed until it reached to equilibrium at room temperature. In contrast, the desorbing of ENR released as increased the temperature. It noticed that MX could induce into $TiO_2$-MX in the presence of higher temperature (Sukidpaneenid et al., 2023). It was also reported that MXene powder could oxidize into $TiO_2$ on MX surface by exposing into long reaction time in DI water (Cao et al., 2017). Therefore, the competition of adsorption may interfere by the growing of $TiO_2$ during adsorption at 50 and 75℃.

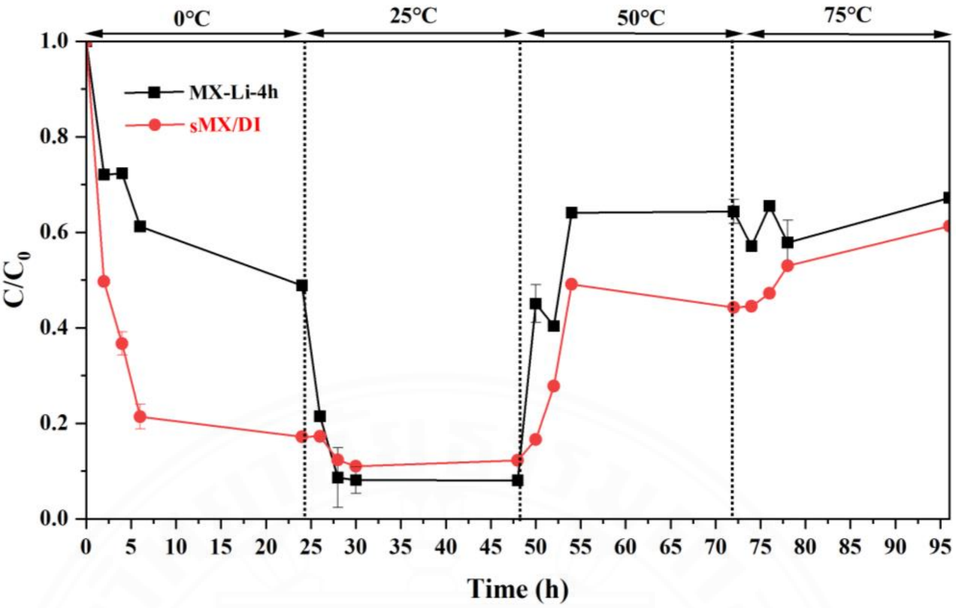

**Figure 4.23** ENR adsorption via different temperature by using MX-Li-4h precursor and sMX/DI sonicating sample: Temperature condition; 0°C, 25°C, 50°C, 75°C, ENR concentration 10ppm, MXene loading 1g/L.

# CHAPTER 5

# CONCLUSIONS AND RECOMMENDATIONS

Antibiotics are a class of beneficial chemical substances that can be promoted aquaculture growth by overcoming pathogenic bacteria, primarily gram-positive and gram-negative bacteria. Overuse of antibiotics has polluted the environment, promoted the trend of resistant-antibiotic pathogenic bacteria and developed multi-drug resistant pathogenic bacteria. The current work focuses on addressing the problem by removing residual amount of antibiotics in aqueous solutions using a simple adsorption with the help of 2D-dimensional material (MXene).

In this work, two-dimensional MXene ($Ti_3C_2T_x$) was successfully synthesized and was further studied on the maximize sorption of enrofloxacin antibiotic. MXene was produced via in-situ HF etching by preparing various fluoride salts (LiF, NaF, KF, $ZnF_2$) with hydrochloric acid (HCl) etchant, confirming that different size of cations which simultaneously intercalated inside the MXene structure, effected on the final product of MXene materials.

Their influences could be also vary depending on reaction time of etching, concentration of reactant either hydrochloric acid or fluoride salts. In this work, we have pointed out that high concentration of the acid, as an etchant, has a substantial effect on producing enough HF forming to remove Al element from the pristine MAX phase precursor. By applying high concentration of acid 9M and fluoride salts 9M, we could minimize the reaction time and could produce layer-structure MXene with different elemental constitution.

As a results, we found that high fluoride salts (9mol/L) including (LiF, NaF, KF, ZnF2) with hydrochloric acid (9mol/L) could etch Al element from MAX phase by just 4 hours. Accordion-like structure multilayer was obtained for all samples as illustrating by SEM analysis. By extending the reaction time to 24 hours, MXene samples was further etched to be a larger interlayer spacing as confirming by XRD pattern and d-spacing calculation. The vast inter-layer space provided essentials candidate for delamination into fewer-layer or single layer as well as beneficial for some applications. However, prolong the etching time may produce undesired impurity as found in NaF-HCl etching system.

MXene sample which made from LiF/HCl system, provided in lagger interlayer spacing, potentially defined as good material for delamination into single layer flake. Combined with the experiment data, UV-Vis spectroscopy analysis results, surface chemistry of zeta potential and particle size distribution, it can be confirmed that the single flake of MXene ($Ti_3C_2T_x$) can fabricate by using dispersion assisted sonication. A well dispersion was obtained of a sample sMX/DI and also high positively charge material. TEM also successfully revealed the fabrication of MXene into monolayer for MX sonication in DI water.

Justifying the accordion-like structure MXene ($Ti_3C_2T_x$) into single flake MXene ($Ti_3C_2T_x$) significantly improved the adsorbing of enrofloxacin contaminant. It was also confirmed that without $Li^+$ intercalation, ENR adsorption performance was also improved for sMX/DI. This is also observed in sMX/LiCl which has richness of Li cation, show lower adsorption than sMX/DI. Furthermore, large amount of $Li^+$ can leach out upon adsorption and not necessary involve in ion-exchange with ENR after MX has already delaminated. Thus, $Li^+$ was only facilitated on enlarge MX space for easily delamination.

A common technique for delamination MX using TBAOH also revealed in this point of view that monolayer which has strongly binding with $TBA^+$, has low chance for ENR molecule to bind on MX surface. Also, a non-intercalant MX-HF which has smaller space in layer structure also show less interaction with ENR molecule since ENR could not penetrate into the active site of layer structure. Thus, the mechanism of ENR adsorption onto monolayer MX can be attribute to the binding of free active site on MX surface.

Moreover, MXene single flake has also ability to adsorb on different pH solutions, with the optimum pH condition is at 5.0 attempting to show the greatest adsorption. At basic condition, ENR adsorption was gradually decreased since the drug transform to anions by deprotonation at the second *pKa* of tertiary amine group. In addition, the model fitting calculation results which the adsorption process follows the Langmuir adsorption isothermal model, with the maximum adsorption capacity 17.45 mg $g^{-1}$. By comparing the performance of ENR adsorption, MX structure uptake ENR molecule well follow by monolayer MXene> cation intercalated multi-layer MXene > multi-layer MXene.

# REFERENCES

Akpotu, S. O., Diagboya, P. N., Lawal, I. A., Sanni, S. O., Pholosi, A., Peleyeju, M. G., . . . Ofomaja, A. E. J. C. E. J. (2023). Designer composite of montmorillonite-reduced graphene oxide-PEG polymer for water treatment: Enrofloxacin sequestration and cost analysis. *453*, 139771.

Alhabeb, M., Maleski, K., Anasori, B., Lelyukh, P., Clark, L., Sin, S., & Gogotsi, Y. (2017). Guidelines for Synthesis and Processing of Two-Dimensional Titanium Carbide (Ti3C2Tx MXene). *Chemistry of Materials, 29*(18), 7633-7644. doi:10.1021/acs.chemmater.7b02847

Anasori, B., Lukatskaya, M. R., & Gogotsi, Y. J. N. R. M. (2017). 2D metal carbides and nitrides (MXenes) for energy storage. *2*(2), 1-17.

Anh, H. Q., Le, T. P. Q., Da Le, N., Lu, X. X., Duong, T. T., Garnier, J., . . . Oeurng, C. (2021). Antibiotics in surface water of East and Southeast Asian countries: A focused review on contamination status, pollution sources, potential risks, and future perspectives. *Science of the Total Environment, 764*, 142865.

Barsoum, M. W., & El-Raghy, T. (2001). The MAX Phases: Unique New Carbide and Nitride Materials. *American Scientist, 89*(4), 334-343. doi:10.1511/2001.28.736

Barsoum, M. W., El-Raghy, T., & Procopio, A. (2000). Synthesis of Ti4AlN3 and phase equilibria in the Ti-Al-N system. *Metallurgical and Materials Transactions A, 31*(2), 373-378. doi:10.1007/s11661-000-0273-1

Benchakar, M., Loupias, L., Garnero, C., Bilyk, T., Morais, C., Canaff, C., . . . Célérier, S. (2020). One MAX phase, different MXenes: A guideline to understand the crucial role of etching conditions on Ti3C2Tx surface chemistry. *Applied Surface Science, 530*, 147209. doi:https://doi.org/10.1016/j.apsusc.2020.147209

Briones, R. M., Sarmah, A. K., & Padhye, L. P. (2016). A global perspective on the use, occurrence, fate and effects of anti-diabetic drug metformin in natural and engineered ecosystems. *Environmental Pollution, 219*, 1007-1020.

Cao, M., Wang, F., Wang, L., Wu, W., Lv, W., & Zhu, J. (2017). Room Temperature Oxidation of Ti3C2MXene for Supercapacitor Electrodes. *Journal of The Electrochemical Society, 164*(14), A3933-A3942. doi:10.1149/2.1541714jes

Chan, R., Chiemchaisri, C., Chiemchaisri, W., Boonsoongnern, A., & Tulayakul, P. (2022). Occurrence of antibiotics in typical pig farming and its wastewater treatment in Thailand. *Emerging Contaminants, 8,* 21-29. doi:https://doi.org/10.1016/j.emcon.2021.12.003

Chen, H., Jing, L., Teng, Y., & Wang, J. (2018). Characterization of antibiotics in a large-scale river system of China: occurrence pattern, spatiotemporal distribution and environmental risks. *Science of the Total Environment, 618,* 409-418.

Dao, X., Hao, H., Bi, J., Sun, S., & Huang, X. (2022a). Surface Complexation Enhanced Adsorption of Tetracycline by ALK-MXene. *Industrial & Engineering Chemistry Research*.

Dao, X., Hao, H., Bi, J., Sun, S., & Huang, X. (2022b). Surface Complexation Enhanced Adsorption of Tetracycline by ALK-MXene. *Industrial & Engineering Chemistry Research, 61*(17), 6028-6036. doi:10.1021/acs.iecr.2c00037

Foo, K. Y., & Hameed, B. H. (2010). Insights into the modeling of adsorption isotherm systems. *Chemical Engineering Journal, 156*(1), 2-10. doi:https://doi.org/10.1016/j.cej.2009.09.013

Gao, G., O'Mullane, A. P., & Du, A. (2017). 2D MXenes: A New Family of Promising Catalysts for the Hydrogen Evolution Reaction. *ACS Catalysis*, *7*(1), 494-500. doi:10.1021/acscatal.6b02754

Ghani, A. A., Shahzad, A., Moztahida, M., Tahir, K., Jeon, H., Kim, B., & Lee, D. S. (2021). Adsorption and electrochemical regeneration of intercalated Ti3C2Tx MXene for the removal of ciprofloxacin from wastewater. *Chemical Engineering Journal, 421*, 127780.

Ghidiu, M., Lukatskaya, M. R., Zhao, M.-Q., Gogotsi, Y., & Barsoum, M. W. (2014a). Conductive two-dimensional titanium carbide 'clay'with high volumetric capacitance. *Nature, 516*(7529), 78-81.

Ghidiu, M., Lukatskaya, M. R., Zhao, M.-Q., Gogotsi, Y., & Barsoum, M. W. J. N. (2014b). Conductive two-dimensional titanium carbide 'clay'with high volumetric capacitance. *516*(7529), 78-81. doi:10.1038/nature13970

Hu, C., Li, F., Zhang, J., Wang, J., Wang, J., & Zhou, Y. (2007). Nb4AlC3: A new compound belonging to the MAX phases. *Scripta Materialia, 57*(10), 893-896. doi:10.1016/j.scriptamat.2007.07.038

Hu, C., Zhang, J., Wang, J., Li, F., Wang, J., & Zhou, Y. (2008). Crystal Structure of V4AlC3: A New Layered Ternary Carbide. *Journal of the American Ceramic Society, 91*(2), 636-639. doi:10.1111/j.1551-2916.2007.02136.x

Ikehata, K., Jodeiri Naghashkar, N., & Gamal El-Din, M. (2006). Degradation of Aqueous Pharmaceuticals by Ozonation and Advanced Oxidation Processes: A Review. *Ozone: Science & Engineering, 28*(6), 353-414. doi:10.1080/01919510600985937

Inman, A., Šedajová, V., Matthews, K., Gravlin, J., Busa, J., Shuck, C. E., . . . Gogotsi, Y. (2022a). Shear delamination of multilayer MXenes. *Journal of Materials Research, 37*(22), 4006-4016. doi:10.1557/s43578-022-00690-3

Inman, A., Šedajová, V., Matthews, K., Gravlin, J., Busa, J., Shuck, C. E., . . . Gogotsi, Y. (2022b). Shear delamination of multilayer MXenes. *Journal of Materials Research*. doi:10.1557/s43578-022-00690-3

Jansomboon, W., Boontanon, S. K., Boontanon, N., Liamleam, W., & Polprasert, C. MONITORING OF ENROFLOXACIN IN IMPORTED PANGASIUS CATFISH PRODUCTS IN THAILAND.

Katugampalage, T., Manyam, J., Kaewsaneha, C., Songkhla, N., Opaprakasit, P., & Sreearunothai, P. (2019). *Synthesis and Characterizations of MXene/Magnetic Nanoparticles Composite Loaded Porous PLGA Microspheres*.

Klein, E. Y., Van Boeckel, T. P., Martinez, E. M., Pant, S., Gandra, S., Levin, S. A., . . . Laxminarayan, R. (2018). Global increase and geographic convergence in antibiotic consumption between 2000 and 2015. *Proceedings of the National Academy of Sciences, 115*(15), E3463-E3470. doi:10.1073/pnas.1717295115

Kumar, M., Chaminda, T., Patel, A. K., Sewwandi, H., Mazumder, P., Joshi, M., & Honda, R. J. E. r. (2020). Prevalence of antibiotic resistance in the tropical rivers of Sri Lanka and India. *188*, 109765.

Kümmerer, K. J. C. (2009). Antibiotics in the aquatic environment–a review–part I. *Chemosphere, 75*(4), 417-434. doi:10.1016/j.chemosphere.2008.11.086

Li, S., Shi, W., Liu, W., Li, H., Zhang, W., Hu, J., . . . Ni, J. (2018). A duodecennial national synthesis of antibiotics in China's major rivers and seas (2005–2016). *Science of the Total Environment, 615*, 906-917. doi:https://doi.org/10.1016/j.scitotenv.2017.09.328

Li, Z., Wang, L., Sun, D., Zhang, Y., Liu, B., Hu, Q., & Zhou, A. (2015). Synthesis and thermal stability of two-dimensional carbide MXene Ti3C2. *Materials Science and Engineering: B, 191*, 33-40. doi:https://doi.org/10.1016/j.mseb.2014.10.009

Lin, Z. J., Zhuo, M. J., Zhou, Y. C., Li, M. S., & Wang, J. Y. (2006). Structural characterization of a new layered-ternary Ta4AlC3 ceramic. *Journal of Materials Research, 21*(10), 2587-2592. doi:10.1557/jmr.2006.0310

Lipatov, A., Alhabeb, M., Lukatskaya, M. R., Boson, A., Gogotsi, Y., & Sinitskii, A. (2016a). Effect of Synthesis on Quality, Electronic Properties and Environmental Stability of Individual Monolayer Ti3C2 MXene Flakes. *Advanced Electronic Materials, 2*(12), 1600255. doi:https://doi.org/10.1002/aelm.201600255

Lipatov, A., Alhabeb, M., Lukatskaya, M. R., Boson, A., Gogotsi, Y., & Sinitskii, A. (2016b). Effect of Synthesis on Quality, Electronic Properties and Environmental Stability of Individual Monolayer Ti3C2 MXene Flakes. *2*(12), 1600255. doi:https://doi.org/10.1002/aelm.201600255

Liu, A., Liang, X., Ren, X., Guan, W., Gao, M., Yang, Y., . . . Ma, T. J. A. F. M. (2020). Recent progress in MXene-based materials: potential high-performance electrocatalysts. *30*(38), 2003437. doi:10.1002/adfm.202003437

Liu, F., Zhou, A., Chen, J., Jia, J., Zhou, W., Wang, L., & Hu, Q. (2017). Preparation of Ti3C2 and Ti2C MXenes by fluoride salts etching and methane adsorptive properties. *Applied Surface Science, 416*, 781-789.

Lukatskaya Maria, R., Mashtalir, O., Ren Chang, E., Dall’Agnese, Y., Rozier, P., Taberna Pierre, L., . . . Gogotsi, Y. (2013). Cation Intercalation and High Volumetric Capacitance of Two-Dimensional Titanium Carbide. *Science, 341*(6153), 1502-1505. doi:10.1126/science.1241488

Lukatskaya, M. R., Mashtalir, O., Ren, C. E., Dall'Agnese, Y., Rozier, P., Taberna, P. L., . . . Gogotsi, Y. (2013). Cation intercalation and high volumetric capacitance of two-dimensional titanium carbide. *Science, 341*(6153), 1502-1505.

Magnuson, M., & Mattesini, M. (2017). Chemical bonding and electronic-structure in MAX phases as viewed by X-ray spectroscopy and density functional theory. *Thin Solid Films, 621*, 108-130. doi:https://doi.org/10.1016/j.tsf.2016.11.005

Maleski, K., Mochalin, V. N., & Gogotsi, Y. (2017). Dispersions of Two-Dimensional Titanium Carbide MXene in Organic Solvents. *Chemistry of Materials, 29*(4), 1632-1640. doi:10.1021/acs.chemmater.6b04830

Mansoorianfar, M., Shahin, K., Hojjati–Najafabadi, A., & Pei, R. (2022). MXene–laden bacteriophage: A new antibacterial candidate to control bacterial contamination in water. *Chemosphere, 290,* 133383. doi:https://doi.org/10.1016/j.chemosphere.2021.133383

Mashtalir, O., Cook, K. M., Mochalin, V. N., Crowe, M., Barsoum, M. W., & Gogotsi, Y. (2014a). Dye adsorption and decomposition on two-dimensional titanium carbide in aqueous media. *Journal of Materials Chemistry A, 2*(35), 14334-14338.

Mashtalir, O., Cook, K. M., Mochalin, V. N., Crowe, M., Barsoum, M. W., & Gogotsi, Y. J. J. o. M. C. A. (2014b). Dye adsorption and decomposition on two-dimensional titanium carbide in aqueous media. *2*(35), 14334-14338.

Mashtalir, O., Naguib, M., Mochalin, V. N., Dall'Agnese, Y., Heon, M., Barsoum, M. W., & Gogotsi, Y. (2013). Intercalation and delamination of layered carbides and carbonitrides. *Nature Communications, 4*(1), 1716. doi:10.1038/ncomms2664

Murray, C. J. L., Ikuta, K. S., Sharara, F., Swetschinski, L., Robles Aguilar, G., Gray, A., . . . Naghavi, M. (2022). Global burden of bacterial antimicrobial resistance in 2019: a systematic analysis. *The Lancet, 399*(10325), 629-655. doi:https://doi.org/10.1016/S0140-6736(21)02724-0

Naguib, M., Kurtoglu, M., Presser, V., Lu, J., Niu, J., Heon, M., . . . Barsoum, M. W. (2011a). Two-Dimensional Nanocrystals Produced by Exfoliation of Ti3AlC2. *Advanced Materials, 23*(37), 4248-4253. doi:https://doi.org/10.1002/adma.201102306

Naguib, M., Kurtoglu, M., Presser, V., Lu, J., Niu, J., Heon, M., . . . Barsoum, M. W. J. A. m. (2011b). Two-dimensional nanocrystals produced by exfoliation of Ti3AlC2. *23*(37), 4248-4253.

Naguib, M., Mashtalir, O., Carle, J., Presser, V., Lu, J., Hultman, L., . . . Barsoum, M. W. J. A. n. (2012). Two-dimensional transition metal carbides. *6*(2), 1322-1331.

Naguib, M., Unocic, R. R., Armstrong, B. L., & Nanda, J. J. D. t. (2015). Large-scale delamination of multi-layers transition metal carbides and carbonitrides "MXenes". *44*(20), 9353-9358.

Natu, V., Pai, R., Wilson, O., Gadasu, E., Badr, H., Karmakar, A., . . . Barsoum, M. W. (2022). Effect of Base/Nucleophile Treatment on Interlayer Ion Intercalation, Surface Terminations, and Osmotic Swelling of Ti3C2Tz MXene Multilayers. *Chemistry of Materials, 34*(2), 678-693. doi:10.1021/acs.chemmater.1c03390

Ötker, H. M., & Akmehmet-Balcıoğlu, I. J. J. o. H. M. (2005). Adsorption and degradation of enrofloxacin, a veterinary antibiotic on natural zeolite. *122*(3), 251-258.

Oulton, R. L., Kohn, T., & Cwiertny, D. M. (2010). Pharmaceuticals and personal care products in effluent matrices: A survey of transformation and removal during wastewater treatment and implications for wastewater management. *Journal of Environmental Monitoring, 12*(11), 1956-1978. doi:10.1039/C0EM00068J

Peng, C., Wei, P., Chen, X., Zhang, Y., Zhu, F., Cao, Y., . . . Peng, F. (2018). A hydrothermal etching route to synthesis of 2D MXene (Ti3C2, Nb2C): Enhanced exfoliation and improved adsorption performance. *Ceramics International, 44*(15), 18886-18893. doi:https://doi.org/10.1016/j.ceramint.2018.07.124

Peng, Q., Guo, J., Zhang, Q., Xiang, J., Liu, B., Zhou, A., . . . Tian, Y. (2014). Unique lead adsorption behavior of activated hydroxyl group in two-dimensional titanium carbide. *Journal of the American Chemical Society, 136*(11), 4113-4116.

Rahman, N., & Raheem, A. J. J. o. E. M. (2022). Fabrication of graphene oxide/inulin impregnated with ZnO nanoparticles for efficient removal of enrofloxacin from water: Taguchi-optimized experimental analysis. *318*, 115525.

Ramasubramanian, B., Reddy, M., Zaghib, K., Armand, M., & Ramakrishna, S. J. N. (2021). Growth mechanism of micro/nano metal dendrites and cumulative strategies for countering its impacts in metal ion batteries: A review. *11*(10), 2476.

Rasool, K., Pandey, R. P., Rasheed, P. A., Buczek, S., Gogotsi, Y., & Mahmoud, K. A. J. M. T. (2019). Water treatment and environmental remediation applications of two-dimensional metal carbides (MXenes). *30*, 80-102. doi:10.1016/j.mattod.2019.05.017

Ren, C. E., Hatzell, K. B., Alhabeb, M., Ling, Z., Mahmoud, K. A., & Gogotsi, Y. (2015). Charge- and Size-Selective Ion Sieving Through Ti3C2Tx MXene Membranes. *The Journal of Physical Chemistry Letters, 6*(20), 4026-4031. doi:10.1021/acs.jpclett.5b01895

Rhee, K. Y., & Gardiner, D. F. J. C. i. d. (2004). Clinical relevance of bacteriostatic versus bactericidal activity in the treatment of gram-positive bacterial infections. *39*(5), 755-756. doi:10.1086/422881

Rico, A., Oliveira, R., McDonough, S., Matser, A., Khatikarn, J., Satapornvanit, K., . . . Van den Brink, P. J. (2014). Use, fate and ecological risks of antibiotics applied in tilapia cage farming in Thailand. *Environmental Pollution, 191*, 8-16.

Rozmysłowska-Wojciechowska, A., Wojciechowski, T., Ziemkowska, W., Chlubny, L., Olszyna, A., & Jastrzębska, A. (2019). Surface interactions between 2D Ti3C2/Ti2C MXenes and lysozyme. *Applied Surface Science, 473*, 409-418.

Shahzad, A., Rasool, K., Miran, W., Nawaz, M., Jang, J., Mahmoud, K. A., & Lee, D. S. (2017). Two-Dimensional Ti3C2Tx MXene Nanosheets for Efficient Copper Removal from Water. *ACS Sustainable Chemistry & Engineering, 5*(12), 11481-11488. doi:10.1021/acssuschemeng.7b02695

Shekhirev, M., Busa, J., Shuck, C. E., Torres, A., Bagheri, S., Sinitskii, A., & Gogotsi, Y. (2022). Ultralarge Flakes of Ti3C2Tx MXene via Soft Delamination. *ACS Nano*. doi:10.1021/acsnano.2c04506

Shekhirev, M., Ogawa, Y., Shuck, C. E., Anayee, M., Torita, T., & Gogotsi, Y. (2022). Delamination of Ti3C2Tx Nanosheets with NaCl and KCl for Improved Environmental Stability of MXene Films. *ACS Applied Nano Materials*. doi:10.1021/acsanm.2c03701

Shen, M., Jiang, W., Liang, K., Zhao, S., Tang, R., Zhang, L., & Wang, J.-Q. (2021). One-Pot Green Process to Synthesize MXene with Controllable Surface Terminations using Molten Salts. *Angewandte Chemie International Edition, 60*(52), 27013-27018. doi:https://doi.org/10.1002/anie.202110640

Shuck, C. E., Ventura-Martinez, K., Goad, A., Uzun, S., Shekhirev, M., & Gogotsi, Y. (2021). Safe Synthesis of MAX and MXene: Guidelines to Reduce Risk During Synthesis. *ACS Chemical Health & Safety, 28*(5), 326-338. doi:10.1021/acs.chas.1c00051

Shuck, C. E., Ventura-Martinez, K., Goad, A., Uzun, S., Shekhirev, M., Gogotsi, Y. J. A. C. H., & Safety. (2021). Safe Synthesis of MAX and MXene: Guidelines to Reduce Risk During Synthesis. doi:10.1021/acs.chas.1c00051

Sinthuchai, D., Boontanon, S. K., Piyaviriyakul, P., Boontanon, N., Jindal, R., & Polprasert, C. (2021). Fate and mass loading of antibiotics in hospital and domestic wastewater treatment plants in Bangkok, Thailand. *Journal of Water, Sanitation and Hygiene for Development, 11*(6), 959-971.

Sukidpaneenid, S., Chawengkijwanich, C., Pokhum, C., Isobe, T., Opaprakasit, P., & Sreearunothai, P. (2023). Multi-function adsorbent-photocatalyst MXene-TiO2 composites for removal of enrofloxacin antibiotic from water. *Journal of Environmental Sciences, 124*, 414-428. doi:10.1016/j.jes.2021.09.042

Tewari, S., Jindal, R., Kho, Y. L., Eo, S., & Choi, K. (2013). Major pharmaceutical residues in wastewater treatment plants and receiving waters in Bangkok, Thailand, and associated ecological risks. *Chemosphere, 91*(5), 697-704.

Trouchon, T., & Lefebvre, S. (2016). A review of enrofloxacin for veterinary use. *Open Journal of Veterinary Medicine, 6*(2), 40-58.

VahidMohammadi, A., Mojtabavi, M., Caffrey, N. M., Wanunu, M., & Beidaghi, M. (2019). Assembling 2D MXenes into Highly Stable Pseudocapacitive Electrodes with High Power and Energy Densities. *31*(8), 1806931. doi:https://doi.org/10.1002/adma.201806931

Verger, L., Natu, V., Ghidiu, M., & Barsoum, M. W. (2019). Effect of Cationic Exchange on the Hydration and Swelling Behavior of Ti3C2Tz MXenes. *The Journal of Physical Chemistry C, 123*(32), 20044-20050. doi:10.1021/acs.jpcc.9b04546

Wan, J., Lacey, S. D., Dai, J., Bao, W., Fuhrer, M. S., & Hu, L. (2016). Tuning two-dimensional nanomaterials by intercalation: materials, properties and applications. *Chemical Society Reviews, 45*(24), 6742-6765. doi:10.1039/C5CS00758E

Wang, X., Garnero, C., Rochard, G., Magne, D., Morisset, S., Hurand, S., . . . Coutanceau, C. (2017). A new etching environment (FeF 3/HCl) for the synthesis of two-dimensional titanium carbide MXenes: a route towards selective reactivity vs. water. *Journal of Materials Chemistry A, 5*(41), 22012-22023.

Watkinson, A. J., Murby, E. J., & Costanzo, S. D. (2007). Removal of antibiotics in conventional and advanced wastewater treatment: Implications for environmental discharge and wastewater recycling. *Water Research, 41*(18), 4164-4176. doi:10.1016/j.watres.2007.04.005

WHO. (2018). WHO report on surveillance of antibiotic consumption: 2016-2018 early implementation.

Wu, Z., Shang, T., Deng, Y., Tao, Y., & Yang, Q.-H. (2020). The Assembly of MXenes from 2D to 3D. *Advanced Science, 7*(7), 1903077. doi:https://doi.org/10.1002/advs.201903077

Yan, Y., Han, H., Dai, Y., Zhu, H., Liu, W., Tang, X., . . . Li, H. (2021). Nb2CTx MXene Nanosheets for Dye Adsorption. *ACS Applied Nano Materials, 4*(11), 11763-11769. doi:10.1021/acsanm.1c02339

Zhang, Q.-Q., Ying, G.-G., Pan, C.-G., Liu, Y.-S., & Zhao, J.-L. (2015). Comprehensive Evaluation of Antibiotics Emission and Fate in the River Basins of China: Source Analysis, Multimedia Modeling, and Linkage to Bacterial Resistance. *Environmental Science & Technology, 49*(11), 6772-6782. doi:10.1021/acs.est.5b00729

Zhang, T., Pan, L., Tang, H., Du, F., Guo, Y., Qiu, T., & Yang, J. (2017). Synthesis of two-dimensional Ti3C2Tx MXene using HCl+ LiF etchant: enhanced exfoliation and delamination. *Journal of Alloys and Compounds, 695*, 818-826.

Zhou, A. (2012). Methods of MAX-phase synthesis and densification – II. In I. M. Low (Ed.), *Advances in Science and Technology of Mn+1AXn Phases* (pp. 21-46): Woodhead Publishing.

Zhou, A., Wang, C.-A., & Hunag, Y. (2003). Synthesis and Mechanical Properties of Ti3AlC2 by Spark Plasma Sintering. *Journal of Materials Science - J MATER SCI, 38*, 3111-3115. doi:10.1023/A:1024777213910

# APPENDIX

# APPENDIX A
# RAW DATA FIGURE

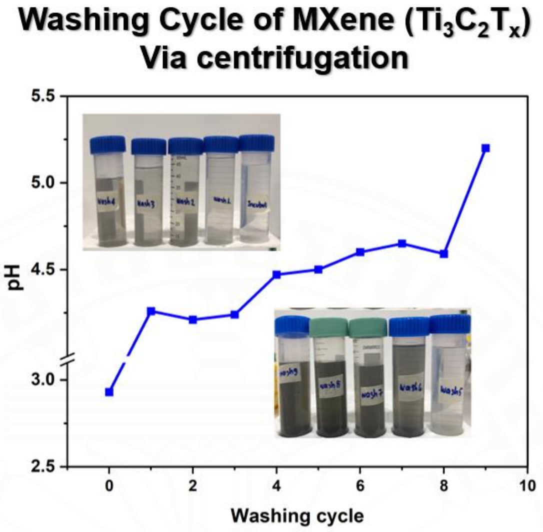

**Figure A.1** Repeat centrifugation cycle were used for washing $Ti_3C_2T_x$ synthesized by etching 1g of MAX phase using 10mL of HCl and 9M NaF etchant. The supernatant of washing solution was monitored of pH until the solution became neutral.

**Table A.1** Phase content matching from XRD measurement of MX etched at various fluoride salts etching.

| Sample | Phase content | | | |
|---|---|---|---|---|
| | % MX | % $Ti_3AlC_2$ MAX phase | % $Na_2AlF_6$ | % $TiO_2$ anatase |
| MX-Li-4h | 53.3% | 40.4% | - | 6.3% |
| MX-Li-24h | 91.3% | 8.70% | - | - |
| MX-Na-4h | 77.1% | - | 22.9% | - |
| MX-Na24h | 45% | - | 55.0% | - |
| MX-K-4h | 97.0% | 3.0% | - | - |
| MX-K-24h | 100% | - | - | - |
| MX-Zn-4h | 95.8% | - | - | 4.2% |
| MX-Zn-24 | 97.8 | - | - | 2.2% |

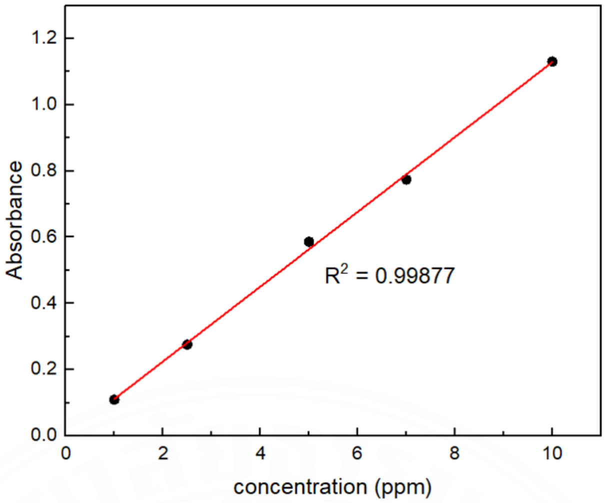

**Figure A.2** Standard curve for enrofloxacin at the maximum absorbance 276nm

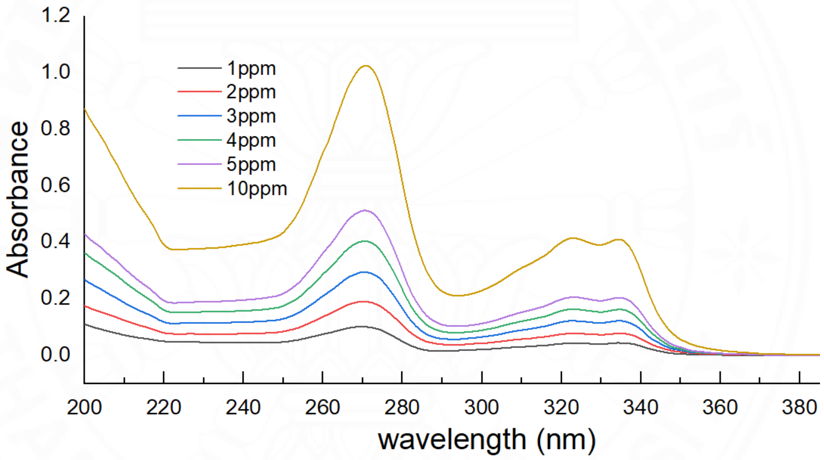

**Figure A.3** Absorbance spectra of enrofloxacin solution at difference concentration

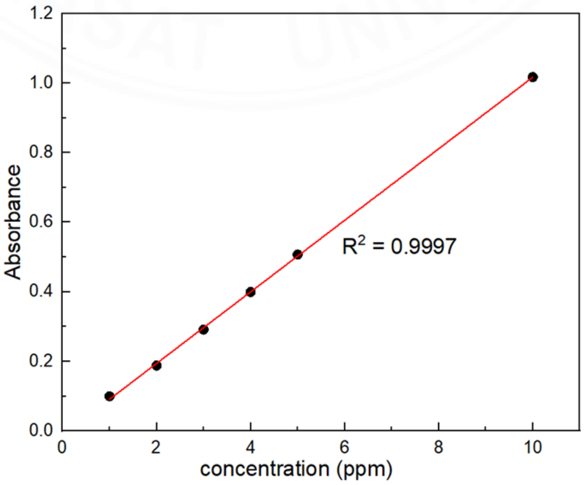

**Figure A.4** Standard curve for enrofloxacin at the maximum absorbance 272nm

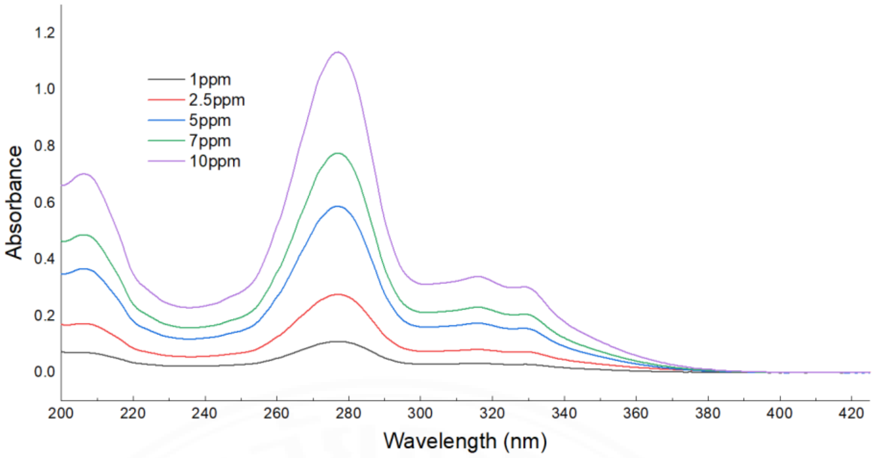

**Figure A.5** Absorbance spectra of enrofloxacin solution at difference concentration

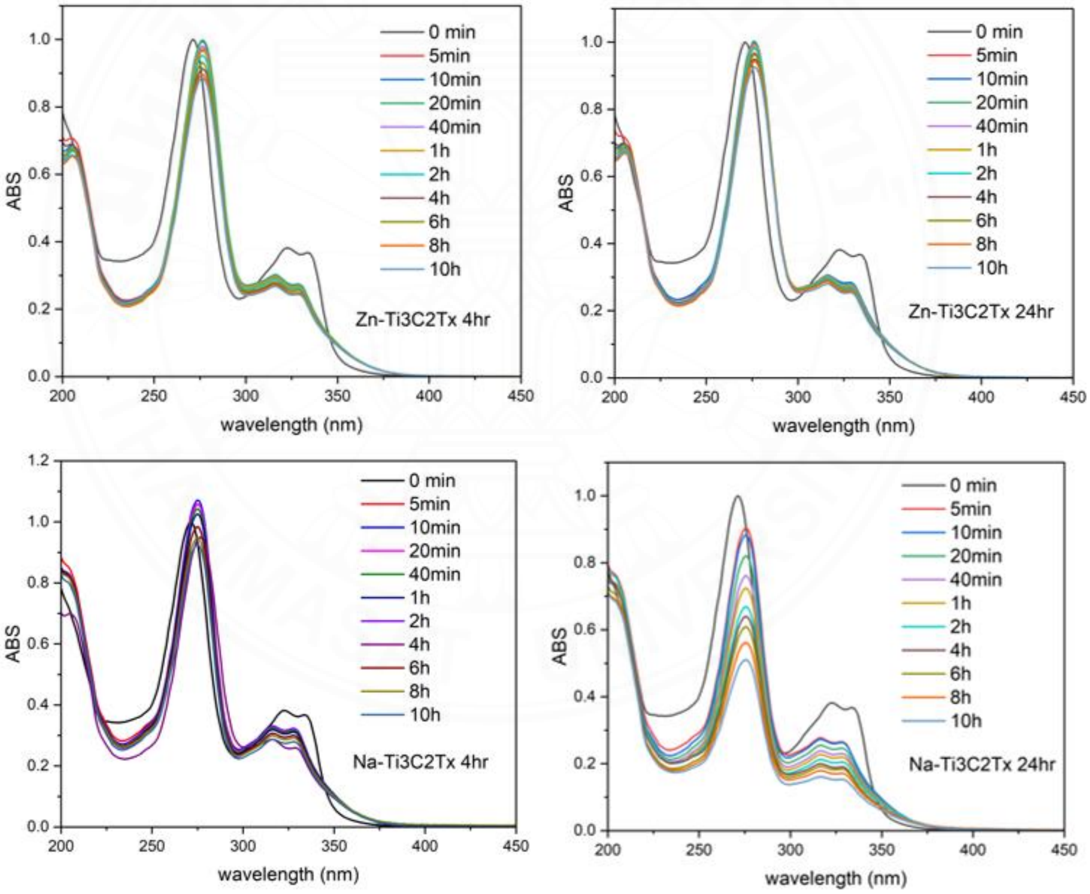

**Figure A.6** ENR absorbance spectra obtained from UV-Vis spectrophotometer during adsorption in the dark condition using multilayer MXene adsorbent

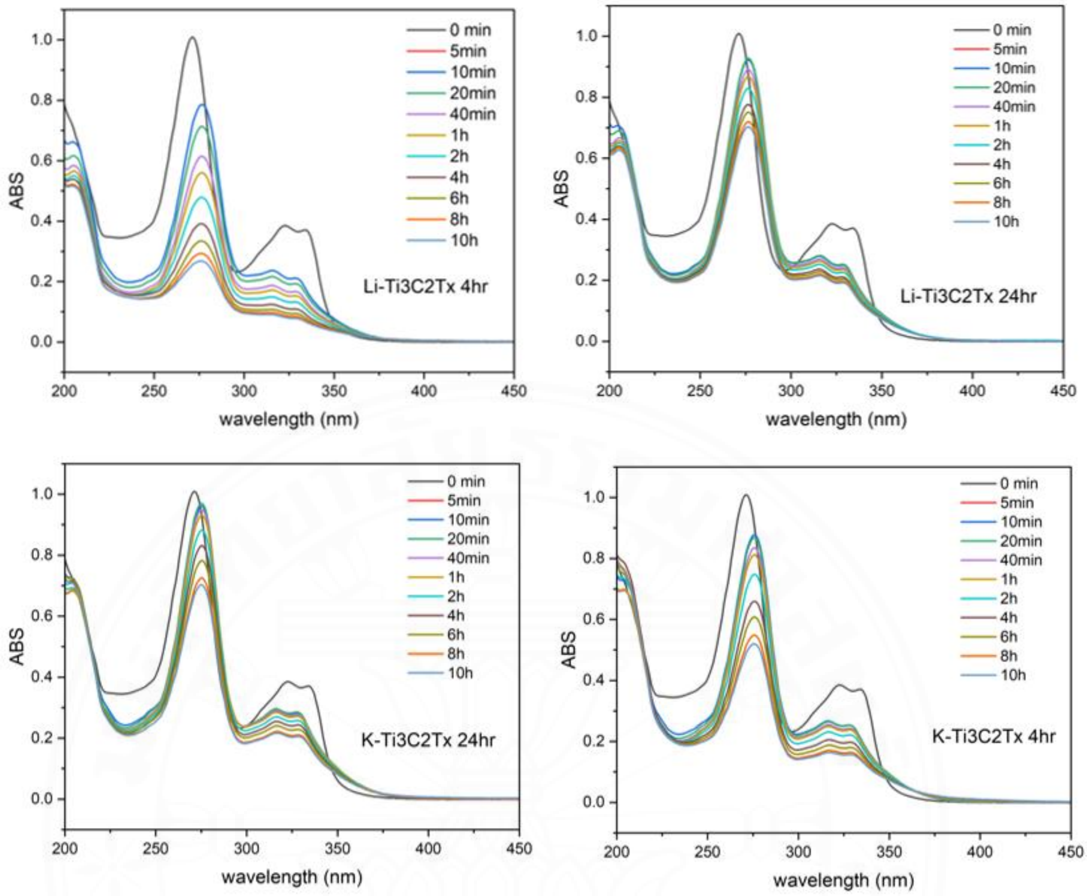

**Figure A.7** ENR absorbance spectra obtained from UV-Vis spectrophotometer during adsorption in the dark condition using multilayer-MXene adsorbent

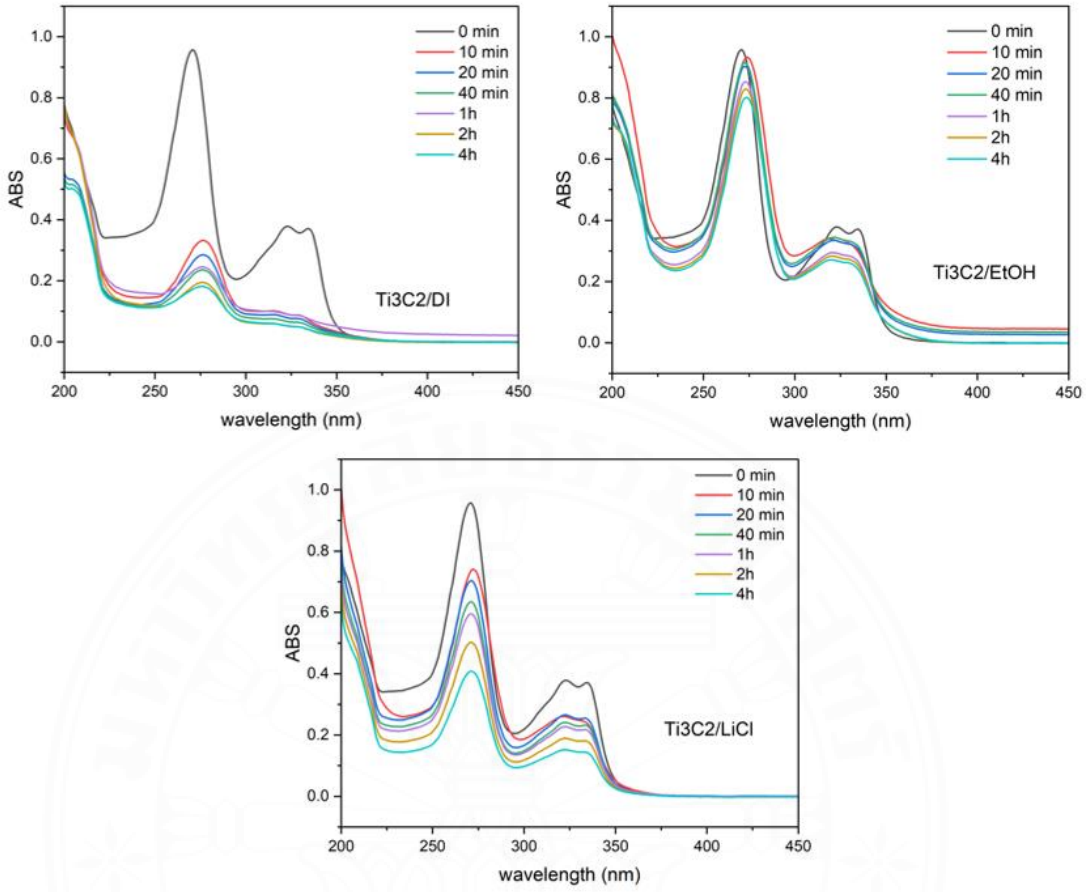

**Figure A.8** ENR absorbance spectra obtained from UV-Vis spectrophotometer during adsorption in the dark condition using monolayer-MXene adsorbent

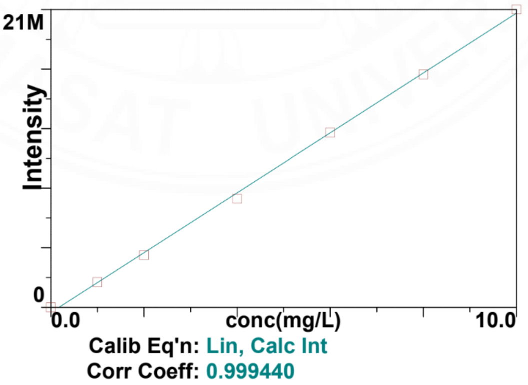

**Figure A.9** Calibration curve of ICP-OES analysis of lithium content in the monolayer-MXene, multilayer-MXene

# BIOGRAPHY

| | |
|---|---|
| Name | Channarith Be |
| Education | 2019: Bachelor of Engineering, Chemical and Food Engineering, Institute of Technology of Cambodia |

Publication

Channarith, B., Thilina, R. K., Paiboon, S., Pakorn, O., & Chamorn, C. (2022). Synthesis and characterizations of MXene ($Ti_3C_2T_x$) for adsorption of an enrofloxacin antibiotic. Proceeding of *11th International Conference on Materials Science and Technology* (pp. 67-72). Thailand.